
Imperial College, London

Albert-Ludwigs-Universität, Freiburg


MSci Thesis

July 7, 2016

# Resonant Enhancement of Velocity-Dependent Casimir-Polder Shifts and Rates


Author:

**Joseph Durnin**

Supervisor:

**Stefan Yoshi Buhmann**

Co-supervisors:

**Juliane Klatt**

**Robert Bennett**

# Abstract

Quantum friction is the velocity-dependent force between two polarisable (but initially unpolarised) objects in relative motion, which is a direct result of quantum-fluctuation mediated energy and momentum transfer. Experimental verification of quantum friction has been unsuccessful so far due to the force's short range nature, however a scenario proposed by Y. Guo and Z. Jacob [*Opt. Express*, 22:26193-26202, 2014] of two parallel plates in relative motion revealed a resonance effect which amplifies substantially the friction force between them. Here a method is presented which investigates in terms of the friction's spectroscopic signatures the more experimentally realisable situation of a moving atom between two plates, on the basis of quantum electrodynamics. This is an extension of previous work on the atomic velocity dependence in the presence of a single plate. Analytical results were obtained for the effects of media on moving atoms for arbitrary geometries, which allowed the calculation of the velocity dependence to lowest order to be calculated for systems which have translational invariance along the atom's direction of motion, as for the results known previously all velocity-dependent terms disappear in this case. No resonance effect of the type discovered by Guo and Jacob could be found for the two-plate set-up, however general expressions for the plate-induced spectroscopic effects on a moving atom were found, and shown to be equivalent to applying a Doppler-shift to the static result. Numerical analysis investigated the behaviour of this system for the well studied case of the $6D_{3/2} \rightarrow 7P_{1/2}$ transition in $^{133}$Cs interacting with sapphire plates, including a detailed analysis of the impact of the relevant atomic, medium and geometric parameters.

Zwischen zwei nicht polarisierten aber polarisierbaren Körpern, welche sich relativ zu einander bewegen, gibt es eine von Quantenfluktuationen vermittelte Kraft, die als Quantenreibung bezeichnet wird. Dieser Effekt ist typischerweise schwach gegenüber der geschwindigkeitsunabhängigen Casimir-Polder-Kraft, und ist daher bis jetzt nicht nachgewiesen worden. Y. Guo und Z. Jacob [*Opt. Express*, 22:26193-26202, 2014] haben einen Resonanzeffekt zwischen zwei sich parallel zueinander bewegenden Platten theoretisch vorhergesagt, der die Quantenreibung vielfach verstärkt. Da diese Situation allerdings vorerst nicht realisierbar ist, wurde hier eine ähnliche Situation erforscht, bei der sich ein Atom zwischen zwei statischen parallelen Platten bewegt, um die spektroskopische Wirkung der Quantenreibung auf das Atom zu berechnen. Diese durch makroskopische QED ausgeführte Rechnung ist verwandt mit der schon vollzogenen Betrachtung der Wirkung einer einzelnen Platte auf ein Atom. Zuerst wurde eine allgemeinere Formulierung der Situation erforscht, in der die geometrieunabhängige Wirkung von Medien auf ein sich bewegendes Atom durch eine Taylor-Reihe in der atomaren Geschwindigkeit berechnet wurde. Die Zwei-Platten-Geometrie wurde dann als Anwendungsbeispiel dieser Ergebnisse benutzt. Der explizite Greensche Tensor der Zwei-Platten-Situation wurde dann verwendet, um zu zeigen, dass die Atomgeschwindigkeitsabhängigkeit des Systems durch eine Doppler-Verschiebung darstellbar ist. Es wurde jedoch kein starker Resonanzeffekt gefunden. Die Eigenschaften der Wechselwirkung zwischen dem $6D_{3/2} \rightarrow 7P_{1/2}$ Übergang in $^{133}$Cs und zwei Saphir-Platten wurde mithilfe numerischer Auswertung erforscht, mit einer ausführlichen Analyse der maßgeblichen atomaren, Medien- und geometrischen Parametern.

# Contents

## Guide to Notation

Vectors are denoted with a right-pointing arrow, e.g. $\vec{v}$. All second rank tensors or matrices are denoted in bold type, e.g. $\mathbf{G}$. Throughout this thesis vector notation is used freely to present expressions involving tensors of rank 1 and 2. Through the use of the following conventions this has been done as unambiguously as possible. In short, any operator, scalar or vector product found on the left (right) hand side of some tensor acts on the leftmost (rightmost) index of that tensor. This combined with the use of the left gradient $\overleftarrow{\nabla}$, implying a gradient acting on the object to the left, means all expressions required can be shown unambiguously in vector notation. For absolute clarity, some examples of this notation are given below in index form. In all examples $(\mathbf{G})_{ij} = G_{ij}$ :

$$(\nabla \cdot \mathbf{G})_k = \sum_i \nabla_i G_{ik} \tag{1}$$

$$(\mathbf{G} \cdot \overleftarrow{\nabla})_k = \sum_i \nabla_i G_{ki} \tag{2}$$

$$(\nabla \times \mathbf{G})_{kl} = \sum_{i,j} \epsilon_{ijk} \nabla_i G_{jl} \tag{3}$$

$$(\mathbf{G} \times \overleftarrow{\nabla})_{kl} = \sum_{i,j} \epsilon_{ijl} G_{ki} \overleftarrow{\nabla}_j = -\sum_{i,j} \epsilon_{ijl} \nabla_i G_{kj} = -\left[ \left( \nabla \times \mathbf{G}^T \right)^T \right]_{kl} \tag{4}$$

Where present $\nabla_A$ should be interpreted as the gradient with respect to the coordinates $\vec{r}_A$, and likewise for all similar notation. When used on a function with 2 position arguments e.g. $f(\vec{r}, \vec{r}\,')$, $\nabla$ and $\nabla'$ refer to derivatives with respect to the first and second position argument respectively, even when the two arguments are not denoted in such a manner as $\vec{r}, \vec{r}\,'$.

Notation of the form $f^{(n)}$ where n is a number is used in various contexts to denote either a) the order in a perturbative expansion, or b) the more usual nth derivative with respect to a function. The context should make which meaning is intended clear.

# Chapter 1

# Introduction

## 1.1 Preface

The work presented here was carried out a part of a junior research group led by Stefan Buhmann, a subgroup of the Quantum Optics and Statistics group headed by Prof. Andreas Buchleitner at the Albert-Ludwigs-Universität, Freiburg im Breisgau. The junior research group focuses on the treatment of dispersion forces and effects as described by Macroscopic Quantum Electrodynamics (QED), a theory of QED which incorporates absorbing and dispersive media (the details of Macroscopic QED will be outlined in the theory chapter of this report). The work contained in this report about velocity dependent Casimir-Polder effects on atoms is closely related to that done by both the group leader Stefan Buhmann, and Juliane Klatt, a 3rd year PhD student in the group.

The initial work presented here was an extension of the treatment of a moving atom in the presence of media using Macrosopic QED carried out by Buhmann and Scheel [1]. They used a series expansion in the atomic velocity to calculate up to linear order the velocity dependence of an atom's spectroscopic properties and experienced friction force due to the media. In this report the calculation of the spectroscopic effects was extended to second order in this velocity series. As discussed in section 3.1, this allowed the lowest order velocity dependence of the atomic dynamics in the presence of a far larger class of geometries to be calculated. These results were then applied to a situation where the linear term does indeed make no contribution to the atomic dynamics, an atom moving in a vacuum cavity between two parallel plates, where the motion is also parallel to the plate surfaces. This was calculated in the non-retarded regime, and following this the two-plate non-retarded system was then considered completely, i.e. to all orders in the velocity dependence. This was achieved by inserting the explicit form of the electromagnetic response tensor for the two-plate system at an earlier stage of the previous calculation, thereby sacrificing generality for a more complete treatment of the two-plate system.

In this work a great deal is owed to Juliane Klatt for her treatment of an atom next to a single dielectric plate; many of the techniques used there were applied to the two-plate set-up. However the two-plate system exhibits significantly more complex behaviour than the single plate system. As the work of Ref. [2] showed, the interaction of a neutral atom with a dielectric plate can be expressed in terms of Fresnel reflection coefficients. A formalism of this kind is used here, and whereas a single reflection off the plate suffices to describe the single-plate system [3], when two-plates are present an infinite number of possible reflections contribute to the final result. The difficulty in treating the expressions analytically compared to the single-plate case meant that the friction force on the atom could not be calculated due to time constraints. However the spectroscopic signatures of the Casimir-Polder effects on the atom were calculated, and in this formalism the electronic transition rates calculated lead directly to the calculation

of the friction force, as was shown in Ref. [4].

## 1.2 Context

The best known example of a dispersion force is the Casimir effect occuring between two parallel uncharged conducting plates situated in the vacuum, where QED predicts that the two plates will experience a mutual attraction. The physical process behind this effect has various interpretations, perhaps the most intuitive being that provided by virtual photons. The free charges in the conducting plates respond to the presence of virtual photons such that the electric field always vanishes at the plate boundaries. This sets a limit on the number of possible virtual photon wavelengths which can exist in the cavity between the two plates, whereas outside the cavity there is an infinite number of possible wavelengths. This leads to a net photon pressure on the plates from outside the cavity, in accordance with QED's prediction and as experimentally measured for this system in 2002 [5]. Such general phenomena between neutral macroscopic bodies are named Casimir effects. The description of these effects given here also corresponds to the interpretation of Casimir and related effects in terms of a redefinition of the vacuum state of the field, and the physical consequences of this redefinition.

An analogous effect occurs between a neutral atom and an uncharged medium, a situation first described for perfect conducting materials around the middle of the 20th century. In the short range unretarded limit this effect was described by Lennard-Jones [6] in 1932 by the method of image charges applied to a quantum mechanical atom, and this work was then extended to include the longer range retarded limit by Casimir and Polder [7] through the use of QED in a second order perturbation theory calculation in 1948. The terminology used for such effects on atoms varies in the literature. Here a Casimir-Polder effect is defined as an effect caused by the presence of macroscopic media on an uncharged atom. A related effect is the well-known attractive van der Waals force between individual atoms. Here the distinction is made between the pairwise van der Waals interaction and the Casimir-Polder interaction, which when considering the media on a microscopic level can be shown [8] to be non-pairwise between atoms.

The understanding of Casimir-Polder effects has a direct application to many areas of interest in physics, chemistry, technology and other fields of study. The standard example in chemistry (which was in fact the subject of Lennard-Jones' 1932 paper [6]) is the description of sorption processes whereby gases interact with surfaces of solids. Modern micro- and nanoelectromechanical systems are systems built on such a small scale that an understanding of the properties of matter and atom-medium interactions on small length scales are vital to explaining their properties. In any system which is cooled substantially an understanding of the zero-point effects of the electromagnetic field must be accounted for to account for any deviations from the 'classical' zero temperature limit. One example of such a consideration is the entanglement of the atoms internal and external degrees of freedom, where due to Casimir-Polder effects the state of an atom and the medium become linked, which has an effect on the dynamics of any such system.

Some more recent theoretical advancements which contributed substantially to the understanding of Casimir-Polder effects are as follows. The work of Wylie and Sype [2] in 1984 was closer in spirit to the description of Casimir-Polder effects in the work presented here; this interpretation of Casimir-Polder effects is implicit in the formulation of Macroscopic QED. They treated the response of a medium to electromagnetic fields with linear response theory, which led to the calculation of the spectroscopic effects on a nearby excited atom, with the medium properties being expressed through the medium's Fresnel coefficients. In a similar approach Fichet et al. showed in 1995 [9] that in the non-retarded limit an enhancement of Casimir-Polder effects can occur when the atomic transition frequency is resonant with a dielectric absorption frequency.

Linear response theory applied to a medium's electromagnetic response provides an interpretation of Casimir-Polder effects in terms of internal fluctuations in the medium by virtue of the fluctuation-dissipation theorem (discussed in section 2.2). The fluctuation interpretation was first hinted at in Lennard-Jones' work [6], where it was required that the mean electron displacement from the nucleus of an atom $\langle \hat{r} \rangle$ vanishes, but $\langle \hat{r}^2 \rangle$, which gives the quantum fluctuations of $\hat{r}$, does not.

Experimentally some key achievements are as follows. The experimental verification of the Lennard-Jones potential (or more precisely a slight modification of this with a more realistic metal conductivity included), which scales with the atom plate separation $R^{-3}$, came in 1969 with the work of Raskin and Kusch [10]. This experiment measured the deflection of a beam of neutral atoms/molecules by a metal cylinder, where the Casimir-Polder force on the atom/molecule is given by the gradient of the Casimir-Polder potential between them and the cylinder $\vec{F} = -\nabla U$. In 1988 Anderson et al. measured [11] the Casimir-Polder force on Rydberg atoms (i.e. atoms with large $\langle \hat{r}^2 \rangle$) near a metallic surface, and achieved results in agreement with the Lennard-Jones potential's [6] linear $\langle \hat{r}^2 \rangle$ dependence. Sandhoghdar et al. [12] investigated spectroscopically the Casimir-Polder interaction energy of Rydberg atoms with two conducting plates in the non-retarded 'Lennard-Jones' limit. They were able to simultaneously verify the $\langle \hat{r}^2 \rangle$ and $R^{-3}$ dependence of the Lennard-Jones potential. Direct detection of the force by measuring the deflection of a beam of neutral sodium atoms by Sukenik et al. [13] followed in 1993, where both the magnitude of the force predicted by QED and the atom-plate separation dependence were confirmed.

One key feature of the above experiments is that they almost all [10, 11, 12, 13] used moving atoms whilst modelling the atom as stationary, i.e. ignoring the velocity dependence of the effects. As shown in Ref. [4] the effects of the atom's velocity are in general non-vanishing, and in many cases lead to quantum friction. This is defined here as a force opposing the direction of motion of the atom which has no classical equivalent. However the results of the above experiments were still valid, because such velocity dependent effects are so small compared to the static effects (which themselves are small enough to have evaded regular detection until the last quarter of the 20th century) that they are undetectable for the experimental sensitivities and system properties used thus far. Therefore to experimentally test the atomic velocity dependence of Casimir-Polder effects in the near future it is necessary to look for some means by which the velocity dependence may be amplified to measurable levels. The motivation for the work presented here came from a paper by Guo and Jacob in Ref. [14], where in the non-retarded limit a resonance effect occurs between two parallel plates in motion relative to each other, such that the plates experience a massively enhanced friction force. This occurs when the Fabry-Perot resonance condition is satisfied. When describing evanescent waves (i.e. in the non-retarded limit) this takes the form $1 - r_1(\omega) r_2(\omega) e^{-2|k_z|L} = 0$, where $r_1$ and $r_2$ are the reflection coefficients of the first and second plate respectively, $L$ is the plate separation, and $|k_z|$ is the wavevector component perpendicular to the plane surface. If the two plates are of the same material, and at some frequency $\omega_{SP}$ this material has a surface plasmon resonance, the motion of one plate can be chosen such that at this frequency $r(\omega') = r(-\omega_{SP}) = r^*(\omega_{SP})$. At the surface plasmon resonance in the non-retarded limit the modulus of the reflection coefficient $|r|$ can be larger than 1. Thus at some $|k_z|$ the Fabry-Perot resonance condition can be exactly satisfied, leading to a large resonance in the vacuum friction between the plates.

However, experimentally realising the above setup such that the resonance condition is met is currently technically impossible. The values quoted in the Guo and Jacob paper [14] were a plate velocity of $c/10$ and a plate separation of 70nm; the velocity required for the resonance scales roughly linearly with the plate separation for $v$ not close to $c$. By comparison in the Sukenik

experiment [13] the smallest (stationary) plate separation achieved was $\sim 1\mu$m for static plates; the difficulties involved in moving plates substantially closer together (let alone moving them at a tenth the speed of light parallel to each other) are currently technically insurmountable. Thus a more experimentally realisable situation is to have two stationary plates with an atom moving between them. This situation has precedent with for example the experiment carried out in Ref. [12]. In this set-up any similar resonant Casimir-Polder effect would be detectable not only in terms of the friction force itself as for the two plates, but also by the effects on the spectroscopic properties of the atom. Thus the proposed set-up is a more experimentally realisable situation with more measurable parameters for investigating Casimir-Polder effects. The calculations will be carried out using Macroscopic QED (MQED). In a similar manner to classical macroscopic electromagnetism, MQED is a useful tool for solving problems involving extended bodies which would be unsolvable using the microscopic theory. The classical macroscopic fields simplify calculations by reformulating the bound charges of a material in terms of electric polarisation and magnetisation fields, which serves to greatly reduce the number of interactions which must be considered when solving a problem. MQED applies a similar methodology to the quantised electromagnetic field. One benefit of calculating velocity dependent effects within MQED along the lines of Ref. [1] is that the calculation of the spectroscopic effects leads naturally to the calculation of the friction force, meaning an experiment can be constructed such that it either detects the friction directly or the friction's spectroscopic signature.

## 1.3 Aims

The aim of the work presented here is to attempt to describe the spectroscopic Casimir-Polder effects on a moving atom between two-plates, and their dependence on experimentally relevant parameters, with a view to finding a resonance which would make the velocity dependent effects sufficiently strong that they could be measured in an experiment. To this end Macroscopic QED will be used to calculate the interaction of an atom with the quantised electromagnetic field, in a way which takes into account the electromagnetic zero-point effects of the medium on the atom. Firstly a more general formulation of the problem of a moving atom in the presence of media will be carried out in a series expansion calculated to second order in the atomic velocity, with a specific application to the two-plate situation. Then by inserting the specific geometry of the two-plate system at an earlier stage in the calculation, an attempt will be made to describe the system without resort to a series expansion which is limited to some order in the atomic velocity. The ideal result would be some massive enhancement of the spectroscopic effects on the atom due to the media for some resonant velocity, by analogy with the result of Guo and Jacob [14]. However even if no such massive resonance exists, it is hoped that the results obtained may nonetheless point to a better understanding of the velocity dependence of Casimir-Polder effects, and how they might be measured most easily. Were such velocity-dependent effects to be detected it would be a confirmation of another aspect of the contemporary understanding of the interaction of atoms and molecules with media on small length scales.

# Chapter 2

# Theoretical Framework

This chapter begins with a summary of the physical origins of Macroscopic QED, with the specific application to the atom-media system brought to the fore. Following this in section 2.2 is an overview of the classical theory of electrodynamics in presence of media, which contains many points relevant to the quantised theory. Macroscopic Quantum Electrodynamics itself is then formulated in detail in section 2.3, and finally in section 2.4 the interaction of an atom with the quantised electromagnetic field in the presence of media is detailed.

## 2.1 Macroscopic QED - Requirements

The aim of the work contained within this report is, in the simplest terms possible, to investigate the electromagnetic effects of macroscopic media on atoms when the electromagnetic field is in its vacuum state. This statement contains all the required information regarding how a theory most suitable to describe the situation at hand might be found. As the interest is in the spectroscopic signatures of the effects on the atom due to media, the quantum mechanical nature of the atom must be taken into account by considering its internal electronic wavefunctions. However the atom's trajectory is treated in a classical manner, i.e. it can be said to have a definite centre of mass motion. This is a form of the Born-Oppenheimer approximation, where the atom's centre of mass motion can be ignored while solving for the system's electronic dynamics. This is valid because in general the nuclear vibrational energies are much smaller than the electronic transition energies, so the transitions are approximately unaffected by the nuclear degrees of freedom [15]. The atom's interaction with the electromagnetic radiation field will in turn be governed by a suitable interacting quantum field theory coupling the atom to the field. Finally the effect of the macroscopic media must be taken into account.

The interaction of an atom with the quantised electromagnetic field in 'free space' (i.e. when no macroscopic media are present) is well understood. The interaction of the atom with the field leads to induced transitions between the electronic states of the atom, where energy is conserved by the emission and/or absorption of photons [15]. The focus on the electronic dynamics is due to the fact that these are almost always the focus of experimental interest. This approach shall be broadly followed here with the inclusion of media, with the focus once again on establishing the quantised field's effects on an atom's internal electronic transitions. With a view to describing the presence of macroscopic bodies in a quantum theory, it is instructive first to consider the equivalent theory in classical electromagnetism. This is motivated by the requirement that the classical limit of the quantum theory corresponds to the classical theory.

## 2.2 Classical Electrodynamics in Media

The microscopic theory of electrodynamics (ED) is clearly unsuited to solving problems involving macroscopic media. 12g of Carbon for example contains $\sim 10^{24}$ particles; to solve the dynamics of this system exactly would be a task disproportionate to the accuracy of the results obtained compared to those obtained when utilising some simpler model of the system. The most common simplification is to space-average the current and charge density, electric and magnetic fields etc., to create more easily manageable continuous charge distributions. These new fields are named the macroscopic fields, and care must be taken when defining them. The key features are that the averaging volume is sufficiently large that the microscopic fluctuations in the current and charge density of the constitutive atoms of the medium are uncorrelated over the averaging distance, but sufficiently small that the value of the averaged field is indeed suitable for the point evaluated. This leads naturally to the separation into free and bound charges in the material, and also to the expression of the individual bound charges as a multipole expansion [16]. Keeping only the dipole elements in this expansion, which can then through the averaging process be expressed as macroscopic polarisation and magnetisation respectively, leads to the well-known macroscopic Maxwell equations and associated constitutive relations without the presence of free charges:

$$\nabla \cdot \vec{D} = 0 \qquad \nabla \cdot \vec{B} = 0$$

$$\nabla \times \vec{E} = -\frac{\partial \vec{B}}{\partial t} \qquad \nabla \times \vec{H} = \frac{\partial \vec{D}}{\partial t} \tag{2.1}$$

$$\vec{D} = \epsilon_0 \vec{E} + \vec{P} \qquad \vec{H} = \frac{1}{\mu_0}\vec{B} - \vec{M} \tag{2.2}$$

Here $\vec{E}$ and $\vec{B}$ are the electric and magnetic fields, and $\vec{D}$ and $\vec{H}$ are the electric and magnetic displacement fields respectively. However, in all work presented here the magnetisation of the medium is assumed to have negligible effects compared to the polarisation. For many materials (e.g. perfect conductors, most dielectrics) this is the case, and henceforth the magnetisation $\vec{M}$ shall always be equal to $\vec{0}$. Next it is assumed that the response of the medium polarisation to an applied electric field is linear and causal. The first assumption is valid for all field strengths normally encountered in experiments in electrodynamics, although for unusually large field strengths it would in principle not hold to good accuracy. It is furthermore useful, although not necessary, to assume that the medium response is isotropic and local. This leads to the following expression for the medium polarisation $\vec{P}$:

$$\vec{P}(\vec{r}, t) = \frac{\epsilon_0}{2\pi} \int_{-\infty}^{\infty} d\tau \cdot \chi(\vec{r}, \tau) \vec{E}(\vec{r}, t - \tau) + \vec{P}_N(\vec{r}, t) \tag{2.3}$$

Here $\chi$ is the scalar response function of the medium, and $\vec{P}_N$ is the noise term corresponding to random fluctuations in the medium occuring independently of any applied field. The response function $\chi(\vec{r}, \tau)$ is required to respect the causality condition of the medium response, meaning that the polarisation at time $t$ cannot depend on the electric field at any time $t' > t$. This leads to the requirement:

$$\chi(\vec{r}, \tau) = 0 \quad \text{when} \quad \tau < 0 \tag{2.4}$$

The assumption made above regarding the linearity of the response will be of great importance when formulating the quantum theory later in this chapter. With regard to the noise polarisation $\vec{P}_N$, constraints are placed on this by the fluctuation dissipation theorem. The fluctuation dissipation theorem is a result of statistical mechanics, and states essentially that if a quantity in a system has a complex response to some applied field, meaning that the imaginary part of the response function (corresponding to dissipation in the system) is non-vanishing, there are necessarily internal fluctuations in this quantity. The reverse argument also holds, and the correlations of the fluctuating quantity $\vec{P}_N$ can be shown [17] to be proportional to the imaginary

part of the response function $\chi(\vec{r},t)$. Thus the presence of the field response term in equation (2.3) necessitates the presence of the noise term.

By taking the time-like Fourier-transform of equations (2.1) - (2.3) according to:

$$f(\omega) = \frac{1}{2\pi}\int_{-\infty}^{\infty} f(t)e^{i\omega t}dt \tag{2.5}$$

and denoting Fourier-transformed functions with an $\omega$ in their argument, they can be written in the simpler form:

$$\begin{aligned} \nabla\cdot\vec{D}(\vec{r},\omega) &= 0 & \nabla\cdot\vec{B}(\vec{r},\omega) &= 0 \\ \nabla\times\vec{E}(\vec{r},\omega) &= i\omega\vec{B}(\vec{r},\omega) & \nabla\times\vec{H}(\vec{r},\omega) &= -i\omega\vec{D}(\vec{r},\omega) \end{aligned} \tag{2.6}$$

$$\vec{D}(\vec{r},\omega) = \epsilon_0\epsilon(\vec{r},\omega)\vec{E}(\vec{r},\omega) + \vec{P}_N(\vec{r},\omega) \qquad \vec{H}(\vec{r},\omega) = \frac{1}{\mu_0}\vec{B}(\vec{r},\omega) \tag{2.7}$$

Here the relative permeability of the medium $\epsilon$ has been identified in terms of the electric response function as:

$$\epsilon(\vec{r},\omega) = 1 + \chi(\vec{r},\omega) \tag{2.8}$$

Later the conjugation properties of these functions will be useful, and from the definition of the Fourier-transform it is clear that $f^*(\omega) = f(-\omega^*)$ holds for all transformed functions $f(\omega)$ when the original function $f(t)$ and its argument $t$ are real.

The Fourier transformed Maxwell equations (2.6) and constitutive relations (2.7) are the most concise expression of the macroscopic theory of classical electrodynamics without sources and with a linear medium response to any applied fields, in that in principle all the fields can be constructed from these equations when suitable boundary conditions and medium properties are used. The medium properties are incorporated by choosing a suitable form for the permittivity function, often (as later in this work) via the Drude-Lorentz model. All the classical foundations have now been laid for the progression to the quantum theory of electrodynamics in the presence of media: Macroscopic QED.

## 2.3 Macroscopic QED - Formulation

The three fundamental requirements placed on Macroscopic QED (MQED) which shall be used to contruct the theory are as follows:

1. The macroscopic Maxwell equations for source-free fields must hold for the quantum operators representing these fields. The interaction of the fields with sources is then described by some Hamiltonian coupling the sources to the field. As the fields are (implicitly) time dependent, the correspondence to the classical theory is easiest to establish in the Heisenberg picture. The transition to the Schrödinger or interaction picture can be made at a later stage.

2. As the fluctuation-dissipation theorem holds equally for quantum and classical systems, the relationship between the noise polarisation and the linear response of the medium polarisation to the electric field is identical to the classical case, except for a correction based on the classical energy scale $k_BT$ being replaced the with quantum energy scale $\hbar\omega$.

3. The constitutive equations (2.7) imply that the electric and magnetic fields can be taken to be the free fields, with the polarisation field reflecting the influence of the media on the displacement field $\vec{D}$. Thus the commutation relations of the electric and magnetic fields must match the free space relations, as they have no dependence on the media.

These conditions can all be satisfied by use of a Fock basis with bosonic annihilation and creation vector operators $\hat{\vec{f}}(\vec{r},\omega)$ corresponding to the electric degrees of freedom of the medium, in accordance with requirement 3 above. These are defined as annihilation and creation operators on a Fock state, and have the bosonic commutator relations (in component form):

$$\left[\hat{f}_i(\vec{r},\omega)\ ,\ \hat{f}_j(\vec{r}\,',\omega')\right] = \left[\hat{f}_i^{\dagger}(\vec{r},\omega)\ ,\ \hat{f}_j^{\dagger}(\vec{r}\,',\omega')\right] = 0 \tag{2.9}$$

$$\left[\hat{f}_i(\vec{r},\omega)\ ,\ \hat{f}_j^{\dagger}(\vec{r}\,',\omega')\right] = \delta_{ij}\delta(\vec{r}-\vec{r}\,')\delta(\omega-\omega')$$

A Hamiltonian for the system which generates the correct time dependence of the operators is sought. The time-dependence of operators in the Heisenberg picture is given by the Heisenberg equation:

$$\frac{d\hat{O}}{dt} = \frac{i}{\hbar}[\hat{H},\hat{O}] \tag{2.10}$$

As the operators are defined in Fourier-space, a Hamiltonian which with the aid of the commutation relation (2.9) and the Heisenberg equation generates the correct time dependence is given by:

$$\hat{H}_F = \int d^3\vec{r}\int_0^{\infty} d\omega\ \hbar\omega\ \hat{\vec{f}}^{\dagger}(\vec{r},\omega)\cdot\hat{\vec{f}}(\vec{r},\omega) \tag{2.11}$$

$$\rightarrow \frac{d}{dt}\hat{f}(\vec{r},\omega) = -i\omega\hat{f}(\vec{r},\omega) \tag{2.12}$$

Time dependence in the above and in the following is not shown for brevity. The task remaining is to use the properties of the field annihilation and creation operators to construct expressions for the noise polarisation and magnetisation operators which satisfy the fluctation dissipation theorem and disappear on the ground state average. Using these the operator form of the Maxwell equations (2.6) can be used to construct all the relevant field operators in terms of the fundamental creation and annihilation operators. It can be shown [18] that the form of the noise operators satisfying the above conditions is:

$$\hat{\vec{P}}_N(\vec{r},\omega) = i\sqrt{\frac{\hbar\epsilon_0}{\pi}\mathrm{Im}[\epsilon(\vec{r},\omega)]}\ \hat{\vec{f}}(\vec{r},\omega) \tag{2.13}$$

With a view to constructing the other fields, the noise current density is defined as:

$$\hat{\vec{J}}_N(\vec{r},\omega) = -i\omega\hat{\vec{P}}_N(\vec{r},\omega) \tag{2.14}$$

Here the divergence of the noise polarisation $\nabla\cdot\vec{P}_N$ was identified as the noise charge density $\rho_N$, and equation (2.14) was then arrived at by inserting this into the charge continuity equation $\dot{\rho}_N + \nabla\cdot\vec{J}_N = 0$. Combining Faraday's law and Ampere's law from the operator form of the Maxwell equations (2.6) with the operator form of the constitutive relations (2.7) leads to the following Helmholtz equation for the electric field operator in terms of the noise current density.

$$\left[-\frac{\omega^2}{c^2}\epsilon(\vec{r},\omega) + \nabla\times\nabla\times\right]\hat{\vec{E}}(\vec{r},\omega) = i\mu_0\omega\hat{\vec{J}}_N(\vec{r},\omega) \tag{2.15}$$

Using the dyadic Green's tensor formalism, the electric and magnetic field operators are given by:

$$\hat{\vec{E}}(\vec{r},\omega) = i\mu_0\omega\int d^3\vec{r}\,'\ \mathbf{G}(\vec{r},\vec{r}\,',\omega)\cdot\hat{\vec{J}}_N(\vec{r}\,',\omega), \tag{2.16}$$

$$\hat{\vec{B}}(\vec{r},\omega) = \mu_0 \int d^3\vec{r}\,' \, \nabla \times \mathbf{G}(\vec{r},\vec{r}\,',\omega) \cdot \hat{\vec{J}}_N(\vec{r}\,',\omega), \tag{2.17}$$

where the Green's tensor $\mathbf{G}(\vec{r},\vec{r}\,',\omega)$ is the solution to the equation:

$$\left[-\frac{\omega^2}{c^2}\epsilon(\vec{r},\omega) + \nabla \times \nabla \times\right] \mathbf{G}(\vec{r},\vec{r}\,',\omega) = \delta(\vec{r}-\vec{r}\,')\mathbf{I}. \tag{2.18}$$

The boundary condition imposed on $\mathbf{G}$ is that in the limit $|\vec{r}-\vec{r}\,'| \to \infty$ the Green's tensor should vanish. As the combination of the Maxwell equations and constitutive relations leading to equations (2.15) and (2.16) can be done equally for the classical fields, the Green's tensor is seen to be equivalent to the classical Green's tensor giving the electric response of a system to the presence of a noise current density. As equation (2.18) is linear in $\mathbf{G}$, a general solution can be constructed as a linear combination of the solution to the inhomogeneous equation $\mathbf{G}^{(0)}$ associated with $\delta(\vec{r}-\vec{r}\,')\mathbf{I}$, and the solution to the homogeneous equation $\mathbf{G}^{(1)}$. For a system with well defined boundaries between $n$ regions of permittivity $\epsilon_n(\omega)$ this allows a removal of position dependence from equation (2.18). The variation in $\epsilon$ for different regions is then accounted for in some region of permittivity $\epsilon_m$ by considering first the bulk effect of a medium of permittivity $\epsilon_m$ and then the effect of transmission/reflection at the boundaries between regions of different $\epsilon$. This is done by identifying $\mathbf{G}^{(0)}$ as the response function of an infinitely extended system of permittivity $\epsilon_m(\omega)$ known as the bulk Green's tensor. Then $\mathbf{G}^{(1)}$ can be identified as the scattering part of the Green's tensor which accounts for reflection and transmission at the boundaries between regions of different permittivities.

In accordance with requirement 3. it is necessary for the electric and magnetic field operators to satisfy the same commutation relations as the free-space operators. The equal-time commutators can indeed be shown [19] to be given by:

$$\left[\hat{\vec{E}}(\vec{r}), \hat{\vec{E}}(\vec{r}\,')\right] = \left[\hat{\vec{B}}(\vec{r}), \hat{\vec{B}}(\vec{r}\,')\right] = 0 \tag{2.19}$$

$$\left[\hat{\vec{E}}(\vec{r}), \hat{\vec{B}}(\vec{r}\,')\right] = \frac{i\hbar}{\epsilon_0}\nabla \times \delta(\vec{r}-\vec{r}\,')\mathbf{I} \tag{2.20}$$

These are in accordance with the free space commutation relations [20].

In principle all the other field operators in the Maxwell equations can now be expressed in terms of the Green's tensor and the noise current density $\hat{\vec{J}}_N$ by use of the Maxwell equations (2.6) and constitutive relations (2.7). However, for the calculations to follow it is convenient to define an auxilary Green's tensor which is directly compatible with the creation and annihilation operators:

$$\hat{\vec{E}}(\vec{r},\omega) = \int d^3\vec{r}\,' \mathbf{G}_e(\vec{r},\vec{r}\,',\omega) \cdot \hat{\vec{f}}(\vec{r}\,',\omega) \tag{2.21}$$

$$\hat{\vec{B}}(\vec{r},\omega) = \frac{1}{i\omega}\int d^3\vec{r}\,' \nabla \times \mathbf{G}_e(\vec{r},\vec{r}\,',\omega) \cdot \hat{\vec{f}}(\vec{r}\,',\omega) \tag{2.22}$$

$$\mathbf{G}_e(\vec{r},\vec{r}\,',\omega) = i\frac{\omega^2}{c^2}\sqrt{\frac{\hbar}{\pi\epsilon_0}\mathrm{Im}[\epsilon(\vec{r}\,',\omega)]}\mathbf{G}(\vec{r},\vec{r}\,',\omega) \tag{2.23}$$

The form of $\mathbf{G}_e$ follows from directly inserting equations (2.13) and (2.14) into equation (2.16). What will be vital for facilitating later calculations are the following properties of the Green's tensor:

$$\mathbf{G}^*(\vec{r},\vec{r}\,',\omega) = \mathbf{G}(\vec{r},\vec{r}\,',-\omega^*) \tag{2.24}$$

$$\int d^3\vec{s}\, \mathbf{G}_e(\vec{r},\vec{s},\omega)\cdot\mathbf{G}_e^{*T}(\vec{r}\,',\vec{s},\omega) = \frac{\hbar\mu_0\omega^2}{\pi}\mathrm{Im}\mathbf{G}(\vec{r},\vec{r}\,',\omega) \tag{2.25}$$

The first of these follows simply from the defining equation (2.16) plus the conjugation property $f^*(\omega) = f(-\omega^*)$ discussed previously, which holds here. The second is more difficult to derive, but follows from multiplying the defining equation (2.18) by $\mathbf{G}$ on the left and right and integrating over a spatial variable to remove the delta function. Using the conjugation property (2.24) leads to the desired result, a full proof is found in [20].

The key points of this section are now restated. A quantum field theory capable of describing the quantised electromagnetic field in the presence of media has been developed in accordance with the three requirements discussed. This theory takes as its input the classical Green's tensor which gives the electromagnetic response of a system, and which depends on both the geometry of the media and the media's relative permittivity functions. The electric field operator was given in terms of the Green's tensor and the bosonic creation and annihilation operators of the field, and through the operator form of the Maxwell equations (2.6), constitutive relations (2.7) and the definition of the noise polarisation operator (2.13), all other operators may be expressed in terms of this quantity. It should be noted that MQED as outlined in this section is derivable from 'free-space' QED by incorporating the effects of the medium as a collection of interacting matter fields [21].

## 2.4 The Atom-Field Interaction

Now that a suitable treatment for the electromagnetic field has been obtained in terms of the classical electromagnetic Green's tensor, the interaction of this field with an atom is considered. In this section for brevity many important results and definitions are stated without proof or detailed explanation, a fuller discussion of these can be found in Ref. [20]. The atom and field are considered as a coupled system, with the interaction between the atom and field governed by an interaction Hamiltonian $\hat{H}_{int}$. Thus, including the internal atomic Hamiltonian $\hat{H}_A$, the total Hamiltonian of the system may be written:

$$\hat{H}_T = \hat{H}_A + \hat{H}_F + \hat{H}_{int} \tag{2.26}$$

The atom-field interaction Hamiltonian most easily derivable from 'free-space' QED [22] is the minimal coupling Hamiltonian. Minimal coupling means the requirement of local-gauge invariance of the quantised electromagnetic field, which can be used to formulate a Lagrangian which leads to the full Hamiltonian of the coupled atom-charge system. However this is seen [15] to simply be equivalent to taking the sum of the individual atom (including Coulomb terms) and field Hamiltonians and then making the replacement:

$$\hat{\vec{p}}_a \rightarrow \hat{\vec{p}}_a - q_a\hat{\vec{A}}(\hat{\vec{r}}_a) \tag{2.27}$$

Here the index $a$ refers to an individual particle, i.e. an individual electron/nucleus rather than the atom as a whole, with $\hat{\vec{p}}_a$ its momentum operator, and $q_a$ is the electric charge of the particle. $\hat{\vec{A}}$ is the vector potential operator of the field, where the electromagnetic field potentials $\hat{\phi}$ and $\hat{\vec{A}}$ are defined by:

$$\hat{\vec{E}} = -\nabla\hat{\phi} - \frac{\partial\hat{\vec{A}}}{\partial t} \tag{2.28}$$

$$\hat{\vec{B}} = \nabla\times\hat{\vec{A}} \tag{2.29}$$

The gauge-fixing condition used here is $\nabla\cdot\hat{\vec{A}} = 0$, i.e. the Coulomb gauge. However, for the present situation an interaction Hamiltonian more amenable to manipulation may be attained

by effecting a transformation $\hat{O} \rightarrow \hat{O}'$ on the operators (and states) describing the system. The transformation is known as a Power-Zienau-Wooley transformation [23], and is given by the following unitary operator:

$$\hat{O}' = \hat{U}\hat{O}\hat{U}^{\dagger} \tag{2.30}$$

$$\hat{U} = \exp\left(\frac{i}{\hbar}\int d^3\vec{r}\,\hat{\vec{P}}_A \cdot \hat{\vec{A}}\right) \tag{2.31}$$

Here $\hat{\vec{P}}_A$ is the atomic polarisation operator, defined as [20]:

$$\hat{\vec{P}}_A(\vec{r}) = \sum_{a \in Atom} q_a \hat{\vec{r}}_a \int_0^1 d\lambda\ \delta(\vec{r} - \hat{\vec{r}}_A - \lambda\hat{\vec{r}}_a) \tag{2.32}$$

Here $q_a$ is the electric charge of the a'th particle of the atom. The index $A$ refers as previously to the atom as a whole, while the index $a$ refers to the constituent particles and their mass, momentum operator etc. Throughout this section all coordinates $\hat{\vec{r}}_a$ and momenta $\hat{\vec{p}}_a$ are given relative to the atomic centre of mass coordinates $\hat{\vec{r}}_A$ and momentum $\hat{\vec{p}}_A$.

Calculating the operators transformed according to (2.30) and (2.31) is a mathematically involved process, consisting of calculating the commutator relations of all atom and field operators with $\hat{\vec{P}}_A$ and $\hat{\vec{A}}$. Rather than present any details the form of the transformed 'multipolar' Hamiltonian is simply stated, and is followed by a discussion of the merits and drawbacks of the transformation.

$$\hat{H}'_A = \frac{1}{2m_A}(\hat{\vec{p}}_A\,')^2 + \sum_n E'_n\,|n'\rangle\,\langle n'| \tag{2.33}$$

$$\hat{H}'_F = \sum_{\lambda=e,m}\int d^3\vec{r}\int_0^{\infty} d\omega\ \hbar\omega\ \hat{\vec{f}}_\lambda\,'(\vec{r},\omega)^{\dagger} \cdot \hat{\vec{f}}_\lambda\,'(\vec{r},\omega) \tag{2.34}$$

$$\begin{aligned}\hat{H}'_{int} = &-\int d^3\vec{r}\,\hat{\vec{P}}'_A \cdot \hat{\vec{E}}' \ - \int d^3\vec{r}\,\hat{\vec{M}}'_A \cdot \hat{\vec{B}}' \\ &+ \sum_{a\in A}\frac{1}{2m_a}\left[\int d^3\vec{r}\,\hat{\vec{\theta}}'_a \times \hat{\vec{B}}'\right]^2 - \frac{1}{m_A}\int d^3\vec{r}\,\hat{\vec{P}}'_A \times \hat{\vec{p}}_A\,' \cdot \hat{\vec{B}}'\end{aligned} \tag{2.35}$$

In the above the atomic operator $\hat{\vec{\theta}}'_a$ is given by:

$$\begin{aligned}\hat{\vec{\theta}}'_a(\vec{r}) = &\frac{m_a}{m_A}\hat{\vec{P}}_A(\vec{r}) + q_a\hat{\vec{r}}_a\,'\int_0^1 d\lambda\ \lambda\,\delta(\vec{r} - \hat{\vec{r}}_A\,' - \lambda\hat{\vec{r}}_a\,') \\ &- \frac{m_a}{m_A}\sum_{b\in Atom} q_b\hat{\vec{r}}_b\,'\int_0^1 d\lambda\ \delta(\vec{r} - \hat{\vec{r}}_A\,' - \lambda\hat{\vec{r}}_b\,')\end{aligned} \tag{2.36}$$

It can be seen that the forms of the atomic and field Hamiltonians remains unchanged from the minimal coupling case. However both the atomic momentum operator and the field creation and annihilation operators are affected by the transformation, as are both the field and atom constituents of the total product state of the system [20]. This can be seen firstly as the transformation contains operators defined over the atom (atomic polarisation operator) and field (vector potential operator) degrees of freedom of the system, and secondly as the internal atomic Hamiltonian term in (2.33) must now be expressed in terms of the transformed eigenstates of the atom. However, as the applied transformation is unitary, the transformed operators and states may be treated as previously as long as the transformation effected is not forgotten when inserting explicit expressions.

Now that the operators have all been transformed, the $'$ denoting the transformed operators is dropped for convenience. The interaction term at first seems no simpler than for the minimal coupling case. However the main benefit of applying this transformation is that (a) in the long-wavelength (dipole) approximation the interaction Hamiltonian takes a particularly simple form (thus the name multipolar Hamiltonian), and (b) in this approximation the momentum operators $\hat{\vec{p}}_a$ coincide with the non-relativistic physical momentum operators $m\hat{\vec{v}}_a$. As a consequence of this the same applies to the total atomic momentum operator according to $\hat{\vec{p}}_A = m\hat{\vec{v}}_A$. The long-wavelength approximation assumes that the atom can be treated as a point, and as the atom has no overall charge the lowest order interaction of such a collection of charges with an electromagnetic field is given by its electric and magnetic dipole terms. Thus this approximation is most valid for 'small' atoms (i.e. non-excited atoms). When only considering the dipole terms the atomic polarisation and magnetisation operators become the electric and magnetic dipole moments operators respectively [23]. This leads to the following form of the interaction Hamiltonian [20]:

$$\hat{H}_{int} = -\hat{\vec{d}} \cdot \hat{\vec{E}}\left(\vec{r}_A\right) - \hat{\vec{\mu}} \cdot \hat{\vec{B}}\left(\vec{r}_A\right) + \vec{v} \cdot \left[\hat{\vec{d}} \times \hat{\vec{B}}\left(\vec{r}_A\right)\right] + \frac{3}{8}\left[\hat{\vec{d}} \times \hat{\vec{B}}(\vec{r}_A)\right]^2 + \sum_{a \in Atom} \frac{q_a^2}{8m_a}\left[\hat{\vec{r}}_a \times \hat{\vec{B}}(\vec{r_A})\right]^2 \quad (2.37)$$

Here $\hat{\vec{d}}$ and $\hat{\vec{\mu}}$ are the canonical electric and magnetic dipole moments respectively. Another benefit of the use of the long-wavelength point-like approximation which is clear in equation (2.37) is that the relevant terms in (2.35) can now be evaluated at the centre of the atom $\vec{r}_A$, removing the need for the spatial integrals. Furthermore as discussed in section 2.1, a key feature of this work is that the atomic motion is treated classically, thus the velocity operator may be replaced by the classical velocity $\vec{v}$. The second term of equation (2.37) is the magnetic dipole interaction, and the last two terms can be shown to correspond to diamagnetic interactions [20]; for a non-magnetic atom both can be discarded. Therefore the interaction Hamiltonian in the long-wavelength approximation for a non-magnetic atom can be written:

$$\hat{H}_{int}(t) = -\hat{\vec{d}} \cdot \hat{\vec{E}}\left(\vec{r}_A(t)\right) + \vec{v} \cdot \left[\hat{\vec{d}} \times \hat{\vec{B}}\left(\vec{r}_A(t)\right)\right] \quad (2.38)$$

Here the time dependence has been shown explicitly to highlight the effect of the atom's motion on the Hamiltonian.

The benefit of applying this transformation is that whereas the full Hamiltonian has many terms, meaning that analytical solutions to problems are not easily identifiable, the multipolar Hamiltonian (2.35) has terms which are easily identifiable with quantities from classical electrodynamics, and can thus be truncated with the physical justification of electric dipole interactions being the dominant interactions. The long-wavelength approximation can then be made, returning the very simple form of (2.38). To summarise, the multipolar Hamiltonian has the benefit of reducing to a very simple form when the electric dipole approximation can be made, thus allowing a large degree of accuracy in calculations without the cumbersomeness of the full Hamiltonian.

The operators used to describe the atom are the atomic flip operators $\hat{A}_{mn}$. When expressed in the orthonormalised eigenbasis of the internal atomic Hamiltonian $\hat{H}_A$, the definition and some basic properties of these operators are as follows:

$$\hat{A}_{mn} = |m\rangle \langle n| \quad (2.39)$$

$$\hat{A}_{ij}\hat{A}_{mn} = |i\rangle \langle j|m\rangle \langle n| = \hat{A}_{in}\delta_{jm} \quad (2.40)$$

$$[\hat{A}_{ij}(t), \hat{A}_{mn}(t)] = \hat{A}_{in}(t)\delta_{jm} - \hat{A}_{mj}(t)\delta_{in} \tag{2.41}$$

The product and commutation relations of the flip operators are derivable from the orthonormality of this basis. The commutation relation (2.41) only applies for equal times. Furthermore:

$$\left\langle \hat{A}_{nn}(t) \right\rangle = \langle \psi(t)|\hat{A}_{nn}|\psi(t)\rangle = \sum_{i,j} c_i^*(t)c_j(t)\,\langle i|n\rangle\,\langle n|j\rangle = |c_n(t)|^2 = P_n(t) \tag{2.42}$$

$$|\psi(t)\rangle = \sum_n c_n(t)\,|n\rangle \tag{2.43}$$

Here $P_n$ is the probability of the atom being in the internal energy eigenstate $|n\rangle$, and the change was made to the Schrödinger picture for simplicity in evaluating the expectation value. Henceforth all work shall be done in the Heisenberg picture, and for brevity the time dependence of all operators is implied if not shown. With the aid of the atomic flip operators the interaction Hamiltonian may be written in a more amenable form. Utilising the orthonormality and completeness of the basis, the dipole moment and Hamiltonian operators of the atom may be re-expressed as follows:

$$\hat{\vec{d}} = \sum_{m,n} |m\rangle\,\vec{d}_{mn}\,\langle n| = \sum_{m,n} \vec{d}_{mn}\hat{A}_{mn} \tag{2.44}$$

$$\hat{H}_A = \sum_n E_n \hat{A}_{nn} \tag{2.45}$$

By inserting this expression into the multipolar interaction Hamiltonian obtained in the previous section, and retaining only terms corresponding to the dipole moment $\vec{d}_{mn}$ in first order, the interaction Hamiltonian takes the form:

$$\hat{H}_{int} = -\sum_{m,n} \hat{A}_{mn}\vec{d}_{mn} \cdot \hat{\vec{E}}(\hat{\vec{r}}_A) + \sum_{m,n} \hat{A}_{mn}\vec{v} \cdot \left[\vec{d}_{mn} \times \hat{\vec{B}}(\vec{r}_A)\right] \tag{2.46}$$

By splitting the time evolution of the relevant operators into the 'free' and 'interaction' terms, whereby the 'free' term corresponds to the time development of an atomic(field) operator when the field(atom) is not present, the Heisenberg equation allows all time developments of operators to be be calculated:

$$\frac{d\hat{O}_{A/F}}{dt} = \frac{i}{\hbar}[\hat{H}, \hat{O}_{A/F}] = \frac{i}{\hbar}[\hat{H}_{A/F}, \hat{O}_{A/F}] + \frac{i}{\hbar}[\hat{H}_{int}, \hat{O}_{A/F}] \tag{2.47}$$

The above can be written because the atom (field) operators commute with the field (atom) Hamiltonian at equal times, as they represent different degrees of freedom. Now it is possible to calculate the time development of the atomic flip operators and the field creation and annihilation operators with recourse to the commutation relations (2.41) for the atomic flip operators, and (2.9) for the field operators [1]:

$$\frac{d\hat{A}_{mn}}{dt} = i\omega_{mn}\hat{A}_{mn} + \frac{i}{\hbar}\sum_k (\hat{A}_{mk}\vec{d}_{nk} - \hat{A}_{kn}\vec{d}_{km}) \cdot [\hat{\vec{E}}(\vec{r}_A) + \vec{v} \times \hat{\vec{B}}(\vec{r}_A)] \tag{2.48}$$

$$\begin{aligned}\frac{d\hat{\vec{f}}(\vec{r},\omega)}{dt} &= -i\omega\hat{\vec{f}}(\vec{r},\omega) + \frac{i}{\hbar}\sum_{m,n} \mathbf{G}_e^{*T}(\vec{r}_A,\vec{r},\omega) \cdot \vec{d}_{mn}\hat{A}_{mn} \\ &\quad + \frac{1}{\hbar\omega}\sum_{m,n} \left\{ \left[\mathbf{G}_e^{*T}(\vec{r}_A,\vec{r},\omega) \times \overleftarrow{\nabla}_A\right] \times \vec{d}_{mn} \right\} \cdot \vec{v}\hat{A}_{mn}\end{aligned} \tag{2.49}$$

Eqn.(2.49) is solved by:

$$\hat{\vec{f}}(\vec{r},\omega,t) = e^{-i\omega(t-t_0)}\hat{\vec{f}}(\vec{r},\omega) + \frac{i}{\hbar}\sum_{m,n}\int_{t_0}^{t} dt' e^{-i\omega(t-t')}\mathbf{G}_e^{*T}(\vec{r}_A(t'),\vec{r},\omega)\cdot\vec{d}_{mn}\hat{A}_{mn}(t')$$
$$+ \frac{1}{\hbar\omega}\sum_{mn}\int_{t_0}^{t} dt' e^{-i\omega(t-t')}\left\{\left[\mathbf{G}_e^{*T}(\vec{r}_A(t'),\vec{r},\omega)\times\overleftarrow{\nabla}_A\right]\times\vec{d}_{mn}\right\}\cdot\vec{v}\hat{A}_{mn}(t') \qquad (2.50)$$

This is easily verified by use of the relation:

$$\frac{d}{dt}\int_{t_0}^{t} dt'\; e^{-i\omega(t-t')}f(t') = f(t) - i\omega\int_{t_0}^{t} dt'\; e^{-i\omega(t-t')}f(t') \qquad (2.51)$$

The theory presented so far in this section provides the basis for all the work presented in chapter 3, and section 3.1 follows directly from here with the particular solution method chosen for this work.

# Chapter 3

# Results

The work to be presented here is an investigation of a single moving atom's internal dynamics in the presence of dispersive media. Three separate approaches are to be carried out, the first a Taylor series expansion in the atomic velocity, then a full treatment of the 2-plate system, and finally a naive Doppler shift applied to the reflection coefficients in the static case result. The Taylor series expansion calculated to second order in the velocity in section 3.1 is applicable to an atom in the presence of any media, and a specific application of the series result is presented here in section 3.2 for the 2-plate set-up. This is a good example of the usefulness of the results of section 3.1 compared to the previous results of Ref. [1] when applied to specific scenarios involving moving atoms, and it also leads naturally on to section 3.3 where the 2-plate situation is treated exactly, i.e. to all orders in the velocity. Finally in section 3.4 the results of 3.3 for a moving atom are shown to be equivalent to the stationary case with all reflections at the plates being evaluated at a Doppler shifted frequency.

## 3.1 Series Approach to Studying the Internal Dynamics of an Atom near General Absorbing Media

Following on directly from the end of section 2.4, the chosen way to proceed is via the Born-Oppenheimer approximation. In the Born-Oppenheimer approximation it is assumed that the dynamics of the atom can be separated into 2 parts describing the electronic dynamics and the centre of mass motion. For describing the electronic dynamics it is assumed that the atom is moving with constant centre of mass motion, with any deviations from this calculated later (i.e. the friction force on the atom). The assumption of centre of mass motion for solving the electronic dynamics of the atom is equivalent to the statement that any forces on the atom are sufficiently weak that its velocity is not substantially changed over the time scale of any internal electronic transitions. With respect to the phenomena investigated this is a reasonable assumption, as the numerical results obtained show that the transition rates are often around $10^{10}\mathrm{s}^{-1}$, over which time scale no reasonable force will produce a noticeable change in the atomic velocity. The second step of the Born-Oppenheimer approximation is to solve exactly the centre of mass motion including any effects ddue to dispersion forces, not carried out in this work but a natural extension of the work presented. Thus implementing the constant velocity Born-Oppenheimer approximation as $\vec{r}_A(t') = \vec{r}_A(t) + (t'-t)\vec{v}$ , a Taylor expansion of the Green's tensor in its first argument around $\vec{r}_A(t)$ can be formulated:

$$\begin{aligned}\mathbf{G}_e^{*T}\left(\vec{r}_A(t'),\vec{r},\omega\right) = \mathbf{G}_e^{*T}\left(\vec{r}_A(t),\vec{r},\omega\right) - (t-t')(\vec{v}\cdot\nabla_A)\mathbf{G}_e^{*T}(\vec{r}_A(t),\vec{r},\omega) \\ + \frac{1}{2}(t-t')^2(\vec{v}\cdot\nabla_A)^2\mathbf{G}_e^{*T}\left(\vec{r}_A(t),\vec{r},\omega\right) + O(v^3) \qquad (3.1)\end{aligned}$$

It should be noted that from this point onwards all factors containing powers of $v^2$ (or $v$ when pertaining to the magnetic field) are original work not contained in the work of Buhmann et al

[1]. From the form of $H_{int}$ given in equation (2.46) it is clear that to complete the calculation to second order in $v$, $\hat{\vec{f}}_\lambda(\vec{r},\omega,t)$ will need to be evaluated to first ($\hat{\vec{f}}^{(1)}_\lambda(\vec{r},\omega,t)$) and second ($\hat{\vec{f}}^{(2)}_\lambda(\vec{r},\omega,t)$) order in $v$:

$$\hat{\vec{f}}^{(1)}(\vec{r},\omega,t) = -\frac{i}{\hbar}\sum_{m,n}\int_{t_0}^{t} dt'(t-t')e^{-i\omega(t-t')}(\vec{v}\cdot\nabla_A)\mathbf{G}_e^{*T}(\vec{r}_A(t),\vec{r},\omega)\cdot\vec{d}_{mn}\hat{A}_{mn}(t') + \frac{1}{\hbar\omega}\sum_{m,n}\int_{t_0}^{t} dt' e^{-i\omega(t-t')}\left\{\left[\mathbf{G}_e^{*T}(\vec{r}_A(t),\vec{r},\omega)\times\overleftarrow{\nabla}_A\right]\times\vec{d}_{mn}\right\}\cdot\vec{v}\hat{A}_{mn}(t') \tag{3.2}$$

$$\hat{\vec{f}}^{(2)}(\vec{r},\omega,t) = \frac{i}{2\hbar}\sum_{m,n}\int_{t_0}^{t} dt'(t-t')^2 e^{-i\omega(t-t')}(\vec{v}\cdot\nabla_A)^2\mathbf{G}_e^{*T}(\vec{r}_A(t),\vec{r},\omega)\cdot\vec{d}_{mn}\hat{A}_{mn}(t') - \frac{1}{\hbar\omega}\sum_{m,n}\int_{t_0}^{t} dt'(t-t')e^{-i\omega(t-t')}(\vec{v}\cdot\nabla_A)\left\{\left[\mathbf{G}_e^{*T}(\vec{r}_A(t),\vec{r},\omega)\times\overleftarrow{\nabla}_A\right]\times\vec{d}_{mn}\right\}\cdot\vec{v}\hat{A}_{mn}(t') \tag{3.3}$$

Using the relations for the electric and magnetic fields obtained in the previous section (2.21) and (2.22), and making use of the property of the Green's tensor (2.25), the electric and magnetic fields can be written in the following form:

$$\hat{\vec{B}}^{(1)}(\vec{r},\omega,t) = -\frac{\mu_0}{\pi}\sum_{m,n}\omega\int_{t_0}^{t} dt'(t-t')e^{-i\omega(t-t')}(\vec{v}\cdot\nabla_A)\nabla\times\mathrm{Im}[\mathbf{G}(\vec{r},\vec{r}_A(t),\omega)]\cdot\vec{d}_{mn}\hat{A}_{mn}(t') - \frac{i\mu_0}{\pi}\sum_{m,n}\int_{t_0}^{t} dt' e^{-i\omega(t-t')}\nabla\times\left\{\left[\mathrm{Im}[\mathbf{G}(\vec{r},\vec{r}_A(t),\omega)]\times\overleftarrow{\nabla}_A\right]\times\vec{d}_{mn}\right\}\cdot\vec{v}\hat{A}_{mn}(t') \tag{3.4}$$

$$\hat{\vec{E}}^{(2)}(\vec{r},\omega,t) = \frac{i\mu_0}{2\pi}\sum_{m,n}\omega^2\int_{t_0}^{t} dt'(t-t')^2 e^{-i\omega(t-t')}(\vec{v}\cdot\nabla_A)^2\mathrm{Im}[\mathbf{G}(\vec{r},\vec{r}_A(t),\omega)]\cdot\vec{d}_{mn}\hat{A}_{mn}(t') - \frac{\mu_0}{\pi}\sum_{mn}\omega\int_{t_0}^{t} dt'(t-t')e^{-i\omega(t-t')}(\vec{v}\cdot\nabla_A)\left\{\left[\mathrm{Im}[\mathbf{G}(\vec{r},\vec{r}_A(t),\omega)]\times\overleftarrow{\nabla}_A\right]\times\vec{d}_{mn}\right\}\cdot\vec{v}\hat{A}_{mn}(t') \tag{3.5}$$

Firstly it is assumed that the atomic dynamics are dominated by the free oscillations of the flip operators at some frequency $\tilde{\omega}_{ab}$, i.e. :

$$\hat{A}_{ab}(t') = e^{i\tilde{\omega}_{ab}(t'-t)}\hat{A}_{ab}(t) \tag{3.6}$$

The exact form of $\tilde{\omega}_{ab}$ can be deduced at a later stage in the calculation, and is given by equation (3.17). Furthermore, from the forms of equations (3.4) and (3.5), it is clear that the fields at a certain time $t$ have a dependence on all times previous to $t$ after the initial time $t_0$. The physical meaning of this is more explicitly shown in (2.50), where the first argument of the Green's tensor is a function of the time integral parameter $t'$. As this argument of the Green's tensor corresponds here to the source of the electromagnetic field, and $r_A(t')$ is the location of the atom at time $t'$, clearly this shows that the fields are dependent on the location of the atom at all previous times. However in general it can be assumed that the atom-field system has no memory of the state of the system at previous times, known as the Markov approximation. A detailed discussion of this assumption and its validity will follow in section 4.1.3, for now it shall

just be assumed. The Markov approximation can be expressed as follows, with the necessary terms including factors of $(t-t^{'})$ obtainable by differentiating both sides with respect to $\omega$:

$$\int_{t_0}^{t} dt' e^{-i\omega(t-t')} \hat{A}_{mn}(t') = \left( \pi\delta(\omega - \tilde{\omega}_{nm}) - i\frac{P}{\omega - \tilde{\omega}_{nm}} \right) \hat{A}_{nm}(t) \tag{3.7}$$

This expression is achieved by taking the lower limit of the integral to minus infinity (the actual implementation of the Markov approximation) and then using the Sokhotski–Plemelj theorem to write this integral as the delta function and principal value integral. These terms must both be considered in a distributional sense. This leads to the final forms of the fields:

$$\begin{aligned}
\hat{\vec{E}}^{\,(2)}(\vec{r},\omega,t) = &-\frac{i\mu_0}{2\pi}\sum_{m,n}\omega^2\frac{d^2}{d\omega^2}\Big(\pi\delta(\omega-\tilde{\omega}_{nm}) - i\frac{P}{\omega-\tilde{\omega}_{nm}}\Big) \\
&\qquad (\vec{v}\cdot\nabla_A)^2 \mathrm{Im}[\mathbf{G}(\vec{r},\vec{r}_A(t),\omega)]\cdot\vec{d}_{mn}\hat{A}_{mn}(t) \\
&-\frac{i\mu_0}{\pi}\sum_{m,n}\omega\frac{d}{d\omega}\Big(\pi\delta(\omega-\tilde{\omega}_{nm}) - i\frac{P}{\omega-\tilde{\omega}_{nm}}\Big)(\vec{v}\cdot\nabla_A) \\
&\qquad \Big\{\Big[\mathrm{Im}[\mathbf{G}(\vec{r},\vec{r}_A(t),\omega)]\times\overleftarrow{\nabla}_A\Big]\times\vec{d}_{mn}\Big\}\cdot\vec{v}\hat{A}_{mn}(t)
\end{aligned} \tag{3.8}$$

$$\begin{aligned}
\hat{\vec{B}}^{\,(1)}(\vec{r},\omega,t) = &-\frac{i\mu_0}{\pi}\sum_{m,n}\omega\frac{d}{d\omega}\Big(\pi\delta(\omega-\tilde{\omega}_{nm}) - i\frac{P}{\omega-\tilde{\omega}_{nm}}\Big) \\
&\qquad (\vec{v}\cdot\nabla_A)\nabla\times\mathrm{Im}[\mathbf{G}(\vec{r},\vec{r}_A(t),\omega)]\cdot\vec{d}_{mn}\hat{A}_{mn}(t) \\
&-\frac{i\mu_0}{\pi}\sum_{m,n}\Big(\pi\delta(\omega-\tilde{\omega}_{nm}) - i\frac{P}{\omega-\tilde{\omega}_{nm}}\Big) \\
&\qquad \nabla\times\Big\{\Big[\mathrm{Im}[\mathbf{G}(\vec{r},\vec{r}_A(t),\omega)]\times\overleftarrow{\nabla}_A\Big]\times\vec{d}_{mn}\Big\}\cdot\vec{v}\hat{A}_{mn}(t)
\end{aligned} \tag{3.9}$$

Returning to eqn. (2.48) it is clear that the time dependence of the atomic flip operators can now be calculated. First however, it is helpful to re-express (2.48) in terms of the Fourier representation of the electric field operators:

$$\begin{aligned}
\frac{d\hat{A}^{(2)}_{mn}}{dt} = &\frac{i}{\hbar}\sum_k\int_0^\infty d\omega\Big\{[\hat{A}_{mk}\vec{d}_{nk} - \hat{A}_{kn}\vec{d}_{km}]\cdot[\hat{\vec{E}}^{(2)}(\vec{r}_A,\omega) + \vec{v}\times\hat{\vec{B}}^{(1)}(\vec{r}_A,\omega)] \\
&+[\hat{\vec{E}}^{(2)\dagger}(\vec{r}_A,\omega) + \vec{v}\times\hat{\vec{B}}^{(1)\dagger}(\vec{r}_A,\omega)]\cdot[\hat{A}_{mk}\vec{d}_{nk} - \hat{A}_{kn}\vec{d}_{km}]\Big\}
\end{aligned} \tag{3.10}$$

From the above forms of (3.8) and (3.9), it is clear that they do not have any dependence on the field creation or annihilation operators. Thus the expectation value of the electromagnetic field in its ground state may be taken trivially in equation (3.10). Inserting (3.8) and (3.9) into (3.10), whilst taking the expectation value of the field in its ground state, yields the following equation of motion for the atomic flip operators:

$$\begin{aligned}
\frac{d\hat{A}^{(2)}_{mn}}{dt} = &-\sum_{k,l}\left[\vec{d}_{nk}\cdot\vec{C}^{(2)}_{kl}\hat{A}_{ml}(t) - \vec{d}_{km}\cdot\vec{C}^{(2)}_{nl}\hat{A}_{kl}(t)\right] \\
&+\sum_{k,l}\left[\vec{d}_{nk}\cdot\vec{C}^{(2)*}_{ml}\hat{A}_{lk}(t) - \vec{d}_{km}\cdot\vec{C}^{(2)*}_{kl}\hat{A}_{ln}(t)\right]
\end{aligned} \tag{3.11}$$

The vector coefficients $\vec{C}^{(2)}_{kl}$ are given by:

$$\begin{aligned}\vec{C}^{(2)}_{kl} = &-\frac{\mu_0}{\pi\hbar}\int_0^\infty d\omega\Big\{\frac{\omega^2}{2}\frac{d^2}{d\omega^2}\Big(\pi\delta(\omega-\tilde{\omega}_{lk})-i\frac{P}{\omega-\tilde{\omega}_{lk}}\Big)(\vec{v}\cdot\nabla')^2\mathrm{Im}\mathbf{G}(\vec{r}_A,\vec{r}_A,\omega)\cdot\vec{d}_{kl}\\
&+\omega\frac{d}{d\omega}\Big(\pi\delta(\omega-\tilde{\omega}_{lk})-i\frac{P}{\omega-\tilde{\omega}_{lk}}\Big)(\vec{v}\cdot\nabla')\Big(\mathrm{Im}\mathbf{G}(\vec{r}_A,\vec{r}_A,\omega)\times\overleftarrow{\nabla}'\Big)\times\vec{d}_{kl}\cdot\vec{v}\\
&+\omega\frac{d}{d\omega}\Big(\pi\delta(\omega-\tilde{\omega}_{lk})-i\frac{P}{\omega-\tilde{\omega}_{lk}}\Big)\vec{v}\times\Big(\nabla\times(\vec{v}\cdot\nabla')\mathrm{Im}\mathbf{G}(\vec{r}_A,\vec{r}_A,\omega)\cdot\vec{d}_{kl}\Big)\\
&+\Big(\pi\delta(\omega-\tilde{\omega}_{lk})-i\frac{P}{\omega-\tilde{\omega}_{lk}}\Big)\vec{v}\times\Big[\Big(\nabla\times\mathrm{Im}\mathbf{G}(\vec{r}_A,\vec{r}_A,\omega)\times\overleftarrow{\nabla}'\Big)\times\vec{d}_{kl}\cdot\vec{v}\Big]\Big\}\end{aligned}\tag{3.12}$$

From the form of equation (3.11) it is clear that the vector coefficients $\vec{C}^{(i)}_{kl}$ combined with the dipole matrix elements $\vec{d}_{kl}$ completely describe the internal dynamics of the atom, with the index $i$ corresponding to the $i$th order velocity correction to the static values. Thus the aim of the work detailed in this chapter is always to find an expression for these coefficients, which can then be used to calculate all the required properties of electronic transitions within the atom.

For a clearer insight into the physical meaning of the coefficients $\vec{C}^{(2)}_{kl}$ it is instructive to consider the dynamics of the electronic transitions to (formally) all orders in $v$ according to [4]. Assuming that the atom has no quasi-degenerate transitions and has a vanishing dipole expectation value in its energy eigenstates (i.e. it is unpolarised), and generalising formally the result of Ref. [4] to all orders of $v$ leads to:

$$\Big\langle\frac{d\hat{A}_{mn}}{dt}\Big\rangle=\Bigg[i\omega_{mn}-\sum_{i=0}^{\infty}\sum_k\Big(\vec{d}_{nk}\cdot\vec{C}^{(i)}_{kn}+\vec{d}_{km}\cdot\vec{C}^{(i)*}_{km}\Big)\Bigg]\Big\langle\hat{A}_{mn}(t)\Big\rangle\tag{3.13}$$

$$\begin{aligned}\Big\langle\frac{d\hat{A}_{nn}}{dt}\Big\rangle=-\sum_{i=0}^{\infty}\sum_k\Big\{&\big[\vec{d}_{nk}\cdot\vec{C}^{(i)}_{kn}+\vec{d}_{kn}\cdot\vec{C}^{(i)*}_{kn}\big]\Big\langle\hat{A}_{nn}(t)\Big\rangle\\
&-\big[\vec{d}_{kn}\cdot\vec{C}^{(i)}_{nk}+\vec{d}_{nk}\cdot\vec{C}^{(i)*}_{nk}\big]\Big\langle\hat{A}_{kk}(t)\Big\rangle\Big\}\end{aligned}\tag{3.14}$$

Here $\omega_{mn}$ is the 'bare' transition frequency between states in free space. From the definition (2.44) of $\vec{d}_{nk}$ it follows that $(\vec{d}_{kn})^*=\vec{d}_{nk}$, thus by assuming the dipole moments to be real (corresponding to a time reversal invariant atomic Hamiltonian) implies $\vec{d}_{kn}=\vec{d}_{nk}$. The form of (3.14) then strongly suggests the identification:

$$\mathrm{Re}\Big(\sum_k\vec{d}_{nk}\cdot\vec{C}^{(i)}_{kn}\Big)=\frac{1}{2}\Gamma^{(i)}_n=\frac{1}{2}\sum_{k<n}\Gamma^{(i)}_{nk}\tag{3.15}$$

Here $\Gamma^{(i)}_n$ is the ith order correction to the static case in a velocity series expansion of the electronic transition rates in the atom. Inserting $i=2$ returns the required interpretation of the result (3.12) above. by identifying that the real part of $\vec{d}_{nk}\cdot\vec{C}_{kn}$ corresponds to the transition rates, from equation (3.13) the imaginary parts of $\vec{d}_{nk}\cdot\vec{C}_{kn}$ can be seen to correspond to a frequency shift in the coherences of the atom. However the total frequency of these coherences is nothing but the atomic frequency $\tilde{\omega}_{ab}$ defined earlier, which can now be expressed in terms of the bare transition frequencies $\omega_{ab}$ as:

$$\tilde{\omega}_{ab}=\omega_{ab}+\delta\omega_a-\delta\omega_b\tag{3.16}$$

Here the $i$th order frequency shifts $\delta\omega^{(i)}_a$ have been defined as:

$$\mathrm{Im}\Big(\sum_k\vec{d}_{nk}\cdot\vec{C}^{(i)}_{kn}\Big)=\delta\omega^{(i)}_n=\sum_k\delta\omega^{(i)}_{nk}\tag{3.17}$$

Here once again the $i = 2$ result corresponds to the result achieved here in equation (3.12).

As an aside, it can be shown [20] by considering only the Green's tensor and the left and right curls acting on it in each respective term of equation (3.12), that each of these terms has a clear physical meaning. Reading from top to bottom these terms describe the electric field response to polarisation, electric field response to magnetisation, magnetic field response to polarisation, and the magnetic field response to magnetisation sources. This interpretation of the different curls of the Green's tensor follows from the duality of the electric and magnetic fields. Furthermore it has been shown for the analogous case in Ref. [4], and can also be shown by direct calculation here, that the middle two terms make no contribution to the atomic dynamics when the dipole moments are real $\vec{d}^*_{mn} = \vec{d}_{nm} = \vec{d}_{mn}$, corresponding to an atomic Hamiltonian which has even parity under time reversal.

## 3.2 Series Approach to the Two-Plate System

In line with the overall aim of the work, here the 2-plate system with an atom in the space between the plates is treated with the results of the previous section. This presents an example of the usefulness of the 2nd order term in shedding light on the velocity dependence of the atomic dynamics for specific geometries, as it shall be seen that the 1st order term vanishes for geometries which are translationally invariant along the atom's direction of motion. First the form of the Green's tensor in the non-retarded limit will be discussed along with a justification for taking this limit, as it forms the basis of the calculations to be carried out throughout the section. Then the series expansion in the atomic velocity up to second order shall be evaluated using this form of the 2-plate Green's tensor.

### 3.2.1 The Two-Plate Green's Tensor

The incorporation of a specific geometry into the theory described thus far is done via the use of the Green's tensor, which is the electromagnetic response function of a system. To insert the Green's tensor into the results obtained in section 3.1, the imaginary part of the scattering Green's tensor is required. The bulk Green's tensor $\mathbf{G}^{(0)}$ for this geometry is the free space tensor, which of course must return the free space transmission rates given by Einstein's well-known formula, with the bare electronic transition frequencies defined as follows:

$$\Gamma^{(0)}_n = \frac{1}{3\pi\epsilon_0\hbar c^3}\sum_{k<n}\omega^3_{nk}|\vec{d}_{nk}|^2 \tag{3.18}$$

$$\hbar\omega_{nk} = E_n - E_k \tag{3.19}$$

Here $E_i$ is the energy of the $i$th electronic state. In principle when media are present the shifted frequencies $\tilde{\omega}_{ab}$ should be used, although in section 4.3 it shall be seen that these are almost always roughly equal to the free space frequencies. Thus the effects of the presence of media are contained within the scattering Green's tensor, which will be used henceforth. Using the conjugation property $\mathbf{G}^{(1)*}(\vec{r},\vec{r}\,',\omega) = \mathbf{G}^{(1)}(\vec{r},\vec{r}\,',-\omega^*)$, for 2 plates of separation $L$ this is given by:

$$\begin{aligned}\mathrm{Im}\mathbf{G}^{(1)}(\vec{r},\vec{r}\,',\omega) = \\ \frac{1}{16\pi^2}\Bigg\{\int\frac{d^2\vec{k}^{\parallel}}{k^{\perp}}e^{i\vec{k}^{\parallel}\cdot(\vec{r}-\vec{r}\,')}\sum_{\sigma=s,p}\Bigg[\frac{r^+_\sigma r^-_\sigma}{D_\sigma}e^{2ik^{\perp}L}(\vec{e}_{\sigma+}\vec{e}_{\sigma+}e^{ik^{\perp}_1(z-z')}+\vec{e}_{\sigma-}\vec{e}_{\sigma-}e^{-ik^{\perp}_1(z-z')}) \\ +\frac{1}{D_\sigma}(r^-_\sigma e^{ik^{\perp}(z+z')}\,\vec{e}_{\sigma+}\vec{e}_{\sigma-}+r^+_\sigma e^{ik^{\perp}(2L-z-z')}\,\vec{e}_{\sigma-}\vec{e}_{\sigma+})\Bigg]-[\omega\to-\omega^*]\Bigg\}\end{aligned} \tag{3.20}$$

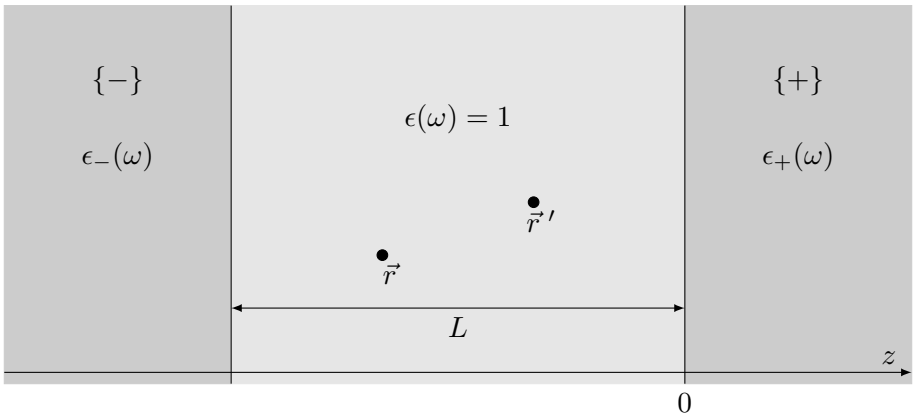


Figure 3.1: The two-plate set-up.

As shown in figure 3.1, the boundary between region $\{+\}$ and the vacuum cavity is $z = 0$, and region $\{-\}$ is a distance $L$ from $\{+\}$. The atomic $z$-coordinate $z_A$ is the closest distance of the atom from $\{+\}$. The label $\sigma$ is used to denote the polarisation state of a wave, where $\vec{e}_{\sigma+}$ and $\vec{e}_{\sigma-}$ are the unit polarisation vectors defined for waves incident on medium $\{+\}$ or $\{-\}$. $r_\sigma^{+/-}(k^\parallel, \omega)$ are the reflection coefficients for the respective polarisation incident on the respective interface. The wavevector $\vec{k}$ has been split into parallel and perpendicular parts with respect to the plane surface as follows:

$$k^\perp(\vec{k}^\parallel, \omega) = \sqrt{(\vec{k})^2 - (\vec{k}^\parallel)^2} = \sqrt{\frac{\epsilon(\omega)\omega^2}{c^2} - (k^\parallel)^2} \tag{3.21}$$

$\mathrm{Im}[k^\perp]$ must always be positive, corresponding to an absorbing medium. This can be deduced from the form of the imaginary part of the Green's tensor (3.20) a negative imaginary part would lead to exponentially increasing terms in the $\vec{k}^\parallel$ integral, leading to an infinite response, which for an absorbing medium cannot be the case. Finally the denominator $D_\sigma$ is given by:

$$D_\sigma = 1 - r_\sigma^+ r_\sigma^- e^{2ik^\perp L} \tag{3.22}$$

Velocity-dependent effects are only expected to be substantial at very small atom-plate separations, i.e. in the non-retarded regime. The requirement for non-retarded, i.e. quasi-instantaneous interactions to dominate is that $z_A \ll c/\omega$, where $z_A$ in this context only means the separation of the atom from either plate, and $\omega$ is the frequency of the wave which here will be close to the atomic transition frequency $\tilde{\omega}_{ab}$. As the interactions are quasi-instantaneous this is equivalent to the speed of light being infinite, which from (3.21) leads to $k^\perp \approx ik^\parallel$. Here the positive root in equation (3.21) was chosen for the reasons given above. By inserting this into the above form of the Green's tensor the non-retarded form is achieved. A further consequence of this assumption is that the magnetic properties of the medium are negligible in comparison to the electric properties, because of the interactions being analogous to electrostatics where no magnetic effects are present. The general formulae for the reflection coefficients between the vaccuum and a non-magnetisable medium ($\mu = 1$) are:

$$r_s^{+-}(k^\parallel, \omega) = \frac{k_{+-}^\perp - k^\perp}{k_{+-}^\perp + k^\perp} \tag{3.23}$$

$$r_p^{+-}(k^\parallel, \omega) = \frac{\epsilon_{+-}(\omega)k_{+-}^\perp - k^\perp}{\epsilon_{+-}(\omega)k_{+-}^\perp + k^\perp} \tag{3.24}$$

However in the non-retarded limit as defined above, it can be seen that $r_s$ becomes 0, and $r_p$ takes the simple form:

$$r_p^{+-}(k^{\parallel},\omega) = r_p^{+/-}(\omega) = \frac{\epsilon_{+/-}(\omega)-1}{\epsilon_{+/-}(\omega)+1} \tag{3.25}$$

The non-retarded limit thus has the further benefits for simplicity of calculation of the $k^{\parallel}$ dependence in the reflection coefficients being removed, and all s-polarised light being transmitted rather than reflected at the plates. Equation (3.20) now takes the following, more manageable form in the non-retarded limit:

$$\begin{aligned}\mathrm{Im}\mathbf{G}^{(1)}(\vec{r},\vec{r}\,',\omega) =& \frac{-i}{16\pi^2}\Bigg\{\int \frac{d^2\vec{k}^{\parallel}}{k^{\parallel}} e^{i\vec{k}^{\parallel}\cdot(\vec{r}-\vec{r}\,')}\Bigg[\frac{r_p^+ r_p^-}{1-r_p^+ r_p^- e^{-2k^{\parallel}L}} e^{-2k^{\parallel}L}(\vec{e}_{p+}\vec{e}_{p+}e^{-k^{\parallel}(z-z')} \\ &+ \vec{e}_{p-}\vec{e}_{p-}e^{k^{\parallel}(z-z')}) + \frac{1}{1-r_p^+ r_p^- e^{-2k^{\parallel}L}}(r_p^- e^{-k^{\parallel}(z+z')}\ \vec{e}_{p+}\vec{e}_{p-} \\ &+ r_p^+ e^{-k^{\parallel}(2L-z-z')}\ \vec{e}_{p-}\vec{e}_{p+})\Bigg] - [\omega \to -\omega^*]\Bigg\}\end{aligned} \tag{3.26}$$

Expressing the $\vec{k}^{\parallel}$ vector in plane polar coordinates $\{k^{\parallel},\phi\}$, the polarisation vectors are:

$$\vec{e}_p^{\,+}\vec{e}_p^{\,+} = \Big(\frac{k^{\parallel}}{k(\omega)}\Big)^2\mathbf{A}(\phi),\ \ \vec{e}_p^{\,-}\vec{e}_p^{\,-} = \Big(\frac{k^{\parallel}}{k(\omega)}\Big)^2\mathbf{A}^*(\phi) \tag{3.27}$$

$$\vec{e}_p^{\,+}\vec{e}_p^{\,-} = \Big[\vec{e}_p^{\,-}\vec{e}_p^{\,+}\Big]^T = \Big(\frac{k^{\parallel}}{k(\omega)}\Big)^2\mathbf{B}(\phi) \tag{3.28}$$

$$\mathbf{A}(\phi) = \begin{bmatrix} -\cos^2(\phi) & -\cos(\phi)\sin(\phi) & -i\ \cos(\phi) \\ -\cos(\phi)\sin(\phi) & -\sin^2(\phi) & -i\ \sin(\phi) \\ -i\ \cos(\phi) & -i\ \sin(\phi) & 1 \end{bmatrix} \tag{3.29}$$

$$\mathbf{B}(\phi) = \begin{bmatrix} \cos^2(\phi) & \cos(\phi)\sin(\phi) & -i\ \cos(\phi) \\ \cos(\phi)\sin(\phi) & \sin^2(\phi) & -i\ \sin(\phi) \\ i\ \cos(\phi) & i\ \sin(\phi) & 1 \end{bmatrix} \tag{3.30}$$

When inserted into equation (3.26) this leads to the form of the Green's tensor used henceforth in this chapter:

$$\begin{aligned}\mathrm{Im}\mathbf{G}^{(1)}(\vec{r},\vec{r}\,',\omega) =& \frac{-i}{16\pi^2}\Bigg\{\int_0^{\infty} dk^{\parallel}\frac{k^{\parallel 2}}{k^2(\omega)}\int_0^{2\pi} d\phi\ e^{i\vec{k}^{\parallel}\cdot(\vec{r}-\vec{r}\,')} \\ &\Bigg[\frac{r_p^+ r_p^-}{1-r_p^+ r_p^- e^{-2k^{\parallel}L}} e^{-2k^{\parallel}L}\Big(e^{-k^{\parallel}(z-z')}\mathbf{A}(\phi) + e^{k^{\parallel}(z-z')}\mathbf{A}^*(\phi)\Big) \\ &+ \frac{1}{1-r_p^+ r_p^- e^{-2k^{\parallel}L}}\Big(r_p^- e^{-k^{\parallel}(z+z')}\ \mathbf{B}(\phi) + r_p^+ e^{-k^{\parallel}(2L-z-z')}\ \mathbf{B}^*(\phi)\Big)\Bigg] \\ &- \big[\omega \to -\omega^*\big]\Bigg\}\end{aligned} \tag{3.31}$$

### 3.2.2 Series Approach - Static Term

Now that the form of the Green's tensor has been established, the vector coefficients $\vec{C}_{ab}^{(n)}$ are to be calculated for $n = 0, 1, 2$. With the assumption of real dipole matrix elements $\vec{d}_{mn}$, the general results of Buhmann et al. for $n = 0, 1$ are as follows:

$$\vec{C}_{kn}^{(0)} = \frac{\mu_0}{\pi\hbar}\left\{\pi\theta(\tilde{\omega}_{nk})\tilde{\omega}_{nk}^2\mathrm{Im}\mathbf{G}^{(1)}(\vec{r}_A,\vec{r}_A,\tilde{\omega}_{nk}) - iP\int_0^{\infty}\frac{\omega^2 d\omega}{\omega-\tilde{\omega}_{nk}}\mathrm{Im}\mathbf{G}^{(1)}(\vec{r}_A,\vec{r}_A,\omega)\right\}\cdot\vec{d}_{kn} \tag{3.32}$$

$$\vec{C}^{(1)}_{kn} = \frac{\mu_0}{\pi\hbar}\Bigg\{(\vec{v}\cdot\nabla')P\int_0^\infty \frac{d\omega}{\omega-\tilde{\omega}_{nk}}\frac{\partial}{\partial\omega}\left[\omega^2 \mathrm{Im}\mathbf{G}^{(1)}(\vec{r}_A,\vec{r}_A,\omega)\right] + i\pi\theta(\tilde{\omega}_{nk})(\vec{v}\cdot\nabla')\frac{\partial}{\partial\tilde{\omega}_{nk}}\left[\tilde{\omega}^2_{nk}\mathrm{Im}\mathbf{G}^{(1)}(\vec{r}_A,\vec{r}_A,\tilde{\omega}_{nk})\right]\Bigg\}\cdot\vec{d}_{kn} \tag{3.33}$$

It can be shown by direct calculation that both terms in (3.33) and the second and third terms of (3.12) vanish for the two plate Green's tensor, although on physical grounds it is also clear that this must be the case. This is due to the translational symmetry of the system in the $x$-$y$ plane. For an atom moving in the plane of the plate surfaces, the labelling of the $x$ and $y$ axes is arbitrary. This means that the results obtained for an atom moving with velocity say $\vec{v} = v\vec{e}_x$ should be identical to a system where the atom is moving with velocity $\vec{v} = -v\vec{e}_x$. Clearly if the sign of the velocity in any expression of the form $(\vec{v}\cdot\nabla')$ is changed, the sign of the whole term is changed. To fit with the symmetry requirement that the same results are achieved for atomic motion in any parallel direction, such terms must be equal to 0. This demonstrates the value of the 2nd order term calculated in section 3.1 to calculating velocity dependent corrections, as for any system with symmetry in the direction of the atom's motion all 1st order terms vanish for the reasons detailed above. As the results of section 3.1 contain terms quadratic in the atomic velocity, the 2nd order terms are expected in general not to vanish.

Proceeding with the calculation, the 0th order term has no spatial derivatives acting on the Green's tensor. The coincidence limit $\vec{r} = \vec{r}\,' = \vec{r}_A$ may thus be taken trivially. As the $k^\parallel$ integrand as presented in (3.31) is not in an amenable form for direct integration, a Taylor expansion of the form $(1-x)^{-1}$ is used to re-express the denominator:

$$\frac{1}{1-r_p^+r_p^-e^{-2k^\parallel L}} = \sum_{j=0}^{\infty}(r_p^+r_p^-)^j e^{-2jLk^\parallel}\ ;\ |r_p^+(\omega)r_p^-(\omega)e^{-2Lk^\parallel}| < 1 \tag{3.34}$$

This expansion in reflection coefficients represents multiple reflections from the two surfaces, with the weighting factor $e^{-2k^\parallel L}$ applied to each term corresponding to an extra reflection of each plate. This has an analogy in the classical electrodynamics problem of a charged particle between two grounded plates, where the solution takes the form of an infinite series of image charges. Regarding the expansion's validity, the inequality on the right hand side must be satisfied for all values of $\omega$ and $k^\parallel$to be integrated over, $0\to\infty$ in both cases. As the exponential term ranges from 1 to 0 in this region, clearly the requirement is that $|r_p^+(\omega)r_p^-(\omega)| < 1$ for all $\omega$. This is not always the case, so care must be taken when considering individual atomic and medium properties. A closer discussion of this point will follow in the discussion section, but for now this should be viewed as a necessary step for following through with analytical calculations, justified because the medium and atomic properties can be manufactured such that this series always converges. Inserting the series expansion into equation (3.31) leads to:

$$\mathrm{Im}\mathbf{G}^{(1)}(\vec{r}_A,\vec{r}_A,\omega) = \frac{-i}{16\pi^2}\int_0^\infty dk^\parallel \frac{k^{\parallel\,2}}{k^2(\omega)}\int_0^{2\pi}d\phi\ \sum_{j=0}^{\infty}(r_p^+r_p^-)^j e^{-2jLk^\parallel} \Bigg[r_p^+r_p^-e^{-2k^\parallel L}\left(\mathbf{A}(\phi)+\mathbf{A}^*(\phi)\right) + r_p^-e^{-2k^\parallel z_A}\,\mathbf{B}(\phi) + r_p^+e^{-2k^\parallel(L-z_A)}\,\mathbf{B}^*(\phi) - \left[\omega\to-\omega^*\right]\Bigg] \tag{3.35}$$

Now the only $\omega$ dependence is contained in the powers of the reflection coefficients, and using the property $r(\omega) - r(-\omega^*) = 2i\ \mathrm{Im}[r(\omega)]$ with the properties of the complex conjugate leads to the conclusion that all powers of $r_p^-$, $r_p^+$ in the above, and any combination thereof, can be replaced by $2i$ times their imaginary part. Here it was also used that all $\omega$ integrals are taken

over the real axis, so conjugation has no effect on any factors of $\omega$ appearing. For completeness it should be noted that this also requires that $k^2(\omega) = k^2(-\omega)$, which from the form of the dispersion relation in free space is trivially seen to be true. Simultaneously carrying out the $k^{\parallel}$ integral leads to:

$$\begin{aligned}\mathrm{Im}\mathbf{G}^{(1)}(\vec{r}_A,\vec{r}_A,\omega) = \frac{1}{32\pi^2 k^2(\omega)L^3}\int_0^{2\pi} d\phi \sum_{j=0}^{\infty}\Bigg\{&\frac{\mathrm{Im}[f_{1,j}(\omega)]}{(1+j)^3}(\mathbf{A}(\phi)+\mathbf{A}^*(\phi)) \\ &+\frac{\mathrm{Im}[f_{2,j}(\omega)]}{(\mathcal{Z}+j)^3}\,\mathbf{B}(\phi)+\frac{\mathrm{Im}[f_{3,j}(\omega)]}{(1-\mathcal{Z}+j)^3}\,\mathbf{B}^*(\phi)\Bigg\} \end{aligned} \tag{3.36}$$

$$\begin{aligned} f_{1,j}(\omega) &= (r_p^+ r_p^-)^{j+1} \\ f_{2,j}(\omega) &= (r_p^+ r_p^-)^{j} r_p^- \\ f_{3,j}(\omega) &= (r_p^+ r_p^-)^{j} r_p^+ \end{aligned} \tag{3.37}$$

Here $\mathcal{Z}$ is the ratio $z_A/L$. The $\phi$ dependence is contained entirely within the matrices $\mathbf{A}(\phi)$ and $\mathbf{B}(\phi)$, meaning that the $\phi$ integral is trivial to evaluate. Carrying out this integral leads to the final form for the Green's tensor:

$$\begin{aligned}\mathrm{Im}\mathbf{G}^{(1)}(\vec{r}_A,\vec{r}_A,\omega) = \frac{1}{32\pi k^2(\omega)L^3}\sum_{j=0}^{\infty}\mathrm{Im}\Bigg\{&\frac{f_{1,j}(\omega)}{(1+j)^3}\begin{bmatrix}-1&0&0\\0&-1&0\\0&0&2\end{bmatrix} \\ &+\left(\frac{f_{2,j}(\omega)}{(\mathcal{Z}+j)^3}+\frac{f_{3,j}(\omega)}{(1-\mathcal{Z}+j)^3}\right)\begin{bmatrix}1&0&0\\0&1&0\\0&0&2\end{bmatrix}\Bigg\}\end{aligned} \tag{3.38}$$

This result may now be inserted directly into equation (3.32), which upon separation into real and imaginary parts gives the 0th order transition rates and frequency shifts:

$$\begin{aligned}\Gamma_n^{(0)} =&2\mathrm{Re}\Big(\sum_k \vec{d}_{nk}\cdot\vec{C}_{kn}^{(0)}\Big) \\ =&\frac{1}{16\pi\hbar\epsilon_0 L^3}\,\theta(\tilde{\omega}_{nk})\sum_k\sum_{j=0}^{\infty}\vec{d}_{nk}\cdot\mathrm{Im}\Bigg\{\frac{2f_{1,j}(\tilde{\omega}_{nk})}{(1+j)^3}\mathbf{N}_- \\ &+\left[\frac{f_{2,j}(\tilde{\omega}_{nk})}{(\mathcal{Z}+j)^3}+\frac{f_{3,j}(\tilde{\omega}_{nk})}{(1-\mathcal{Z}+j)^3}\right]\mathbf{N}_+\Bigg\}\cdot\vec{d}_{kn}\end{aligned} \tag{3.39}$$

$$\begin{aligned}\delta\omega_n^{(0)} =&\mathrm{Im}\Big(\sum_k \vec{d}_{nk}\cdot\vec{C}_{kn}^{(0)}\Big) \\ =&\frac{-1}{32\pi^2\hbar\epsilon_0 L^3}\sum_k\sum_{j=0}^{\infty}P\int_0^{\infty}\frac{d\omega}{\omega-\tilde{\omega}_{nk}}\vec{d}_{nk}\cdot\mathrm{Im}\Bigg\{\frac{2f_{1,j}(\omega)}{(1+j)^3}\mathbf{N}_- \\ &+\left[\frac{f_{2,j}(\omega)}{(\mathcal{Z}+j)^3}+\frac{f_{3,j}(\omega)}{(1-\mathcal{Z}+j)^3}\right]\mathbf{N}_+\Bigg\}\cdot\vec{d}_{kn}\end{aligned} \tag{3.40}$$

Here the matrices $\mathbf{N}_\pm$ are defined as:

$$\mathbf{N}_\pm = \begin{bmatrix}\pm1&0&0\\0&\pm1&0\\0&0&2\end{bmatrix} \tag{3.41}$$

### 3.2.3 Series Approach - Velocity-Dependent Term

To simplify the second order calculation, it is noted that the fourth term in (3.12) can be shown [20] to be the part of the Green's tensor which gives the response of the magnetic field to a magnetisation source, and the first term gives the response of the electric field to a polarisation source. As in the non-retarded regime (as discussed in section 3.2.1) the latter will be the dominant interaction, for the following calculation the fourth term of (3.12) is discarded, as are the second and third terms following the previous discussion regarding terms containing $(\vec{v}\cdot\nabla')$. This leaves the relevant term as:

$$\vec{C}^{(2)}_{kn} = -\frac{\mu_0}{\pi\hbar}\int_0^\infty d\omega \left[\frac{\omega^2}{2}\frac{d^2}{d\omega^2}\Big(\pi\delta(\omega-\tilde{\omega}_{nk}) - i\frac{P}{\omega-\tilde{\omega}_{nk}}\Big)(\vec{v}\cdot\nabla')^2 \mathrm{Im}\mathbf{G}(\vec{r}_A,\vec{r}_A,\omega)\right]\cdot\vec{d}_{kn} \quad (3.42)$$

Without loss of generality, it may be assumed that the atom is travelling in the positive $x$ direction with velocity $v$. Thus $\vec{v}\cdot\nabla' = v\partial_{x'}$. From the form of the Green's tensor (3.31) it is clear that under the $k^\parallel$ and $\phi$ integrals the action of this operator under the integrals is:

$$(\vec{v}\cdot\nabla')^2 = -(\vec{v}\cdot k^\parallel)^2 = -v^2 k^{\parallel 2}\cos^2(\phi) \quad (3.43)$$

Inserting this directly into (3.31) and then taking the coincidence limit by analogy with the 0th order calculation leads to:

$$\begin{aligned}\vec{C}^{(2)}_{kn} =& \frac{-i\mu_0 v^2}{32\pi^3\hbar}\int_0^\infty d\omega\int_0^\infty dk^\parallel\int_0^{2\pi} d\phi\,\omega^2\frac{d^2}{d\omega^2}\Big(\pi\delta(\omega-\tilde{\omega}_{nk}) - i\frac{P}{\omega-\tilde{\omega}_{nk}}\Big)\\ &\left\{\frac{k^{\parallel\,4}\cos^2(\phi)}{k^2(\omega)}\left[\frac{r_p^+ r_p^-}{1-r_p^+ r_p^- e^{-2k^\parallel L}}e^{-2k^\parallel L}\left(\mathbf{A}(\phi)+\mathbf{A}^*(\phi)\right)\right.\right.\\ &\left.\left.+\frac{1}{1-r_p^+ r_p^- e^{-2k^\parallel L}}\left(r_p^- e^{-2k^\parallel z_A}\,\mathbf{B}(\phi) + r_p^+ e^{-2k^\parallel(L-z_A)}\,\mathbf{B}^*(\phi)\right)\right] - [\omega\to-\omega^*]\right\}\cdot\vec{d}_{kn}\end{aligned} \quad (3.44)$$

Using the Taylor expansion (3.34) to again put the $k^\parallel$ integrand into a manageable form leads to:

$$\begin{aligned}\vec{C}^{(2)}_{kn} =& \frac{-i\mu_0 v^2}{32\pi^3\hbar}\int_0^\infty d\omega\int_0^\infty dk^\parallel\int_0^{2\pi} d\phi\,\omega^2\frac{d^2}{d\omega^2}\Big(\pi\delta(\omega-\tilde{\omega}_{nk}) - i\frac{P}{\omega-\tilde{\omega}_{nk}}\Big)\\ &\left\{\frac{k^{\parallel\,4}\cos^2(\phi)}{k^2(\omega)}\sum_{j=0}^\infty (r_p^+ r_p^-)^j e^{-2jLk^\parallel}\left[r_p^+ r_p^- e^{-2k^\parallel L}\Big(\mathbf{A}(\phi)+\mathbf{A}^*(\phi)\Big)\right.\right.\\ &\left.\left.+\Big(r_p^- e^{-2k^\parallel z_A}\,\mathbf{B}(\phi) + r_p^+ e^{-2k^\parallel(L-z_A)}\,\mathbf{B}^*(\phi)\Big)\right] - [\omega\to-\omega^*]\right\}\cdot\vec{d}_{kn}\end{aligned} \quad (3.45)$$

The $k^\parallel$ integral can now be carried out:

$$\begin{aligned}\vec{C}^{(2)}_{kn} =& \frac{-3i\mu_0 v^2}{128\pi^3\hbar L^5}\int_0^\infty d\omega\int_0^{2\pi} d\phi\,\omega^2\frac{d^2}{d\omega^2}\Big(\pi\delta(\omega-\tilde{\omega}_{nk}) - i\frac{P}{\omega-\tilde{\omega}_{nk}}\Big)\left\{\frac{\cos^2(\phi)}{k^2(\omega)}\sum_{j=0}^\infty (r_p^+ r_p^-)^j\right.\\ &\left[\frac{r_p^+ r_p^-}{(1+j)^5}\Big(\mathbf{A}(\phi)+\mathbf{A}^*(\phi)\Big) + \left(\frac{r_p^-}{(\mathcal{Z}+j)^5}\,\mathbf{B}(\phi) + \frac{r_p^+}{(1-\mathcal{Z}+j)^5}\,\mathbf{B}^*(\phi)\right)\right]\\ &\left.- [\omega\to-\omega^*]\right\}\cdot\vec{d}_{kn}\end{aligned} \quad (3.46)$$

By the same reasoning as previously, all products of reflection coefficients and the subtraction of the expression with $\omega \to -\omega$ can be replaced by the imaginary part of the functions (3.37):

$$\vec{C}^{(2)}_{kn} = \frac{3\mu_0 v^2}{64\pi^3\hbar L^5}\int_0^\infty d\omega \int_0^{2\pi} d\phi\, \omega^2 \frac{d^2}{d\omega^2}\Big(\pi\delta(\omega-\tilde{\omega}_{nk}) - i\frac{P}{\omega-\tilde{\omega}_{nk}}\Big)\frac{\cos^2(\phi)}{k^2(\omega)}\sum_{j=0}^{\infty} \left[\frac{\mathrm{Im}[f_{1,j}(\omega)]}{(1+j)^5}\Big(\mathbf{A}(\phi)+\mathbf{A}^*(\phi)\Big) + \left(\frac{\mathrm{Im}[f_{2,j}(\omega)]}{(\mathcal{Z}+j)^5}\,\mathbf{B}(\phi) + \frac{\mathrm{Im}[f_{3,j}(\omega)]}{(1-\mathcal{Z}+j)^5}\,\mathbf{B}^*(\phi)\right)\right]\cdot\vec{d}_{kn} \tag{3.47}$$

Carrying out the $\phi$ integral, and then separating into real and imaginary parts thus yields the expressions for the 2nd order corrections to the transition rates and frequency shifts:

$$\begin{aligned}\Gamma^{(2)}_n &= 2\mathrm{Re}\Big(\sum_k \vec{d}_{nk}\cdot\vec{C}^{(2)}_{kn}\Big)\\ &= \frac{3v^2}{32\pi\hbar\epsilon_0 L^5}\,\theta(\tilde{\omega}_{nk})\sum_k\sum_{j=0}^{\infty}\vec{d}_{nk}\cdot\mathrm{Im}\left[\frac{2[f_{1,j}(\tilde{\omega}_{nk})]''}{(1+j)^5}\mathbf{M}_- \right.\\ &\left. + \left(\frac{[f_{2,j}(\tilde{\omega}_{nk})]''}{(\mathcal{Z}+j)^5} + \frac{[f_{3,j}(\tilde{\omega}_{nk})]''}{(1-\mathcal{Z}+j)^5}\right)\mathbf{M}_+\right]\cdot\vec{d}_{kn}\end{aligned} \tag{3.48}$$

$$\begin{aligned}\delta\omega^{(2)}_n &= \mathrm{Im}\Big(\sum_k \vec{d}_{nk}\cdot\vec{C}^{(2)}_{kn}\Big)\\ &= \frac{-3v^2}{32\pi^2\hbar\epsilon_0 L^5}\sum_k\sum_{j=0}^{\infty}P\int_0^\infty\frac{d\omega}{(\omega-\tilde{\omega}_{nk})^3}\vec{d}_{nk}\cdot\mathrm{Im}\left[\frac{2f_{1,j}(\omega)}{(1+j)^5}\mathbf{M}_- \right.\\ &\left. + \left(\frac{f_{2,j}(\omega)}{(\mathcal{Z}+j)^5} + \frac{f_{3,j}(\omega)}{(1-\mathcal{Z}+j)^5}\right)\mathbf{M}_+\right]\cdot\vec{d}_{kn}\end{aligned} \tag{3.49}$$

Here the matrices $\mathbf{M}_\pm$ are defined as:

$$\mathbf{M}_\pm = \begin{bmatrix}\pm\frac{3}{4} & 0 & 0\\ 0 & \pm\frac{1}{4} & 0\\ 0 & 0 & 1\end{bmatrix} \tag{3.50}$$

## 3.3 Complete Approach to the Two-Plate System

Having made an approach to the two-plate system based on evaluating the terms in a Taylor series expansion in the atomic velocity, a full treatment of the atomic dynamics with respect to the atomic velocity is now attempted. The broad aim is to show that a full treatment of a moving atom between two plates yields results equivalent to that of a stationary atom with the plates reflecting at a Doppler-shifted frequency. As again in the non-retarded limit electric interactions are dominant over magnetic ones, for this case only electric terms shall be considered. The working of section 3.1 until equation (2.50) can be followed exactly, and by discarding the magnetic term (as the non-retarded limit is again considered) this leads to:

$$\hat{\vec{f}}(\vec{r},\omega,t) = e^{-i\omega(t-t_0)}\hat{\vec{f}}(\vec{r},\omega) + \frac{i}{\hbar}\sum_{a,b}\int_{t_0}^{t} dt' e^{-i\omega(t-t')}\mathbf{G}^{*T}_e(\vec{r}_A(t'),\vec{r},\omega)\cdot\vec{d}_{ab}\hat{A}_{ab}(t') \tag{3.51}$$

Following the calculation further, making no perturbative expansion in the atomic velocity, leads to the following form for the electric field operator (the equivalent of equation (3.5)):

$$\hat{\vec{E}}(\vec{r}_A,\omega,t) = e^{-i\omega(t-t_0)}\hat{\vec{E}}(\vec{r}_A,\omega,t_0) + \frac{i\mu_0}{2\pi}\sum_{a,b}\omega^2\int_{t_0}^{t} dt' e^{-i\omega(t-t')}\mathrm{Im}\mathbf{G}(\vec{r}_A(t),\vec{r}_A(t'),\omega)\cdot\vec{d}_{ab}\hat{A}_{ab}(t') \quad (3.52)$$

The steps assuming the oscillatory character of the flip operators as per equation (3.6), inserting equation (3.52) into (2.48) while ignoring the magnetic term, and then taking expectation values with the electric field in its ground state such that the free field terms vanish can all be carried out as previously. As $\vec{d}^*_{ba} = \vec{d}_{ab}$ from their definition in equation (2.44), the forms of equations (3.13) and (3.14) suggest defining scalar coefficients such that $C_{ab} = \vec{d}_{ab}\cdot\vec{C}_{ba}$, as both equations are seen to be expressible purely in terms of these coefficients and their complex conjugates. These then have the form:

$$C_{ab} = \frac{\mu_0}{\pi\hbar}\int_0^\infty d\tau\int_0^\infty \omega^2 d\omega\; e^{-i(\omega-\tilde{\omega}_{ab})\tau}\vec{d}_{ab}\cdot\mathrm{Im}\mathbf{G}^{(1)}(\vec{r}_A,\vec{r}_A\,',\omega)\cdot\vec{d}_{ba} \quad (3.53)$$

Here $\tau = t - t'$, $\vec{r}_A = \vec{r}_A(t)$, $\vec{r}_A\,' = \vec{r}_A(t')$. The upper limit of the $\tau$ integral was extended to infinity as a way of implementing the Markov approximation, the details of which shall be further explained in section 4.1.3. This form for the coefficients shall be used henceforth. By making the constant velocity approximation (assuming any friction force on the atom to have little effect on the atomic velocity over the relevant time scales) $\vec{r}_A = \vec{r}_A\,' + \vec{v}\tau$, the imaginary part of the non-retarded scattering Green's tensor (3.31) reads:

$$\begin{aligned}\mathrm{Im}\mathbf{G}^{(1)}(\vec{r}_A,\vec{r}_A\,',\omega) =& \frac{-i}{16\pi^2}\Bigg\{\int_0^\infty dk^\parallel\frac{k^{\parallel\,2}}{k^2(\omega)}\int_0^{2\pi}d\phi\; e^{ik^\parallel v\tau\cos(\phi)} \\ &\Bigg[\frac{r_p^+r_p^-}{1-r_p^+r_p^-e^{-2k^\parallel L}}e^{-2k^\parallel L}\left(\mathbf{A}(\phi)+\mathbf{A}^*(\phi)\right)+ \\ &\frac{1}{1-r_p^+r_p^-e^{-2k^\parallel L}}\left(r_p^-e^{-2k^\parallel z_A}\,\mathbf{B}(\phi)+r_p^+e^{-2k^\parallel(L-z_A)}\,\mathbf{B}^*(\phi)\right)\Bigg] \\ &-[\omega\to-\omega^*]\Bigg\}\end{aligned} \quad (3.54)$$

Here again it was assumed without loss of generality that the atomic velocity is purely in the positive $x$ direction, for the reasons described in the previous section. Introducing for convenience of notation a redefined matrix:

$$\frac{1}{2}(\mathbf{A}(\phi)+\mathbf{A}^*(\phi))\to\mathbf{A}(\phi) = \begin{bmatrix}-\cos^2(\phi) & -\cos(\phi)\sin(\phi) & 0\\ -\cos(\phi)\sin(\phi) & -\sin^2(\phi) & 0\\ 0 & 0 & 1\end{bmatrix} \quad (3.55)$$

Equation (3.54) can thus be written:

$$\begin{aligned}\mathrm{Im}\mathbf{G}^{(1)}(\vec{r}_A,\vec{r}_A\,',\omega) = \frac{-i}{16\pi^2}\Bigg\{&\int_0^\infty dk^\parallel\frac{k^{\parallel\,2}}{k^2(\omega)}\int_0^{2\pi}d\phi\; e^{ik^\parallel v\tau\cos(\phi)}\Bigg[\frac{2r_p^+r_p^-}{1-r_p^+r_p^-e^{-2k^\parallel L}}e^{-2k^\parallel L}\mathbf{A}(\phi) \\ &+\frac{1}{1-r_p^+r_p^-e^{-2k^\parallel L}}\left(r_p^-e^{-2k^\parallel z_A}\,\mathbf{B}(\phi)+r_p^+e^{-2k^\parallel(L-z_A)}\,\mathbf{B}^T(\phi)\right)\Bigg] \\ &-[\omega\to-\omega^*]\Bigg\}\end{aligned} \quad (3.56)$$

Once again expanding the denominator in a reflection coefficient power series as per (3.34), the above becomes:

$$\begin{aligned}\mathrm{Im}\mathbf{G}^{(1)}(\vec{r}_A,\vec{r}_A\,',\omega) =&\frac{-i}{16\pi^2}\Bigg\{\int_0^\infty dk^\parallel \frac{{k^\parallel}^2}{k^2(\omega)}\int_0^{2\pi} d\phi\; e^{ik^\parallel v\tau\cos(\phi)}\sum_{j=0}^{\infty}(r_p^+r_p^-)^j e^{-2jLk^\parallel}\\ &\Big[2r_p^+r_p^-e^{-2k^\parallel L}\mathbf{A}(\phi)+r_p^-e^{-2k^\parallel z_A}\;\mathbf{B}(\phi)+r_p^+e^{-2k^\parallel(L-z_A)}\;\mathbf{B}^T(\phi)\Big]\\ &-[\omega\to-\omega^*]\Bigg\}\end{aligned} \tag{3.57}$$

Inserting this into the expression for the coefficients (3.53) gives:

$$\begin{aligned}C_{ab} = \frac{-i\mu_0}{16\pi^3\hbar}\int_0^\infty d\tau\int_0^\infty \omega^2 d\omega\; e^{-i(\omega-\tilde{\omega}_{ab})\tau}\int_0^\infty {k^\parallel}^2 dk^\parallel\int_0^{2\pi} d\phi\; e^{ik^\parallel v\tau\cos(\phi)}\vec{d}_{ab}\cdot\\ \Bigg\{\frac{1}{k^2(\omega)}\sum_{j=0}^{\infty}(r_p^+r_p^-)^j e^{-2jLk^\parallel}\Big[2r_p^+r_p^-e^{-2k^\parallel L}\mathbf{A}(\phi)+r_p^-e^{-2k^\parallel z_A}\;\mathbf{B}(\phi)\\ +r_p^+e^{-2k^\parallel(L-z_A)}\;\mathbf{B}^T(\phi)\Big]-[\omega\to-\omega^*]\Bigg\}\cdot\vec{d}_{ba}\end{aligned} \tag{3.58}$$

Proceeding as previously, the products of reflection coefficients can be grouped together and written in terms of the functions (3.37):

$$\begin{aligned}C_{ab} = \frac{1}{8\pi^3\hbar\epsilon_0}\int_0^\infty d\tau\int_0^\infty d\omega\; e^{-i(\omega-\tilde{\omega}_{ab})\tau}\int_0^\infty {k^\parallel}^2 dk^\parallel\int_0^{2\pi} d\phi\; e^{ik^\parallel v\tau\cos(\phi)}\vec{d}_{ab}\cdot\sum_{j=0}^{\infty}e^{-2jLk^\parallel}\\ \Big\{2\mathrm{Im}[f_{1,j}(\omega)]e^{-2k^\parallel L}\mathbf{A}(\phi)+\mathrm{Im}[f_{2,j}(\omega)]e^{-2k^\parallel z_A}\;\mathbf{B}(\phi)\\ +\mathrm{Im}[f_{3,j}(\omega)]e^{-2k^\parallel(L-z_A)}\;\mathbf{B}^T(\phi)\Big\}\cdot\vec{d}_{ba}\end{aligned} \tag{3.59}$$

The $k^\parallel$ integral can now be carried out, leading to:

$$\begin{aligned}C_{ab} =&\frac{1}{4\pi^3\hbar\epsilon_0}\int_0^\infty d\tau\int_0^\infty d\omega\; e^{-i(\omega-\tilde{\omega}_{ab})\tau}\int_0^{2\pi} d\phi\;\sum_{j=0}^{\infty}\vec{d}_{ab}\cdot\Bigg\{\frac{2\mathrm{Im}[f_{1,j}(\omega)]}{[2(1+j)d-iv\tau\cos(\phi)]^3}\mathbf{A}(\phi)\\ &+\frac{\mathrm{Im}[f_{2,j}(\omega)]}{[2(jd+z_A)-iv\tau\cos(\phi)]^3}\;\mathbf{B}(\phi)+\frac{\mathrm{Im}[f_{3,j}(\omega)]}{[2((1+j)d-z_A)-iv\tau\cos(\phi)]^3}\;\mathbf{B}^T(\phi)\Bigg\}\cdot\vec{d}_{ba}\end{aligned} \tag{3.60}$$

Due to the difficult form of the denominators in the above equation, a Taylor expansion in terms of the following parameters is advantageous:

$$s_{1,j}=\frac{v}{2L(1+j)}\;;\;s_{2,j}=\frac{v}{2(jL+z_A)}\;;\;s_{3,j}=\frac{v}{2(L(1+j)-z_A)} \tag{3.61}$$

$$[1-is_{n,j}\cos(\phi)\tau]^{-3}=\frac{1}{2}\sum_{k=0}^{\infty}(k+1)(k+2)[is_{n,j}\cos(\phi)]^k\tau^k\;;\;|s_{n,j}\cos(\phi)\tau|<1 \tag{3.62}$$

It is instructive to look closer at the convergence requirements for this expansion. These are equivalent to:

$$v\tau<2z_A\;;\;v\tau<2(L-z_A) \tag{3.63}$$

If $L = 2z_A$, as can often be assumed to be the case, and the time scale of the interaction is taken to be the inverse of the atomic transition frequency $\tilde{\omega}_{ab}$, this reduces to the more intuitive:

$$v \ll L\tilde{\omega}_{ab} \tag{3.64}$$

Typical atomic transition frequencies are in the optical regime $10^{14}$Hz [24], and experimentally the current upper limit on accessible velocities is less than $10^4 \text{ms}^{-1}$. This would set a lower limit on the plate separation of roughly 1Å, roughly the size of an atom. Thus it can be seen that for almost all realistic situations the above expansion is valid. Equation (3.60) may now be written:

$$\begin{aligned} C_{ab} =& \frac{1}{8\pi^3\hbar\epsilon_0 L^3}\int_0^\infty d\tau \int_0^\infty d\omega\, e^{-i(\omega-\tilde{\omega}_{ab})\tau}\int_0^{2\pi} d\phi \sum_{j,k=0}^{\infty}(k+1)(k+2)[i\cos(\phi)]^k\tau^k\vec{d}_{ab}\cdot \\ & \left\{\frac{2\text{Im}[f_{1,j}(\omega)]s_{1,j}^k}{(1+j)^3}\mathbf{A}(\phi) + \frac{\text{Im}[f_{2,j}(\omega)]s_{2,j}^k}{(\mathcal{Z}+j)^3}\,\mathbf{B}(\phi) + \frac{\text{Im}[f_{3,j}(\omega)]s_{3,j}^k}{(1-\mathcal{Z}+j)^3}\,\mathbf{B}^T(\phi)\right\}\cdot\vec{d}_{ba} \end{aligned} \tag{3.65}$$

Here once again $\mathcal{Z}$ is the ratio $z_A/L$. As in section (3.1), the $\tau$ integral may be evaluated by using the Markov approximation, corresponding to the system having no memory of its state at previous times. The integral has already been extended to infinity in accordance with the Markov approximation, so as previously the $\tau$ integral can be evaluated as:

$$\int_0^\infty \tau^k e^{-i(\omega-\tilde{\omega}_{ab})\tau}d\tau = i^k\frac{d^k}{d\omega^k}\left(\pi\delta(\omega-\tilde{\omega}_{ab}) - i\frac{P}{\omega-\tilde{\omega}_{ab}}\right) \tag{3.66}$$

After insertion into equation (3.65) this leads to:

$$\begin{aligned} C_{ab} =& \frac{\mu_0}{8\pi^3\hbar\epsilon_0 L^3}\int_0^\infty d\omega \int_0^{2\pi} d\phi \sum_{j,k=0}^{\infty}(-1)^k(k+1)(k+2)\cos^k(\phi)\vec{d}_{ab}\cdot \\ & \left\{\frac{2\text{Im}[f_{1,j}(\omega)]s_{1,j}^k}{(1+j)^3}\mathbf{A}(\phi) + \frac{\text{Im}[f_{2,j}(\omega)]s_{2,j}^k}{(\mathcal{Z}+j)^3}\,\mathbf{B}(\phi) + \frac{\text{Im}[f_{3,j}(\omega)]s_{3,j}^k}{(1-\mathcal{Z}+j)^3}\,\mathbf{B}^T(\phi)\right\} \\ & \cdot\vec{d}_{ba}\frac{d^k}{d\omega^k}\left(\pi\delta(\omega-\tilde{\omega}_{ab}) - i\frac{P}{\omega-\tilde{\omega}_{ab}}\right) \end{aligned} \tag{3.67}$$

First the delta function contribution to the $\omega$ integral is considered. By partially integrating the expression with respect to the delta function this term becomes:

$$\begin{aligned} C_{ab}^{\delta} =& \frac{\mu_0}{8\pi^2\hbar\epsilon_0 L^3}\int_0^{2\pi} d\phi \sum_{j,k=0}^{\infty}(-1)^k(k+1)(k+2)\cos^k(\phi)\vec{d}_{ab}\cdot\frac{d^k}{d\omega^k}\left\{\frac{2\text{Im}[f_{1,j}(\omega)]s_{1,j}^k}{(1+j)^3}\mathbf{A}(\phi)\right. \\ & \left.+\frac{\text{Im}[f_{2,j}(\omega)]s_{2,j}^k}{(\mathcal{Z}+j)^3}\,\mathbf{B}(\phi) + \frac{\text{Im}[f_{3,j}(\omega)]s_{3,j}^k}{(1-\mathcal{Z}+j)^3}\,\mathbf{B}^T(\phi)\right\}\Bigg|_{\omega=\tilde{\omega}_{ab}}\cdot\vec{d}_{ba} \end{aligned} \tag{3.68}$$

Now the principal value integral term must be evaluated. By writing explicitly the imaginary part of the functions $f_{n,j}(\omega)$ in terms of the function and its complex conjugate, this term $I_k$ is given by:

$$\begin{aligned} I_k =& P\int_0^\infty \text{Im}[f_{n,j}(\omega)]\frac{d^k}{d\omega^k}\Big(\frac{1}{\omega-\tilde{\omega}_{ab}}\Big)d\omega = (-1)^k k!\,P\int_0^\infty \frac{\text{Im}[f_{n,j}(\omega)]}{(\omega-\tilde{\omega}_{ab})^{k+1}}d\omega \\ =& \frac{(-1)^k k!}{2i}\,P\int_0^\infty \frac{f_{n,j}(\omega)}{(\omega-\tilde{\omega}_{ab})^{k+1}}d\omega + \frac{k!}{2i}\,P\int_{-\infty}^0 \frac{f_{n,j}(\omega)}{(\omega+\tilde{\omega}_{ab})^{k+1}}d\omega \end{aligned} \tag{3.69}$$

The last term of (3.69) was arrived at by recalling the conjugation property of the reflection coefficients $r^*(\omega) = r(-\omega^*)$ which follows from the conjugation property of $\epsilon(\omega)$, and then

identifying that the functions $f_{n,j}(\omega)$ have the same property, which follows from their definition (3.37). The integration paths for the two terms in the above equation are shown in figure 3.2, where A denotes the path for the first term and B the path for the second. Due to the finiteness of the functions $f_{n,j}(\omega)$ along the real axis, the residues of the integrands on the bottom line of (3.69) obey the (k+1) order pole formula. Thus the residue part of $I_k$ is given by:

$$I_k^{res} = (-1)^k \pi \left\{ \frac{d^k}{d\omega^k} \mathrm{Re}[f_{n,j}(\omega)] \right\} \Big|_{\omega=\tilde{\omega}_{ab}} \theta(\tilde{\omega}_{ab}) \tag{3.70}$$

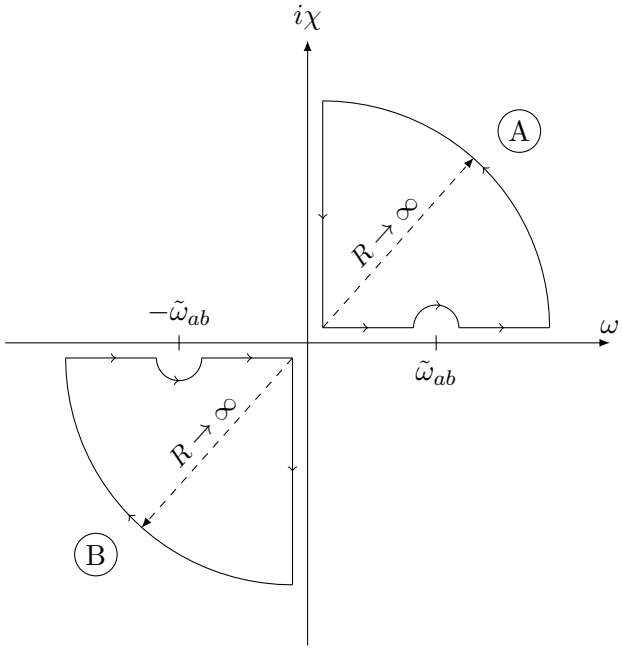


Figure 3.2: The contours to be integrated over for the two parts A and B of the first and second terms in equation (3.69) respectively.

From the form of equation (3.69) the integrals over the quarter-circle arcs in figure 3.2 can be shown to vanish in the limit $R \to \infty$ (care must only be taken with the k = 0 term, where the properties of the reflection coefficients for $R \to \infty$ must be used to show that the integral vanishes). Thus the remaining integral terms consist purely of the the two integrals along the imaginary axes. Separating the integral $I_k$ into contributions due to the residue terms and the integrals along the imaginary axes, the integral terms can be expressed as follows:

$$I_k = I_k^{res} + I_k^{int} \tag{3.71}$$

$$\begin{aligned} I_k^{int} =& \frac{(-1)^k k!}{2} \int_0^\infty \frac{f_{n,j}(i\chi)}{(-\tilde{\omega}_{ab} + i\chi)^{k+1}} d\chi - \frac{k!}{2} \int_0^\infty \frac{f_{n,j}(i\chi)}{(\tilde{\omega}_{ab} + i\chi)^{k+1}} d\chi \\ =& \frac{k!}{2} \int_0^\infty \frac{f_{n,j}(i\chi)}{(\tilde{\omega}_{ab} - i\chi)^{k+1}} d\chi + \frac{k!}{2} \int_0^\infty \frac{f_{n,j}(i\chi)}{[(\tilde{\omega}_{ab} - i\chi)^{k+1}]^*} d\chi \\ =& -\frac{k!}{2} \int_0^\infty d\chi \, \frac{(i\chi + \tilde{\omega}_{ab})^{k+1} + (-i\chi + \tilde{\omega}_{ab})^{k+1}}{(\chi^2 + \tilde{\omega}_{ab}^2)^{k+1}} f_{n,j}(i\chi) \end{aligned} \tag{3.72}$$

By combining the results for the residue and integral terms, the final value of $I_k$ is:

$$\begin{aligned} I_k = (-1)^k \pi \, \theta(\tilde{\omega}_{ab}) \Big[ \frac{d^k}{d\omega^k} \mathrm{Re}[f_{n,j}(\omega)] \Big] \Big|_{\omega=\tilde{\omega}_{ab}} \\ - \frac{k!}{2} \int_0^\infty d\chi \, \frac{(i\chi + \tilde{\omega}_{ab})^{k+1} + (-i\chi + \tilde{\omega}_{ab})^{k+1}}{(\chi^2 + \tilde{\omega}_{ab}^2)^{k+1}} f_{n,j}(i\chi) \end{aligned} \tag{3.73}$$

The first term in $I_k$ is identified as a resonant contribution (as it is evaluated purely at the transition frequency $\tilde{\omega}_{ab}$) and the second term is identified as the non-resonant contribution as the integral samples complex frequencies other than the transition frequency $\tilde{\omega}_{ab}$. This result can now be inserted into (3.67) and combined with (3.68) to give:

$$\begin{aligned}
C_{ab}^{res} &= \frac{1}{8\pi^2\hbar\epsilon_0 L^3}\int_0^{2\pi} d\phi \sum_{j,k=0}^{\infty}(-1)^k(k+1)(k+2)\cos^k(\phi)\theta(\tilde{\omega_{ab}})\vec{d}_{ab}\cdot \\
&\quad \frac{d^k}{d\omega^k}\left\{\frac{(2\mathrm{Im}[f_{1,j}(\omega)]-2i\mathrm{Re}[f_{1,j}(\omega)])\,s_{1,j}^k}{(1+j)^3}\mathbf{A}(\phi)+\frac{(\mathrm{Im}[f_{2,j}(\omega)]-i\mathrm{Re}[f_{2,j}(\omega)])\,s_{2,j}^k}{(\mathcal{Z}+j)^3}\,\mathbf{B}(\phi)\right. \\
&\quad \left.+\frac{(\mathrm{Im}[f_{3,j}(\omega)]-i\mathrm{Re}[f_{3,j}(\omega)])\,s_{3,j}^k}{(1-\mathcal{Z}+j)^3}\,\mathbf{B}^T(\phi)\right\}\Bigg|_{\omega=\tilde{\omega}_{ab}}\cdot\vec{d}_{ba} \\
&= \frac{-i}{8\pi^2\hbar\epsilon_0 L^3}\int_0^{2\pi} d\phi \sum_{j,k=0}^{\infty}(-1)^k(k+1)(k+2)\cos^k(\phi)\theta(\tilde{\omega_{ab}})\vec{d}_{ab}\cdot \\
&\quad \left\{\frac{2f_{1,j}(\omega)s_{1,j}^k}{(1+j)^3}\mathbf{A}(\phi)+\frac{f_{2,j}(\omega)s_{2,j}^k}{(\mathcal{Z}+j)^3}\,\mathbf{B}(\phi)+\frac{f_{3,j}(\omega)s_{3,j}^k}{(1-\mathcal{Z}+j)^3}\,\mathbf{B}^T(\phi)\right\}\Bigg|_{\omega=\tilde{\omega}_{ab}}\cdot\vec{d}_{ba} \qquad (3.74)
\end{aligned}$$

$$\begin{aligned}
C_{ab}^{nres} &= \frac{i}{16\pi^3\hbar\epsilon_0 L^3}\int_0^{2\pi} d\phi \sum_{j,k=0}^{\infty}(k+2)!\cos^k(\phi)\int_0^{\infty} d\chi\,\frac{(i\chi+\tilde{\omega}_{ab})^{k+1}+(-i\chi+\tilde{\omega}_{ab})^{k+1}}{(\chi^2+\tilde{\omega}_{ab}^2)^{k+1}} \\
&\quad \vec{d}_{ab}\cdot\left\{\frac{2f_{1,j}(i\chi)s_{1,j}^k}{(1+j)^3}\mathbf{A}(\phi)+\frac{f_{2,j}(i\chi)s_{2,j}^k}{(\mathcal{Z}+j)^3}\,\mathbf{B}(\phi)+\frac{f_{3,j}(i\chi)s_{3,j}^k}{(1-\mathcal{Z}+j)^3}\,\mathbf{B}^T(\phi)\right\}\cdot\vec{d}_{ba} \qquad (3.75)
\end{aligned}$$

The summation over the index $k$ is then identified to be the series expansion of a $k^{\|}$ integral over a Doppler shifted frequency. The origin of this identification is detailed in section 3.4. Furthermore, after this step the summation over $j$ can be seen to be identical to equation (4.4), which was also the origin of the $j$ summation, with $r(\omega)$ evaluated instead at the new Doppler-shifted frequency. Thus both sums can be removed, and the above can be re-expressed as:

$$\begin{aligned}
C_{ab}^{res} &= \frac{-i}{8\pi^2\hbar\epsilon_0}\int_0^{2\pi} d\phi\int_0^{\infty} dk^{\|}\,\frac{(k^{\|})^2}{1-r_p^+(\tilde{\omega}'_{ab})r_p^-(\tilde{\omega}'_{ab})e^{-2Lk^{\|}}}\vec{d}_{ab}\cdot \\
&\quad \Big[2\mathbf{A}(\phi)e^{-2Lk^{\|}}r_p^+(\tilde{\omega}'_{ab})r_p^-(\tilde{\omega}'_{ab})+\mathbf{B}(\phi)e^{-2L\mathcal{Z}k^{\|}}r_p^+(\tilde{\omega}'_{ab}) \\
&\quad +\mathbf{B}^T(\phi)e^{-2L(1-\mathcal{Z})k^{\|}}r_p^-(\tilde{\omega}'_{ab})\Big]\cdot\vec{d}_{ba}\theta(\tilde{\omega}_{ab}) \qquad (3.76)
\end{aligned}$$

$$\begin{aligned}
C_{ab}^{nres} &= \frac{i}{8\pi^3\hbar\epsilon_0}\int_0^{2\pi} d\phi\int_0^{\infty} dk^{\|}\int_0^{\infty} d\chi\,\frac{(k^{\|})^2}{1-r_p^+(i\chi)r_p^-(i\chi)e^{-2Lk^{\|}}}\,\frac{\tilde{\omega}'^2_{ab}}{(\tilde{\omega}'^2_{ab}+\chi^2)} \\
&\quad \vec{d}_{ab}\cdot\Big[2\mathbf{A}(\phi)e^{-2Lk^{\|}}r_p^+(i\chi)r_p^-(i\chi)+\mathbf{B}(\phi)e^{-2L\mathcal{Z}k^{\|}}r_p^+(i\chi) \\
&\quad +\mathbf{B}^T(\phi)e^{-2L(1-\mathcal{Z})k^{\|}}r_p^-(i\chi)\Big]\cdot\vec{d}_{ba} \qquad (3.77)
\end{aligned}$$

Here the Doppler shifted frequency $\tilde{\omega}'_{ab}$ is given by:

$$\tilde{\omega}'_{ab} = \tilde{\omega}'_{ab}\,(k^{||},\phi) = \tilde{\omega}_{ab} + vk^{||}\cos(\phi) \qquad (3.78)$$

When the atom is in the centre of the cavity between the plates, i.e. $\mathcal{Z} = 1/2$, the equations take the simpler form:

$$C_{ab}^{res} = \frac{-i}{8\pi^2\hbar\epsilon_0}\int_0^{2\pi} d\phi \int_0^{\infty} dk^{\parallel} \frac{(k^{\parallel})^2}{1 - r_p^+(\tilde{\omega}'_{ab})r_p^-(\tilde{\omega}'_{ab})e^{-2Lk^{\parallel}}}\vec{d}_{ab}\cdot \Big[2\mathbf{A}(\phi)e^{-2Lk^{\parallel}}r_p^+(\tilde{\omega}'_{ab})r_p^-(\tilde{\omega}'_{ab})\theta(\tilde{\omega}_{ab}) + \mathbf{B}(\phi)e^{-Lk^{\parallel}}r_p^+(\tilde{\omega}'_{ab})\theta(\tilde{\omega}_{ab}) + \mathbf{B}^T(\phi)e^{-Lk^{\parallel}}r_p^-(\tilde{\omega}'_{ab})\theta(\tilde{\omega}_{ab})\Big]\cdot\vec{d}_{ba} \quad (3.79)$$

$$C_{ab}^{nres} = \frac{i}{8\pi^3\hbar\epsilon_0}\int_0^{2\pi} d\phi \int_0^{\infty} dk^{\parallel} \int_0^{\infty} d\chi \frac{(k^{\parallel})^2}{1 - r_p^+(i\chi)r_p^-(i\chi)e^{-2Lk^{\parallel}}} \frac{\tilde{\omega}'^2_{ab}}{(\tilde{\omega}'^2_{ab} + \chi^2)}\,\vec{d}_{ab}\cdot \Big[2\mathbf{A}(\phi)e^{-2Lk^{\parallel}}r_p^+(i\chi)r_p^-(i\chi) + \mathbf{B}(\phi)e^{-Lk^{\parallel}}r_p^+(i\chi) + \mathbf{B}^T(\phi)e^{-Lk^{\parallel}}r_p^-(i\chi)\Big]\cdot\vec{d}_{ba} \quad (3.80)$$

## 3.4 Doppler Shift Approach to the Two-Plate System

The key result of the previous section is that a Doppler shifted frequency (3.78) contains all the velocity dependence of the atom. From the form of (3.59) it is clear that the frequency dependence of the coefficients $C_{ab}$ is contained in the reflection coefficient functions $f_{n,j}(\omega)$ and the factor $e^{-i\omega\tau}$, i.e. there is no dependence on the properties of the atom. Thus the moving atom should give identical results to a stationary atom with the plates reflecting at a Doppler shifted frequency. Using the formalism of section 3.3 this can be verified mathematically, although as the details of the calculation are almost identical to those carried out in the previous section only the key points will be noted here. First the coincidence limit of the imaginary part of the scattering Green's tensor (3.31) is taken, which combined with the re-definition (3.55) and the expansion (3.34) gives:

$$\mathrm{Im}\mathbf{G}^{(1)}(\vec{r}_A, \vec{r}_A\,', \omega) = \frac{-i}{16\pi^2}\Bigg\{\int_0^{\infty} dk^{\parallel}\frac{(k^{\parallel})^2}{k^2(\omega)}\int_0^{2\pi} d\phi \sum_{j=0}^{\infty}(r_p^+r_p^-)^j e^{-2jLk^{\parallel}} \Big[2r_p^+r_p^-e^{-2k^{\parallel}L}\mathbf{A}(\phi) + r_p^-e^{-2k^{\parallel}z_A}\,\mathbf{B}(\phi) + r_p^+e^{-2k^{\parallel}(L-z_A)}\,\mathbf{B}^T(\phi)\Big] - [\omega \to -\omega^*]\Bigg\} \quad (3.81)$$

Insertion into equation (3.53) with the reflection coefficients evaluated at the Doppler-shifted frequency $\omega + vk^{\parallel}\cos\phi$ yields:

$$C_{ab} = \frac{\mu_0}{8\pi^3\hbar\epsilon_0}\int_0^{\infty} dk^{\parallel}(k^{\parallel})^2\int_0^{2\pi} d\phi\int_0^{\infty} d\tau\int_0^{\infty} d\omega\; e^{-i(\omega-\tilde{\omega}_{ab})\tau}\sum_{j=0}^{\infty} e^{-2jLk^{\parallel}}\vec{d}_{ab}\cdot \Big\{2\mathrm{Im}[f_{1,j}(\omega + vk^{\parallel}\cos\phi)]e^{-2k^{\parallel}L}\mathbf{A}(\phi) + \mathrm{Im}[f_{2,j}(\omega + vk^{\parallel}\cos\phi)]e^{-2k^{\parallel}z_A}\,\mathbf{B}(\phi) + \mathrm{Im}[f_{3,j}(\omega + vk^{\parallel}\cos\phi)]e^{-2k^{\parallel}(L-z_A)}\,\mathbf{B}^T(\phi)\Big\}\cdot\vec{d}_{ba} \quad (3.82)$$

Applying the Markov approximation as per equation (3.66) leads to:

$$C_{ab} = \frac{\mu_0}{8\pi^3\hbar\epsilon_0}\int_0^{\infty} dk^{\parallel}(k^{\parallel})^2\int_0^{2\pi} d\phi\int_0^{\infty} d\omega\;\sum_{j=0}^{\infty} e^{-2jLk^{\parallel}}\left(\pi\delta(\omega-\tilde{\omega}_{ab}) - i\frac{P}{\omega-\tilde{\omega}_{ab}}\right)\vec{d}_{ab}\cdot \Big\{2\mathrm{Im}[f_{1,j}(\omega + vk^{\parallel}\cos\phi)]e^{-2k^{\parallel}L}\mathbf{A}(\phi) + \mathrm{Im}[f_{2,j}(\omega + vk^{\parallel}\cos\phi)]e^{-2k^{\parallel}z_A}\,\mathbf{B}(\phi) + \mathrm{Im}[f_{3,j}(\omega + vk^{\parallel}\cos\phi)]e^{-2k^{\parallel}(L-z_A)}\,\mathbf{B}^T(\phi)\Big\}\cdot\vec{d}_{ba} \quad (3.83)$$

Evaluating the $\omega$ integral as in section 3.3 gives:

$$C_{ab}^{res} = \frac{-i\mu_0}{8\pi^2\hbar\epsilon_0}\int_0^\infty dk^\parallel (k^\parallel)^2 \int_0^{2\pi} d\phi \sum_{j=0}^{\infty} e^{-2jLk^\parallel}\vec{d}_{ab}\cdot \Big\{2f_{1,j}(\tilde{\omega}_{ab}+vk^\parallel\cos\phi)e^{-2L(1+j)k^\parallel}\mathbf{A}(\phi) + f_{2,j}(\tilde{\omega}_{ab}+vk^\parallel\cos\phi)e^{-2L(j+\mathcal{Z})k^\parallel}\mathbf{B}(\phi) + f_{3,j}(\tilde{\omega}_{ab}+vk^\parallel\cos\phi)e^{-2L(j+1-\mathcal{Z})k^\parallel}\mathbf{B}^T(\phi)\Big\}\cdot\vec{d}_{ba} \quad (3.84)$$

$$C_{ab}^{nres} = \frac{i\mu_0}{8\pi^3\hbar\epsilon_0}\int_0^{2\pi} d\phi \int_0^\infty dk^\parallel\ (k^\parallel)^2 \sum_{j=0}^{\infty}\int_0^\infty d\chi\ \frac{\tilde{\omega}_{ab}'^2}{(\tilde{\omega}_{ab}'^2+\chi^2)}\ [r^+(i\chi)r^-(i\chi)]^j\ \vec{d}_{ab}\cdot \Big\{2\mathbf{A}(\phi)e^{-2L(1+j)k^\parallel}r^+(i\chi)r^-(i\chi) + \mathbf{B}(\phi)e^{-2L(j+\mathcal{Z})k^\parallel}r^+(i\chi) + \mathbf{B}^T(\phi)e^{-2L(j+1-\mathcal{Z})k^\parallel}r^-(i\chi)\Big\}\cdot\vec{d}_{ba} \quad (3.85)$$

By reconstructing the $(1-r_p^+(\tilde{\omega}_{ab}')r_p^-(\tilde{\omega}_{ab}')e^{-2Lk^\parallel})^{-1}$-like terms from the infinite sum over $j$ in the above, these results can be seen to be identical to (3.76) and (3.77), confirming that physically the two systems considered are identical, corresponding simply to a Galilean reference frame transformation. The only step needing confirmation is that from equations (3.74) and (3.75) to equations (3.76) and (3.77). This can now be reverse engineered from equations (3.84) and (3.85) respectively by expanding the $k^\parallel$ integral in a power series, and then evaluating to show the equivalence.

This result also implies that the atom's properties remain unchanged from their static case when moving relative to the reference frame. Mathematically this assumption was added in equation (3.7), an intemediary step in arriving at equation (3.53), where taking the atomic flip operator $\hat{A}_{mn}(t')$ outside the $t'$ integral corresponded to assuming the dynamics of the atom remain roughly constant on the time scale of interactions.

# Chapter 4

# Discussion

The first section of the previous chapter was dedicated to the problem of a moving atom in the presence of dielectric or metallic media. The only loss of generality regarding the media distribution is that the atom moves in free space, otherwise the results are completely general. This is reflected by the fact that no properties of the Green's tensor representing the electromagnetic response of the system were assumed beyond those following from its defining equation (2.18). This led to a series expansion in the atomic velocity along the lines of the work carried out in Refs. [1, 4] for the 0th and 1st order terms in the velocity $\vec{v}$. In this work the 2nd order term was calculated, which returned as a final result:

$$\begin{aligned}\vec{C}^{(2)}_{kl} = &-\frac{\mu_0}{\pi\hbar}\int_0^\infty d\omega\Big\{\frac{\omega^2}{2}\frac{d^2}{d\omega^2}\Big(\pi\delta(\omega-\tilde{\omega}_{lk})-i\frac{P}{\omega-\tilde{\omega}_{lk}}\Big)(\vec{v}\cdot\nabla')^2\mathrm{Im}\mathbf{G}(\vec{r}_A,\vec{r}_A,\omega)\cdot\vec{d}_{kl}\\
&+\omega\frac{d}{d\omega}\Big(\pi\delta(\omega-\tilde{\omega}_{lk})-i\frac{P}{\omega-\tilde{\omega}_{lk}}\Big)(\vec{v}\cdot\nabla')\left(\mathrm{Im}\mathbf{G}(\vec{r}_A,\vec{r}_A,\omega)\times\overleftarrow{\nabla}'\right)\times\vec{d}_{kl}\cdot\vec{v}\\
&+\omega\frac{d}{d\omega}\Big(\pi\delta(\omega-\tilde{\omega}_{lk})-i\frac{P}{\omega-\tilde{\omega}_{lk}}\Big)\vec{v}\times\left(\nabla\times(\vec{v}\cdot\nabla')\mathrm{Im}\mathbf{G}(\vec{r}_A,\vec{r}_A,\omega)\cdot\vec{d}_{kl}\right)\\
&+\Big(\pi\delta(\omega-\tilde{\omega}_{lk})-i\frac{P}{\omega-\tilde{\omega}_{lk}}\Big)\vec{v}\times\left[\left(\nabla\times\mathrm{Im}\mathbf{G}(\vec{r}_A,\vec{r}_A,\omega)\times\overleftarrow{\nabla}'\right)\times\vec{d}_{kl}\cdot\vec{v}\right]\Big\}\end{aligned}\tag{4.1}$$

The vector coefficient $\vec{C}^{(2)}_{kl}$ contains the information about the second order velocity-dependent corrections to the spectroscopic properties of the atom, as detailed at the end of section 3.1. The second order term has a particular usefulness when treating systems with translational invariance along the atom's direction of motion, because as detailed near the beginning of section 3.2.2 the 1st order velocity corrections disappear in this case.

An example of such a system is the case which is to be the main focus of this discussion section, an atom moving in a vacuum cavity between two parallel dielectric plates. In section 3.3 the two-plate system was considered in the non-retarded limit exactly, i.e. to all orders in $v$. This result was then shown in section 3.4 to be equivalent to a Doppler shift applied to the frequencies at which the reflection coefficients were evaluated, with the full result for the dominant resonant terms as follows:

$$\begin{aligned}C^{res}_{ab} = \frac{-i}{8\pi^2\hbar\epsilon_0}\int_0^{2\pi}d\phi\int_0^\infty dk^{\parallel}\,\frac{(k^{\parallel})^2}{1-r_p^+(\tilde{\omega}'_{ab})r_p^-(\tilde{\omega}'_{ab})e^{-2Lk^{\parallel}}}\vec{d}_{ab}\cdot\\
\Big\{2\mathbf{A}(\phi)e^{-2Lk^{\parallel}}r_p^+(\tilde{\omega}'_{ab})r_p^-(\tilde{\omega}'_{ab})+\mathbf{B}(\phi)e^{-2L\mathcal{Z}k^{\parallel}}r_p^+(\tilde{\omega}'_{ab})\\
+\mathbf{B}^T(\phi)e^{-2L(1-\mathcal{Z})k^{\parallel}}r_p^-(\tilde{\omega}'_{ab})\Big\}\cdot\vec{d}_{ba}\theta(\tilde{\omega}_{ab})\end{aligned}\tag{4.2}$$

The resonant contributions to the medium-induced transition rates $\Gamma_{ab}$ and frequency shifts $\delta\omega_{ab}$ for a given transition $a \to b$ are given in terms of the above result by:

$$\Gamma_{ab} = 2\mathrm{Re}\left[C_{ab}^{res}\right] \qquad \delta\omega_{ab} = \mathrm{Im}\left[C_{ab}^{res}\right] \tag{4.3}$$

This chapter begins with a discussion of the validity of the results obtained in chapter 3, followed by a comparison of the three approaches to the treatment of the system carried out in the same chapter. These were the velocity series expansion, the full treatment of velocity, and finally the application of the Doppler shift. Section 4.3 then goes through in detail the interpretation of the results obtained, with numerical examples illustrating the arguments. Finally section 4.4 considers the applicability of the work presented to possible future experiments.

## 4.1 Validity of Results

In this section all assumptions and approximations will be examined in terms of their validity and accuracy.

### 4.1.1 Reflection Coefficient Series

In the work carried out in section 3.2 until the end of the chapter, the following Taylor expansion with associated convergence requirement was made:

$$\frac{1}{1 - r_p^+ r_p^- e^{-2k^\parallel L}} = \sum_{j=0}^{\infty} (r_p^+ r_p^-)^j e^{-2jLk^\parallel} \;;\; |r_p^+(\omega) r_p^-(\omega)| < e^{2Lk^\parallel} \tag{4.4}$$

At the time it was noted that the convergence of the series is not guaranteed for all values of $\omega$ and $k^\parallel$, here this is investigated more thoroughly. To demonstrate this, a Drude-Lorentz model reflection function is plotted in figure 4.1. For a Drude-Lorentz model dielectric in the non-retarded limit where only a single resonance is considered, the p-reflection coefficient is given by:

$$\epsilon(\omega) = \eta\left(1 + \frac{\omega_P^2}{\omega_T^2 - \omega^2 - i\gamma\omega}\right) \tag{4.5}$$

$$r_p(\omega) = \frac{\epsilon(\omega) - 1}{\epsilon(\omega) + 1} \tag{4.6}$$

Here $\omega_P$ is the plasma frequency, $\omega_T$ is the resonant frequency of the material, $\gamma$ is the absorption coefficient of the material, and $\eta$ accounts for the effects due to other resonances.

Normally energy conservation would require that $|r(\omega)|$ is less than or equal to 1, however this requirement does not hold for the non-retarded limit as all waves are evanescent, i.e. carry no energy. Thus from figure 4.1 it is clear that at least in some regime this Taylor series does not converge. The convergence limit shown in figure 4.1 is that for $k^\parallel = 1/L$, which is roughly where the terms of the form $\left(k^\parallel\right)^2 e^{-2k^\parallel L}$ in the result (4.2) are maximum. Within the Drude-Lorentz model it can be shown by direct calculation from equations (4.5) and (4.6) that the condition for some region of $|r(\omega)|$ to be larger than or equal to 1 is (here setting $\eta = 1$ such that the material only has one resonance):

$$\omega_P^4 - 2\gamma^2\left(\omega_P^2 + 2\omega_T^2\right) + \gamma^4 \geq 0 \tag{4.7}$$

Should this condition be satisfied, by the same method it is possible to show that the region in which $|r| \geq 1$ is given by:

$$\omega_- \leq \omega \leq \omega_+ \tag{4.8}$$

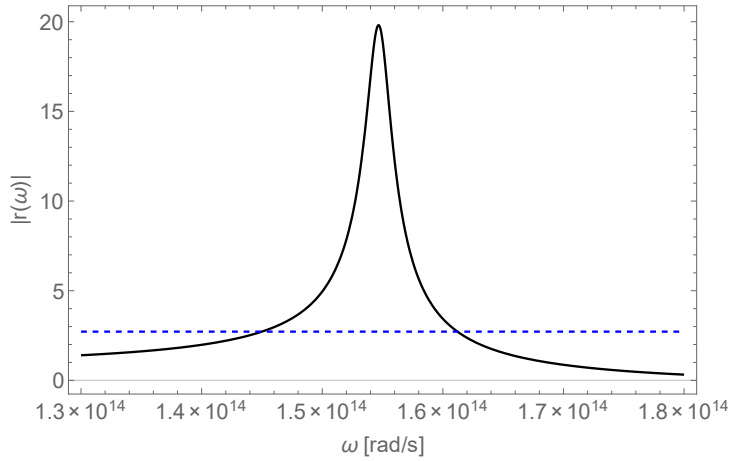


Figure 4.1: A plot of $|r(\omega)|$ in the non-retarded limit for the sapphire Drude-Lorentz parameters $\eta = 2.71$, $\omega_T = 1.08 \times 10^{14}$rad/s, $\omega_P = 1.2\omega_T$, $\gamma = 0.02\omega_T$. The convergence limit at $k^{\parallel} = 1/L$, given by $|r(\omega)| = e$, is shown in dashed red.

$$\omega_{\pm} = \sqrt{\frac{\left(\omega_P^2 + 2\omega_T^2 - \gamma^2\right) \pm \sqrt{\gamma^4 - 2\gamma^2\left(\omega_P^2 + 2\omega_T^2\right) + \omega_P^4}}{2}} \tag{4.9}$$

Now the rationale and justification for the expansion in section 3.2 will be briefly discussed. In the treatment of the two-plate Green's tensor in chapter 3, this Taylor series was used as a necessary evil to allow an analytic solution to some of the integrals present in equation (3.58), and the equivalent stage in sections 3.2.2, 3.2.3 and 3.4. Implicit in this Taylor series is a description of the processes involved being an infinite sum of multiple reflections off the two plate surfaces, as can be seen from the form of equation (4.4). This is analogous to the solution to the classical problem of a charge situated between two grounded plates, where the solution takes the form of an infinite series of image charges in both plates. Thus when the Taylor series diverges, as it does for the above material properties, the physical interpretation of the interaction being described by an infinite sum of reflections breaks down, opening up the possibility of unexpected behaviour in the non-retarded regime. Importantly, as for non-evanescent waves $|r|$ cannot be larger than 1 due to energy conservation, such behaviour is not possible outside the non-retarded limit.

To summarise, the Taylor series expansion was made to allow a further analytical treatment of the problem, which for materials where equation (4.7) does not hold is convergent. Using this, various analytical results have been obtained, and crucially the existence of a Doppler-shift phenomenon was shown.

### 4.1.2 Velocity Constraints

In the sections covering the two-plate system, a series expansion was used with the convergence requirement:

$$v \ll 2z_A\tilde{\omega}_{ab} \tag{4.10}$$

Here $z_A$ refers not as previously to the distance from one plate, but refers equally to the distance from either plate. As discussed in section 3.3 when the expansion was introduced, an atomic resonance frequency in the optical range ($\tilde{\omega} \sim 10^{14}$rad/s) and atomic velocity $v < 10^4\text{ms}^{-1}$ leads to a minimum plate separation of roughly 1 Å, or comparable in size to the Bohr radius $a_0$. As an extreme example, one might consider an atom with a large but non-relativistic velocity, for example $\sim 10^5\text{ms}^{-1}$, and a small resonance frequency $\sim 10^{13}$rad/s. In this case the atom-plate separation would have to be more than 10nm. However plate separations in experiments are

usually larger than this. For example in the direct measurement of the static Casimir-Polder force in Ref. [13] the plate separation was roughly $1\mu$m, and the closest atom-plate separation achieved was roughly 0.2 $\mu$m. No experiment since then has made any significant advances on this in terms of atom-plate separation.

Alternatively it may be taken that atom-plate separations are of the order of $1\mu$m, which together with the optical transition frequencies quoted above leads to the velocity requirement being $v \ll 10^8 \text{ms}^{-1}$. This ties in with a further non-explicit approximation made throughout the work, namely that the system can be treated non-relativistically. Details of the differences between relativistic and non-relativistic formulations of QED, and a thorough discussion of both can be found in Ref. [23]. Essentially however, for low energy physics where the particles (i.e. the moving atom in this case) are moving non-relativistically this is a perfectly valid treatment, where the atom is treated in a non-relativistic manner and the electromagnetic field equations are not expressed in a manifestly covariant formulation. This non-relativistic approximation thus sets the actual upper limit on the maximum velocity in this situation, normally taken to be something of the order of $10^6 \text{ms}^{-1}$. As long as this is satisfied the velocity presents no foreseeable source of limitation on the validity of the results.

### 4.1.3 Markovianity of the System

In chapter 3 it was assumed that the system being described is Markovian, i.e. that the field has essentially no memory of its state at previous times. This allows the simplification of formulae throughout the chapter by virtue of equation (3.7), which allows the dependence of the fields at all previous times to be reduced to a pure dependence on the time of evaluation of the field: $t$. More specifically a Markovian system may be described as one in which the state of a system at some time $t > t'$ can be described by the system's state at a time $t'$ and the relevant propagator, details of which can be found in Ref. [25].

In the context of this work, the Markov approximation means that the response of the electromagnetic field to the atom's internal dynamics is sufficiently fast that the atom's field-induced dynamics at time $t$ are describable solely in terms of the electromagnetic field at the same time $t$. This was inserted into the results when taking the lower limit of the $t'$ integral to $-\infty$ in equation (3.7). As discussed in Ref. [4], an ideal Markovian system is one in which the field spectrum is completely flat, in the case of the Drude-Lorentz model used in section 4.3 this corresponds to an infinite resonance width $\gamma$. This is because $1/\gamma$ gives an estimate of the field time scale, so only the part of the time integral between $t - 1/\gamma$ and $t$ contributes meaningfully to the results of the integral which was approximated as equation (3.7). Thus if $1/\gamma$ is substantially smaller than the atomic time scales defined by the inverse of the transition rate $1/\Gamma$, the field response can be approximated as infinitely fast, the Markovian approximation of the system's behaviour holds, and the $t'$ integral can be safely extended to $-\infty$. As such the value $\Gamma/\gamma$ gives an indication of how accurately the system can be treated as Markovian, with this holding to good accuracy when $\Gamma/\gamma \ll 1$. This will typically place some constraint on the plate separation $L$, for example the static two-plate setup result (3.39) for the transition rates $\Gamma$ has an $L^{-3}$ dependence. This sets some lower bound on the plate separations which are compatible with the Markov approximation, dependent on the medium properties and atomic transition frequency. The results of section 4.3 will show $\Gamma$ of the order $10^7 - 10^8 \text{s}^{-1}$, as opposed to the resonance width $\gamma \simeq 2 \times 10^{12} \text{rad/s}$, meaning that the system is Markovian to a good degree of accuracy.

### 4.1.4 Non-Retarded Limit

For the work of sections 3.2, 3.3 and 3.4 it was assumed that the the system could be treated in the non-retarded limit. As discussed when implementing the non-retarded form of the Green's tensor in section 3.2.1, this limit corresponds to distances much smaller than the atomic transition wavelengths. This regime is defined by $z_A \ll c/\omega_A$, where as in the previous section $z_A$ is the distance of the atom from either plate, and $\omega_A$ is the atomic transition frequency to be considered. This leads to an upper limit on $z_A$ which presents a possible problem for experiments where achieving small separations is a considerable challenge. As discussed previously the atom-plate separations achievable in experiments are normally of the order 200nm [13] and larger, a conservative estimate on the atom-plate separation $z_A$ is thus $1\mu$m. When considering atomic transitions with frequencies in the optical spectrum $\sim 10^{14}$rad/s, this sets an upper bound on $z_A$ in the non-retarded limit of $z_A \sim 3\mu$m. Thus as long as $z_A$ is chosen suitably, the non-retarded limit is a good approximation for almost all realistic systems where the effects of quantum friction could possibly be experimentally measured. It should furthermore be mentioned that molecules [24] and Rydberg atoms [26] generally have larger transition wavelengths than atoms and may thus be treated in the non-retarded limit over larger distance scales.

### 4.1.5 Zero Temperature

The assertion that the field is in its ground state is equivalent to the assertion that the temperature of the atom's surroundings is 0K at $t = t_0$, as the general thermal state of the field for $T = 0$K is simply the ground state of the system [4]. However it is a central result of thermodynamics that no system can ever be cooled to 0K. Nevertheless it can be shown that the temperature of the system has to be high before its effects on the initial field state must be taken into account. The electromagnetic field is a bosonic field, thus its state populations have a Bose-Einstein distribution for finite temperature, given as a frequency distribution by:

$$n(\omega, T) = \frac{1}{\exp\left(\frac{\hbar\omega}{k_B T}\right) - 1} \tag{4.11}$$

Using this equation it is possible to calculate the population of photon states at the atomic transition frequency, i.e. the frequency regime where the effects investigated in this work dominate over thermal effects. Considering a system at room temperature $T = 293$K and the transition frequency $1.544 \times 10^{14}$ rad/s for the transition in caesium considered later in section 4.3 leads to a photon population density of 0.018. This number is small, so to a good degree of accuracy the field can be considered to be at 0K for this transition at room temperature. However as the effect of thermal photons on the processes involved have not been investigated, a cooled system would produce a far lower number of photons. For example a system cooled to 150K would have a photon population density of $3.66 \times 10^{-4}$ at the given frequency. In fact in the measurement of the Casimir-Polder force in Ref. [13] it was estimated that black body effects accounted for roughly 1% of the measured effects. This shows that experimentally a sufficiently low temperature can be achieved such that temperature effects are negligible for atomic transitions in the optical range. Further details regarding the treatment of finite temperature can be found in Ref. [4].

Regarding an atom in a thermal state, the initial state of the atom was not specified at any point in the calculations. The stage at which the initial atomic state would be inserted would be in solving equations (3.13) and (3.14), i.e. the atom's spectroscopic properties themselves do not depend on the atom's initial electronic state. Were the friction force to be calculated for the two-plate set-up, it would be expected to depend in some way on the initial atomic state in analogy to the calculation of the friction force in a series approach for a general distribution of media [1, 4].

### 4.1.6 Born-Oppenheimer Approximation

Throughout chapter 3 it was assumed for the purposes of solving for the electronic dynamics that the atom moves with a constant velocity parallel to the two plates, the Born-Oppenheimer approximation. As discussed when it was introduced, the approximation can be introduced without disallowing the possibility of later calculating the friction force on the atom given that certain conditions are met. Here several sources of inaccuracy regarding the constant motion approximation are discussed. Firstly, the static Casimir-Polder force between an atom and a dielectric plate will produce an attractive force between them. For an atom exactly in the centre of the plates these forces will cancel, but for any other position the atom will experience a net force towards the nearer plate. This force increases the closer the atom is to the plate. By analogy with Refs. [1, 3] there is also expected to be a velocity dependent force opposing the atom's direction of motion, the friction force whose spectroscopic effects were examined in this report.

The validity of the approximation thus reduces to 2 points:

- Does the atomic velocity change sufficiently over the time scale of the interaction that this must be taken into account?
- If so, is the velocity dependence of the transition rates sufficiently flat that any changes in velocity can be ignored to a good degree of accuracy when considering the rates?

Regarding the first of these points, the atom must be found very close to the centre of the cavity, and the time scale of an experiment must be sufficiently short that no significant deflection due to these effects occurs. For the velocity dependent friction force the force is normally of a very small order of magnitude (thus the continued absence of experimental detection), so for realistic timescales the change in velocity is likely to be small. However, for the sake of argument it can be assumed that this force does have a significant effect on the atomic velocity, here the second point is also generally satisfied as the numerical results of this chapter will show. Crucially, there are no sharp peaks anywhere in the velocity dependence of the numerical results given later in the chapter. Thus by following the above guidance, uniform motion can be a good approximation assuming that the experiment is suitably constructed.

### 4.1.7 Long-Wavelength Approximation

In constructing the interaction Hamiltonian in section 2.4 the long-wavelength approximation was made. In the multipolar coupling scheme used throughout the work presented here, this enables the expression of the interaction Hamiltonian (2.46) in a very simple form. However this approximation rests on the assumption that the interaction of the atom with the field can be described purely as an electric dipole interaction. For atom-light interaction the long-wavelength approximation is valid if the wavelength of the light interacting with the atom is much larger than the atom's size [23]. For the atomic transition frequency $\omega = 1.544 \times 10^{14}$ rad/s quoted for the numerical results later in the chapter this corresponds to a wavelength of $12.2\mu$m, several orders of magnitude larger than an atom's size. For small point like atoms this is a good approximation, and although molecules and Rydberg atoms are larger in size, they also typically have larger transition wavelengths as discussed previously. Thus in general the long-wavelength approximation holds to good accuracy. Were it not to hold in some situation, the next highest order terms in such an expansion (by analogy with the perturbation theory calculation found in [15]) would correspond to the electric quadrupole and magnetic dipole terms. Also, when considering such higher order terms it would not be clear whether the diamagnetic terms in the multipole expansion of equation (2.35) could be discarded, so any attempt to include higher order terms would necessarily include a far larger number of terms in the interaction Hamiltonian. The

results of this work can only be considered applicable for atoms or molecules suitably small, non-magnetic, and with large enough transition wavelengths that their magnetic dipole and electric quadrupole terms can be safely ignored compared to the electric dipole terms. In practise the experimental work quoted in the introduction section all agreed with theory taken to electric dipole order.

## 4.2 Comparison of Approaches

In total three approaches were made to the analysis of the internal dynamics of a moving atom between two parallel dielectric plates. Here a discussion of the merits and drawbacks of each approach is presented. The three approaches are:

1. The Taylor expansion in the atomic velocity formulated generally in section 3.1 and applied specifically to the two-plate scenario in sections 3.2.2 and 3.2.3.

2. The insertion of the 2-plate Green's tensor into the calculation at an early stage of the calculation used in approach 1 to show the equivalence with a Doppler shift, calculated in section 3.3.

3. The naive insertion of a Doppler shift to the explicit 2-plate Green's tensor calculation, detailed in section 3.4.

Each will now be discussed in turn.

Approach 1 has the clear benefit of being applicable to any geometry; at no point are any assumptions made about the properties of the Green's tensor beyond the general properties derivable from the defining equation (2.15). This generality is why no complete treatment of the atomic velocity dependence is possible, only by making further assumptions about the form of the Green's tensor or by inserting an explicit tensor as in approaches 2 and 3 can a full treatment be attempted. The second main benefit of this approach is that it is capable of including magnetic terms with relative ease, something considerably harder when treating the dynamics completely (i.e. considering all terms in the velocity series expansion). This is beneficial when the system to be considered is not to be considered in the non-retarded limit, as there the magnetic terms no longer disappear. The treatment of the two-plate set-up was significantly simplified by the possibility of ignoring the magnetic terms due to it being considered in the non-retarded limit. However for larger distances between the atom and plates the non-retarded limit becomes a poor approximation, and the inclusion of magnetic field terms becomes necessary. Outside of the non-retarded limit the non-retarded form of the two-plate tensor may of course not be used either, making treatment of the system even more mathematically awkward. However the simpler form of the series used in approach 1 also better facilitates the inclusion of a more complex Green's tensor than the more difficult calculations of section 3.3.

Approach 2 is to be viewed as a necessary step on the way to applying a naive Doppler shift to the frequency received by the plates in approach 3. The key point of approach 2 is that by using a full description (subject to the convergence conditions discussed earlier) of the electric interactions of the two-plate system not limited to some order in $v$, it can be shown that the velocity dependence of the transition rates and frequency shifts can be included in the results by a Doppler-shifted frequency being received at the plates. This is by no means a trivial result, as the two-plate set-up does not always have analagous behaviour to the simpler single-plate setup, where the Doppler shift can be inserted without too much insecurity due to the interpretation of a single-reflection off a plate describing the process accurately. The main achievement of this work is to show that the problem can be significantly simplified (in the non-retarded limit at least) by inserting the velocity dependence of the results directly into the frequency dependence.

This enables immediately the possibility of considering the velocity dependence of results to all orders, rather than requiring a Taylor series expansion of the type found in section 3.1. The drawbacks are as already mentioned the limitation to the non-retarded limit as magnetic effects were not accounted for, and also the specification of the two-plate system over a more general distribution of media.

## 4.3 Numerical Results

This section contains a discussion of the results obtained at the end of section 3.3, which describe the effects of the electric interaction of a moving atom with two parallel plates on the atom's rates and shifts in the non-retarded limit.

Throughout this section unless noted otherwise the following material and atom properties will be used. A Drude-Lorentz model permeability function describing a material with one dominant resonance is used:

$$\epsilon(\omega) = \eta\left(1 - \frac{\omega_P^2}{\omega^2 - \omega_T^2 + i\gamma\omega}\right) \tag{4.12}$$

$$r_p(\omega) = \frac{\epsilon(\omega) - 1}{\epsilon(\omega) + 1} \tag{4.13}$$

For a given material this is characterised by the plasma frequency $\omega_P$, the absorption frequency $\omega_T$, the resonance width parameter $\gamma$, and finally $\eta$ which accounts for the effects of other resonances in the material. The parameters used in this section correspond to those of an atom of $^{133}$Cs in the presence of sapphire plates, where the caesium $6D_{3/2} \rightarrow 7P_{1/2}$ transition is very close in frequency ($1.544 \times 10^{14}$rad/s) to the resonant requency of sapphire [9]. The dipole moment for this transition is assumed to be isotropic and has a magnitude of $5.85 \times 10^{-29}$ Cm, and the Drude-Lorentz parameters for sapphire are $\omega_T = 1.08 \times 10^{14}$rad/s, $\omega_P = 1.2\omega_T$, $\gamma = 0.02\omega_T$, $\eta = 2.71$. The plate separation will be taken to be $L = 1\mu$m, as experimentally this is a distance as small as can be normally achieved (the Sukenik measurement of the Casimir-Polder force [13] for example achieved a separation of $\sim 1\mu$m). Furthermore, the main focus shall be on the transition rate $\Gamma = 2\text{Re}[C]$ for this transition in caesium, and only the resonant contributions shall be considered. The imaginary part of $r(i\chi)$ can be shown to be 0 because of the property $r^*(i\chi) = r((-i\chi)^*) = r(i\chi)$, which is a general property of these functions as discussed in chapter 2, although it also follows from the above definitions (4.12) and (4.13). If all terms including the reflection coefficient $r(i\chi)$ have no imaginary part, the expression for the non-resonant coefficients (3.77) must be purely imaginary, meaning that they contribute nothing to the decay rates. For completeness the real part of $r(i\chi)$ is shown in figure 4.2.

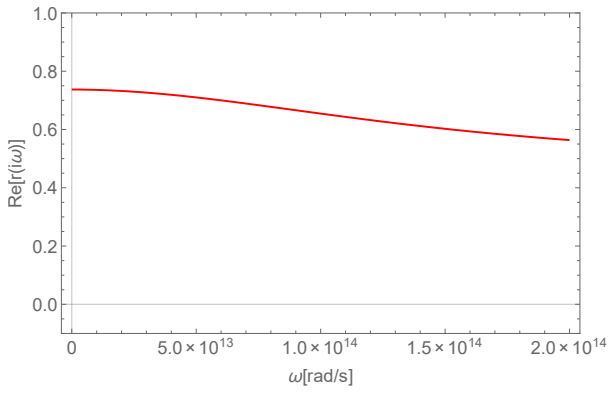


Figure 4.2: Plot of the real part of the non-retarded reflection coefficient for a purely imaginary argument $i\omega$.

### 4.3.1 Atomic Position

First to be considered is the dependence of the transition rates and frequency shifts on the position of the atom, shown in figure 4.3. A key feature of this diagram is that the smallest medium induced transition rate $\Gamma_{ab}$ and frequency shift $\delta\omega_{ab}$ is found when the atom is exactly in the centre of the 2 plates, at values of $1.69 \times 10^6 s^{-1}$ and $-1.36 \times 10^5$rad/s respectively. This is in comparison to the free space transition rate for this transition, which is given by the Einstein A-coefficient as $\Gamma_0 = \tilde{\omega}^3 |\vec{d}|^2 / 3\pi\epsilon_0\hbar c^3 = 5.31 \times 10^4 s^{-1}$. Thus in this case the rate of electronic transitions due to the media is roughly 2 orders of magnitude larger than the rate of transitions in free space, which in principle should be measurable. In comparison, consider the form of the shifted transition frequency $\tilde{\omega}_{ab} = \omega_{ab} + \delta\omega_a - \delta\omega_b$. Assuming all other transitions involved in the sum (3.17) to contribute a negligible amount due to being far from the medium resonance, $\delta\omega_a \simeq \delta\omega_b \simeq \delta\omega_{ab}$, it can be seen that the total shift in the transition frequency will be very small. Thus in the plots to follow the focus will be on the transition rates due to media rather than the frequency shifts, as experimentally these are far more likely to be detected. The smallness of the transition frequency shift compared to the bare transition frequency also justifies the insertion of the bare transition frequency $\omega_{ab} = 1.544 \times 10^{14}$rad/s rather than the shifted frequency $\tilde{\omega}_{ab} = \omega_{ab} + \delta\omega_a - \delta\omega_b$ into the results of section 3.3 when evaluating the results numerically. In principle if a frequency shift for any particular transition were large it would be necessary to solve for the shifted transition frequency perturbatively.

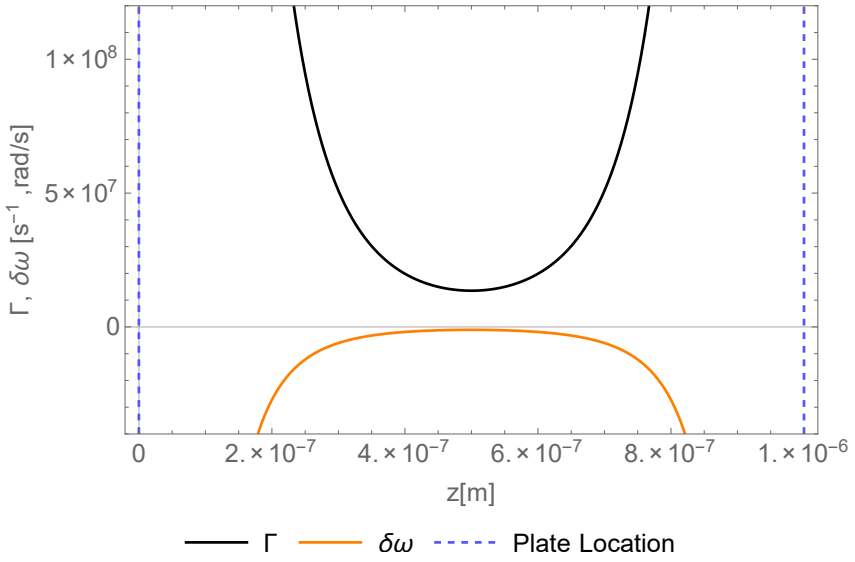


Figure 4.3: Plot of the resonant contributions to the medium-induced atomic transition rate $\Gamma$ and frequency shift $\delta\omega$ as a function of the atomic coordinate $z$ with $v = 10^3 \text{ms}^{-1}$ between two plates with a separation of $1\mu$m. The two plates are located at the blue dotted lines.

In figure 4.3 the position dependence is only shown for a range of atom-plate separations close to the centre of the cavity. This is because of the attractive Casimir-Polder force between an atom and a plate, which scales (for the single plate) with $z^{-4}$ in the non-retarded limit [20], where $z$ is the distance of the atom from the plate. In the centre of the cavity this attractive force must be zero as the two forces from the two plates cancel, however moving closer to one plate strongly increases the attractrive force. Thus in any experimental apparatus only atoms which are reasonably close to the centre can be considered to be unaffected by this force, an important point as in the work presented here the possibility of motion perpendicular to the

plane surface was not considered.

### 4.3.2 Atomic Transition Frequency and Velocity

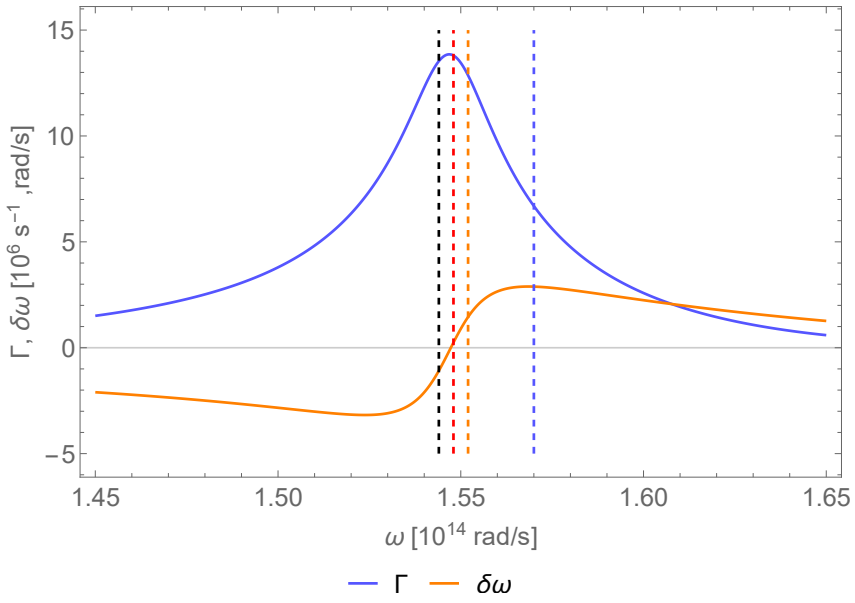


Figure 4.4: Plot of the resonant contributions to the medium-induced atomic transition rate $\Gamma$ and frequency shift $\delta\omega$ as a function of the atomic resonance frequency $\omega$ for a static atom in the centre of two plates of separation $1\mu$m. The dashed vertical lines show the locations of the colour-labelled detunings from the resonance used in figures 4.5 and 4.6.

The atomic transition frequency and velocity are closely related to one another by virtue of the Doppler shift introduced in equation (3.78). Figure 4.4 shows the dependence of the electronic transition rate and frequency on the bare resonance frequency of this transition. The transition rate peaks almost exactly at the transition frequency of the transition in caesium discussed earlier, at $\omega = 1.544 \times 10^{14}$rad/s. The frequency shift is at its most positive and negative for slightly larger and small atomic frequencies respectively, however for the reasons just given the focus will be on the transition rates for the remainder of this chapter. Figure 4.4 shows the static case, however it provides a useful intuition as to how the Doppler shift will affect the results for the moving atom. For the static case the reflection coefficients are all evaluated at the atomic resonance $\tilde{\omega}_{ab}$, which for the moving atom becomes $\tilde{\omega}'_{ab} = \tilde{\omega}_{ab} + vk^{\parallel}\cos(\phi)$. Both $k^{\parallel}$ and $\phi$ are variables to be integrated over, complicating matters, however the key point is that the inclusion of the atom's motion leads to a sampling of frequencies other than the atom's transition frequency. The 'amount' of spreading/sampling is given by the velocity $v$, and also the range of $k^{\parallel}$ around which the the $k^{\parallel}$ integral contributes most. The factors of $\left(k^{\parallel}\right)^2 e^{-2k^{\parallel}L}$ in the results (3.76) mean that this region can be taken to be in the vicinity of $k^{\parallel} \sim 1/L$ where this $k^{\parallel}$ integrand is maximum. Thus by using the fact that $\cos(\phi)$ ranges from $-1$ to 1 over a cycle, the amount of sampling for a given velocity is roughly given by $2v/L$. Using the estimates quoted in section 4.1: $v \simeq 10^4 \text{ms}^{-1}$ and $L \simeq 10^{-6}$m leads to a sampling of around $10^{10}\text{s}^{-1}$. This is much smaller than the transition frequency of the caesium transition considered here $\omega \sim 10^{14}$rad/s, which leads to the expectation that velocity dependent effects on the atomic transition rates are small compared to the static effects.

The spreading however does imply certain behaviour regarding how the velocity of an atom will affect its medium-induced transition rates. If $|d\Gamma/d\omega|$ is larger on the side of the resonance,

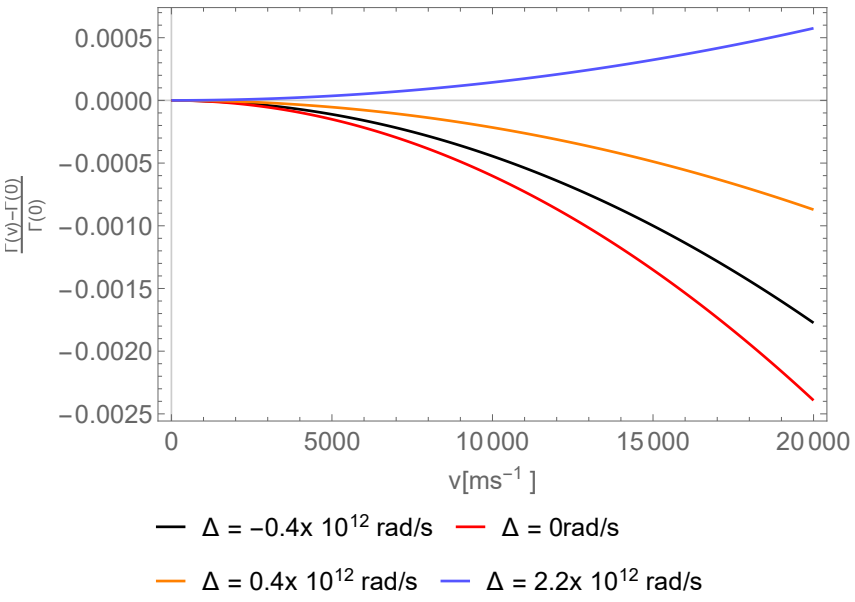


Figure 4.5: The velocity dependent transition rates proportional to the static rates evaluated for 4 different detunings $\Delta$ from the resonance. The case $\Delta = -0.4 \times 10^{12}$ rad/s corresponds to the actual resonance frequency for the caesium transition $6D_{3/2} \rightarrow 7P_{1/2}$.

i.e. $d^2\Gamma/d\omega^2$ is $> 0$ to the left of the resonance or $< 0$ to the right, then the velocity spreading will lead to a larger $\Gamma$ than for the static case. The reverse holds if the change of the gradient is the opposite way around. This matches exactly with what is shown in figure 4.5. In this figure the velocity dependence of the transition rates for four possible transition frequencies is shown, with a larger range of velocities than previously shown to highlight the dependence's behaviour at larger $v$. The black line corresponds to the actual transition frequency for the resonant caesium transition, the other lines to other transition frequencies near the resonance, which is roughly (as seen from figure 4.4) at $\omega = 1.548 \times 10^{14}$rad/s. Being situated very near to the resonance the smearing caused due to the larger velocities do indeed lead to a smaller transition rate for the caesium transition, as here $d\Gamma/d\omega > 0$ and $d^2\Gamma/d\omega^2 < 0$ by inspection. However the fact that the transition does not lie exactly on the resonance can be seen from the plot for $\Delta = 0$rad/s compared to the caesium frequency plot, which has a stronger negative velocity dependence as smearing in both directions from the resonant frequency leads to smaller transition rates. As expected, the transition rate for $\Delta = 2.2 \times 10^{12}$rad/s does indeed increase with velocity compared to the static case, as is expected from the previous discussion and figure 4.4. A final point to note is that the increase/decrease of the transition rates caused by the atomic velocity is indeed small compared to the static rates, the origin of which can be traced to the amount of smearing ($\sim 10^{10}$rad/s) compared to the scale of the transition frequencies ($\sim 10^{14}$rad/s). To find a large effect due to the atomic motion the ideal situation would be to have a combination of:

- a transition frequency at the region of largest/most negative $d^2\Gamma/d\omega^2$ depending which side of the resonance the transition frequency is on. Thus the maximum effect is achieved by the argument above.
- a small medium resonance frequency to bring the factor $vk^{\parallel}_{max}$ closer in magnitude to the frequency.
- a very small plate separation such that the integral over $k^{\parallel}$ contributes mostly in a region of larger $k^{\parallel}$.

- a larger atomic velocity.

The first two of these may simply be achieved by finding a suitable material and atomic transition which achieves these aims, the limitations on the second two points have already been discussed in section 4.1.

### 4.3.3 One Moving and One Stationary Plate

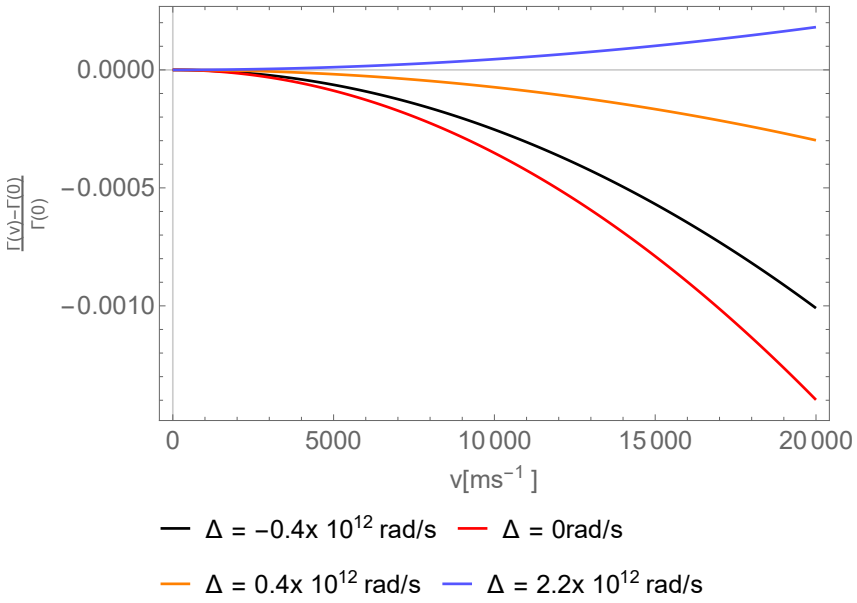


Figure 4.6: The transition rates compared to the static rates for a system where the atom and one plate are stationary and the second plate moves with velocity $v$, plotted as a function of this velocity $v$ for the four different detunings $\Delta$ of figure 4.5.

Here it is investigated whether a system of the type originally envisaged by Guo and Jacob [14], two plates in relative motion such that the Fabry-Perot resonance condition is satisfied, might be realised by the formalism here. This approach would have the advantage of having an atom in the centre of the plates whose internal or external dynamics might be used as a probe of the velocity dependent effects. The initial problem that presents itself is that the treatment of the system here is not Lorentz covariant, so is thus unsuitable for the relativistic treatment given to the plates in the above work. Furthermore the requirements placed on the velocity in section 4.1.2 will be presumed still to hold. Taking the non-relativistic limit of the results given in [14] and assuming the main contribution to the results occurs at the wavevector $k^{\parallel} = L^{-1}$ as previously leads to the resonance velocity $v_{res} = 2\omega_{ab}L$, where $\omega_{ab}$ is the atomic resonance frequency, and $L$ is the plate-plate separation. However this is clearly at odds with the requirement in section 4.1.2: $v \ll 2\omega_{ab}z_A$, where $z_A$ is the atom-plate separation, as $z_A < L$. This means that the treatment of the system here is not suited for dealing with exactly the kind of resonance discussed in Ref. [14]. It is nevertheless interesting to consider the system for smaller single-plate velocities to see if an amplification of the transition rates occurs in such a system for smaller velocities. As it was shown that the movement of the atom can be accounted for by inserting a Doppler shift to the frequency received at the plate, the movement of a single plate next to a stationary second plate and atom is accounted for by inserting the Doppler shifted frequency into one plate's reflection coefficients but not the other's. The results for a range of plate velocities are plotted in figure 4.6. However by inspection the results are very similar to the (far easier to experimentally realise) moving atom and stationary plates scenario

considered until now, but with a smaller velocity dependent shift. Thus the results of this work may be applied to the moving plate within a certain range of plate velocities, but no significant enhancement of the medium-induced effects is seen.

### 4.3.4 Plate Separation

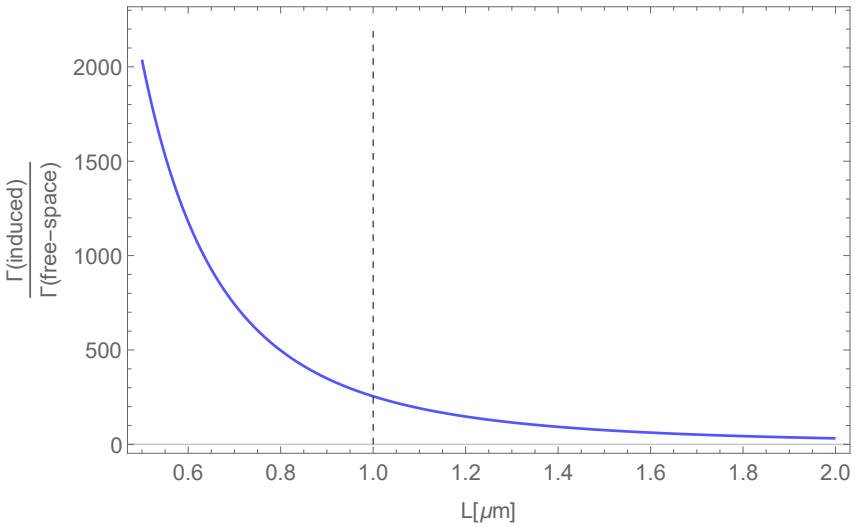


Figure 4.7: Plot of the medium-induced atomic transition rate $\Gamma$ as a function of the plate separation $L$ for a stationary atom situated in the centre of the plates. The results are normalised to the free space transition rates $\Gamma_0 = \tilde{\omega}^3|\vec{d}|^2/3\pi\epsilon_0\hbar c^3 = 5.31 \times 10^4 s^{-1}$.

The dependence of the transition rates on the plate separation $L$ is plotted in figure 4.7, which shows clearly the expected increasing effect as the plates are brought closer together. As discussed previously, the $1\mu$m plate separation used throughout this chapter and plotted as the dotted line in figure 4.7 is based on the achievements of previous experiments [13], and can be viewed as a realistic expectation of the results obtainable in some future experiment. However it also shows a clear motivation for attempting to bring the plates closer together, as the medium-induced transition rates rise sharply as the plate separation is reduced.

### 4.3.5 Dipole Moment

The dependence of $C_{ab}$ and thus $\Gamma$ on the dipole moment, ignoring its directionality, scales with $d_{ab}^2$. Thus a simple way of increasing the effect of medium induced transition rates and frequency shifts would be to use an atom with a large dipole moment, most simply achieved by using a large 'Rydberg' atom. However, in section 2.3 the long-wavelength approximation was made, meaning that the atom was treated as a point-like electric dipole. Using that atom sizes in their ground states are normally of the order $\sim 0.1$nm [27], with a transition in the optical range $\lambda \sim 10\mu$m, shows that generally the treatment of an atom as a dipole is correct to about 5 orders of magnitude. Thus for atoms the dipole moment may (theoretically) be taken to be as large as is realistic for a single atom, i.e. as calculated from the 'size' of an excited atom. In principle the same argument holds for small molecules, however very many molecules are polarised in their energy eigenstates, meaning that the assumption made at the end of section 3.1 no longer holds. If a suitable unpolarised molecule can be found, in general it should also be suitable for use in these results, assuming its transition wavelengths are not especially small.

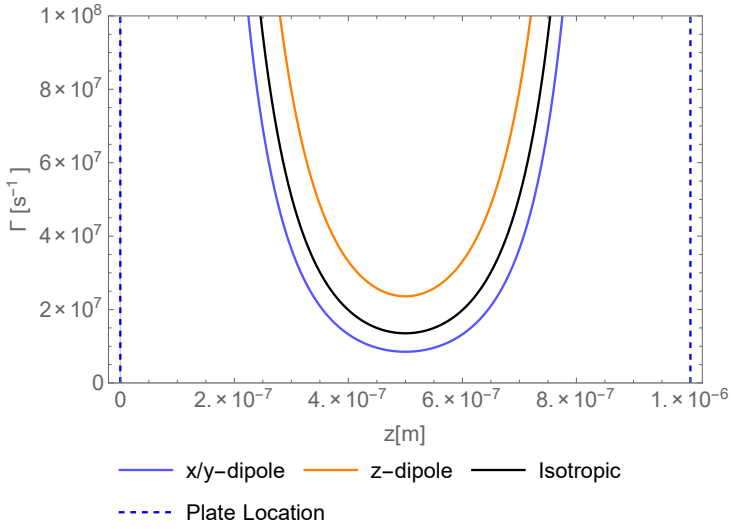


Figure 4.8: The position dependence of the medium-induced transition rates for an atom with velocity $3 \times 10^3$ ms$^{-1}$ for three possible dipole orientations.

With regard to the directionality of the dipole moment, as the system has 3 distinguished directions, the results are expected to distinguish between all axes. By assuming real dipole moments (which occur as a result of the atom having a time-reversal invariant Hamiltonian), i.e. $\vec{d}_{ab} = \vec{d}_{ba}$, it is easy to show from the form of equations (3.30), (3.55) and (3.76) that the dependence of C on the dipole moment can be expressed as:

$$C_{ab} \propto \int_0^{2\pi} d\phi \left[\mp \cos^2(\phi) d_x^2 \mp \sin^2(\phi) d_y^2 \mp \cos(\phi)\sin(\phi)\, d_x d_y + d_z^2\right] F(\phi) \tag{4.14}$$

Here the dipole moment was split into its cartesian components $d_i$. The minus signs refer to terms including $\mathbf{A}(\phi)$ and plus to $\mathbf{B}(\phi)$, and $F(\phi)$ refers to the other $\phi$ dependences. For simplicity in all the other plots of this section the dipole moment is assumed to be isotropic, i.e. proportional to $(1,1,1)^T$ in cartesian coordinates. Figure 4.8 shows the effect a dipole moment of specific directionality has on the transition rates, with the isotropic result of figure 4.3 given for comparison. A dipole moment in the $z$-direction produces the largest medium induced transition rate, however the difference between a dipole in the $x$ or $y$ direction produces no distinguishable difference. This can be attributed to the general weakness of velocity dependent effects, they do not contribute sufficiently to the results to substantially break the symmetry of results for dipoles in the $x$ or $y$ axes. From the form of equation (4.14) it is clear that for the cases presented in figure 4.8 the results are independent of the sign of $d_i$ as long as either $d_x$ or $d_y$ are 0. However more generally when it is not the case that either $d_x$ or $d_y$ is 0, a change in the sign of either of these will change the transition rate due to the sign of the third term of (4.14) changing. No such change occurs for $d_z$ as the system is symmetric with respect to a reflection in the $x$-$y$ plane at $z = -L/2$ (see figure 3.1). Figure 4.8 does however reinforce the choice of an isotropic dipole moment in the other plots, as it leads transition rates slower than a purely z-dipole, but faster than an x or y dipole. A final point is that in the $v = 0$ limit of the above equation, it is easy to see from equation (3.76) that $F(\phi) = 1$, meaning that by inspection of equation (4.14) that the red and blue curves in figure 4.8 must coincide, although this effect is so small that in figure 4.3 it is not apparent. This matches the physical requirement that when the atom is stationary there is no longer any distinction between the x and y axes.

### 4.3.6 Non-Equal Plates

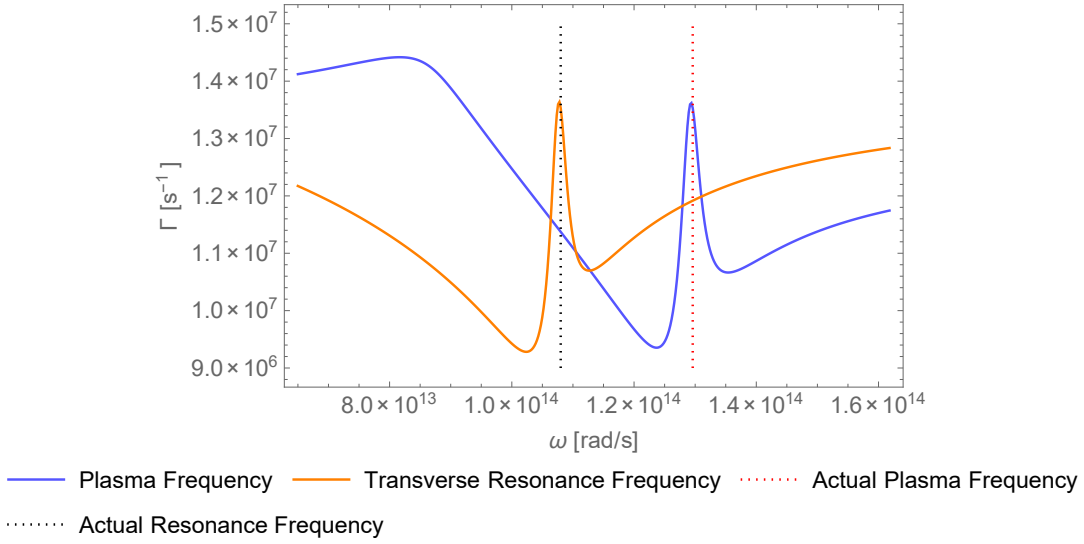


Figure 4.9: The dependence of the medium-induced transition rate $\Gamma$ on the plasma frequency $\omega_P$ and lateral transition frequency $\omega_T$ of one of the plates when each are independently varied. All other parameters are kept constant as for the sapphire-caesium system and the system is considered for $v = 3 \times 10^3 \text{ms}^{-1}$ and $z_A = L/2$.

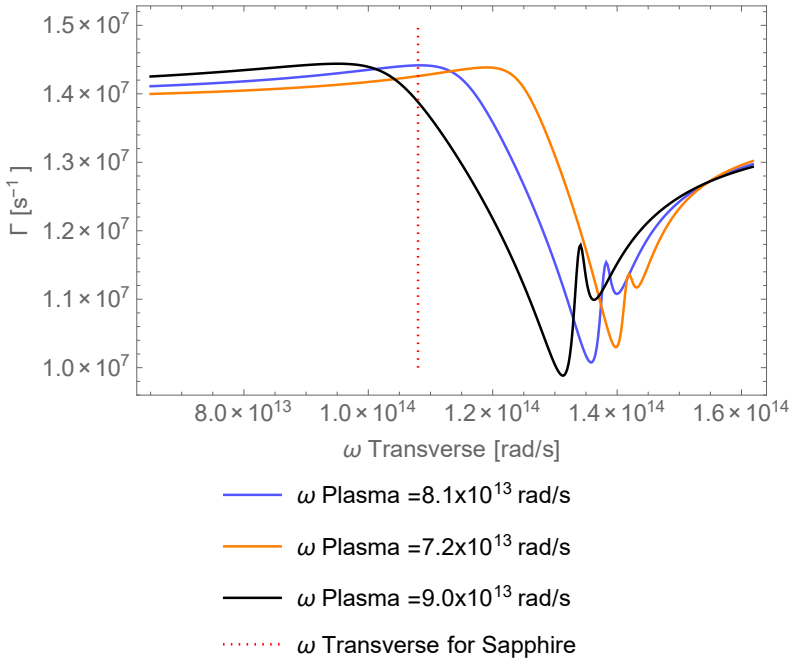


Figure 4.10: The dependence of the medium-induced transition rate $\Gamma$ on the lateral transition frequency $\omega_T$ of one of the plates for several plasma frequencies $\omega_P$ near the largest peak of figure 4.9. All other parameters are again kept constant as for the sapphire-caesium system and the system is considered for $v = 3 \times 10^3 \text{ms}^{-1}$ and $z_A = L/2$.

One further possibility which can be investigated using the results of this work is whether substantially different results can be achieved by the use of two plates whose dielectic properties are not identical. This is done most simply by keeping the properties of one plate fixed and varying the plasma frequency $\omega_P$ and transverse resonance frequency $w_T$ for the second plate independently of each other. The result of such varying of the Drude-Lorentz parameters is shown in figure 4.9. The key feature is that the actual parameters for sapphire correspond to local maxima, so there is no slight tweaking of material parameters which would lead to substantial enhancement of the effects due to the media. However, the second peak in the vicinity of $\omega_P = 8.1 \times 10^{13}\text{s}^{-1}$ is worth investigating to see if further adjustements to the parameters in this region produce a significantly larger effect. However as figure 4.10 shows, when evaluated over a range of $\omega_T$ for 3 possible values of $\omega_P$ near this resonance, all peaks of the transition rates $\Gamma$ are of similar order to the largest peak in figure 4.9, and also in a similar region. Thus there appears to be no simple way to use the possibility of two plates of different dielectric properties to enhance the effects of the medium on a moving atom, at least not by merely changing the frequency parameters of one medium.

### 4.3.7 Non-Additivity of Results

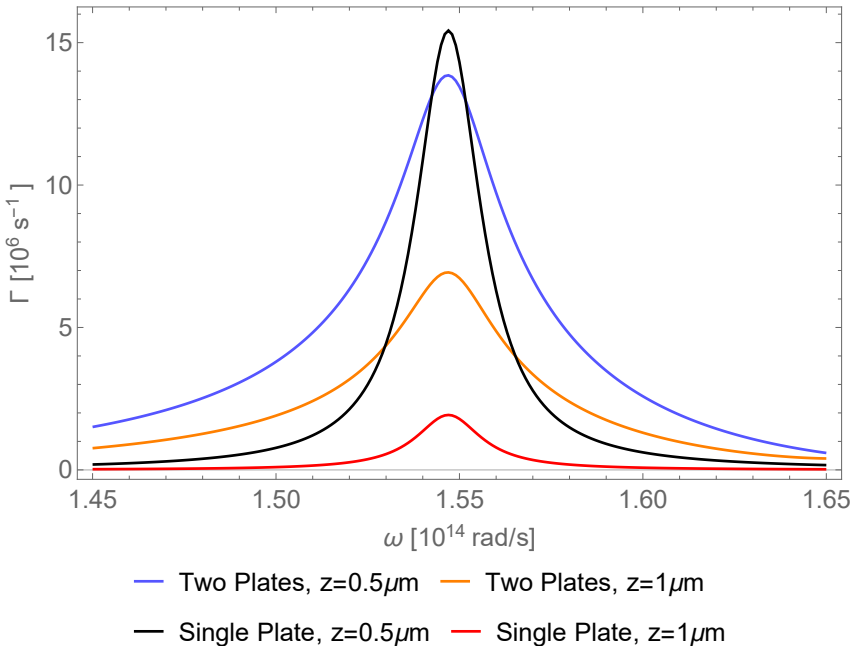


Figure 4.11: A comparison of the medium-induced transition rates $\Gamma$ for the double-plate result with the single-plate result, plotted as a function of the atomic transition frequency $\omega$ for two different atom-plate separations $z$.

The rationale for carrying out the investigation of the Casimir-Polder effects on a moving atom between two parallel plates, as detailed in the Introduction, was to establish if it might offer a route to detection of velocity dependent Casimir-Polder effects. These effects are sufficiently weak that in experiments to date (e.g. [12, 13]) they may be safely ignored compared to the static effects, thus any foreseeable experimental detection of these effects would require a significant enhancement of the velocity dependence. Figure 4.11 shows a comparison of the decay rates induced by the double plate system, as opposed to the results for an atom next to a single plate. The single plate result can either be quoted from the results of Ref. [3], or can be reached by taking the results of section 3.3 in the limit $r^-(\omega) \to 0$. From figure 4.11 it can be seen that the behaviour of the two-plate system is completely different from the single-plate system, and

thus that the approximation of the double-plate system as two single-plates does not in general give accurate results. For the $0.5\mu$m atom-plate separation used mostly throughout this chapter the double plate set-up actually results in medium-induced transition rates smaller than if there were only one plate present. However for the larger $1\mu$m separation the two plate set-up leads to the more intuitive larger transition rates. The key difference between the double and single plate result is the factor of $[1 - r^2(\omega)e^{-2k^{\parallel}L}]^{-1}$, and as it was shown in section 4.1.1 that $|r(\omega)|$ can be much larger than 1 near the resonance, this shows how the effect of the double-plate set-up on the atomic dynamics can in some situations be smaller than the single plate. By changing $L$ as is done in figure 4.11 (as for the two-plate situation here $L = 2z$), and thus changing the amount of the $k^{\parallel}$ integral where $|[1 - r^2(\omega)e^{-2k^{\parallel}L}]^{-1}|$ is less than one, this factor can be made to contribute more than for the single plate case. This is exactly what is seen for the atom-plate separation $z = 1\mu$m in figure 4.11, where the double plate rates are much larger than for the single plate. Thus to achieve a reasonable enhancement of the effect by adding another plate to the single-plate set-up requires careful tuning of the atom-plate separation, although of course as shown in figure 4.7 a smaller plate separation also leads to larger medium-induced transition rates. An experiment must therefore maximise the effects by controlling these two dependences in a suitable manner.

## 4.4 Applicability to Experiment

As discussed in section 4.3.3, the work here is not capable of treating or finding a resonance of the type found by Guo and Jacob [14], due to constraints on the velocities for which the results presented here are valid. However the general velocity dependence of Casimir-Polder effects for an atom moving between two plates has been formulated, with several indications of how these effects might be made larger such that they may reach experimentally measurable levels. Experimental confirmation of the results presented here for the velocity dependence of Casimir-Polder effects would indicate how accurate the results of the experiments mentioned in section 1 are. This is because almost all of the experiments discussed in the introduction section involved moving atoms whose interaction with matter was calculated as though they were static [10, 11, 12, 13], and identifying the limitations of this approximation is vital to furthering the understanding of and ability to experimentally investigate Casimir-Polder effects.

The work here presented a calculation of the spectroscopic effects, which have been measured in analogous static situations by Ref. [12]. However the calculation of the friction force on the atom can also be calculated directly [4] from the expressions obtained here for the medium-induced transition rates. Thus a theory capable of describing both measurable quantities has been established here, although due to time constraints it could not be carried out in its entirety.

# Chapter 5

# Conclusions

## 5.1 Summary

The aim of this work was to find a resonance in the Casimir-Polder transition rates and shifts experienced by an atom moving between two parallel plates. This was an attempt to find a situation whereby the velocity-dependence of the medium-induced rates and shifts would become large enough that it would in principle become experimentally measurable. As a first step the transition rates and frequency shifts were calculated using Macroscopic QED for arbitrary geometries in a series expansion in the atomic velocity $v$, where the contribution of this work was to calculate the second order term in $v$ in addition to the zeroth and first order terms given in Refs. [1, 4]. This result was then applied to the two-plate scenario, and here it was shown that unlike the first order term in $v$ the second order term makes a contribution to the atom's shifts and rates.

Following this the two-plate geometry was treated to all orders in $v$ in the non-retarded limit by inserting the specific form of the two-plate Green's tensor at an earlier stage in the calculation of the medium-induced rates and shifts. The results obtained in this way are the main focus of the work. The specific example of the $6D_{3/2} \rightarrow 7P_{1/2}$ transition in $^{133}$Cs, which is close to a resonance in a sapphire medium, was evaluated numerically, and here it was shown that the medium-induced effects are much larger for the transition rates than for the frequency shifts when compared to the free-space effects. For this reason, and also because the transition rates lead directly to the calculation of the friction force on the atom [4], the discussion chapter was devoted mostly to an investigation of the characteristics of the medium-induced transition rates. As expected the transition rates were shown to increase for smaller plate separations. However when comparing to the results for an atom next to a single plate [3] it was shown that the double plate geometry gives slower transition rates than the single plate system for the $0.5\mu$m atom-plate separation achieved by Sukenik et al. [13], when the atom-plate separation is equal for both systems. For larger atom-plate separations it was shown that the double plate system does produce faster rates than the single-plate system.

The effect of the atomic velocity on the results was shown to be equivalent to evaluating the reflections of evanescent waves off the surfaces at a non-relativistically Doppler-shifted frequency. This means that the velocity dependence of the system depends itself on the detuning of the atom and medium resonances, as a result of the fact that the Doppler-shift leads to a spreading of the frequencies sampled in the wavevector integrals used in calculating the rates and shifts. However no strong resonance which substantially exceeds the static result was found for any velocity. Furthermore it was shown that the velocity constraints in this analysis are mutually exclusive with the velocities required to use the atom as a probe of the massive resonance of the moving two-plate system proposed by Guo and Jacob [14]. For an isotropic atomic electric

dipole moment $\vec{d}$ the dependence of the transition rates was shown to recover the Lennard Jones [6] $d^2$ dependence, although the rates caused by a non-isotropic dipole moment are heavily orientation dependent.

With the results of this work and Ref. [3] it should be possible in principle to maximise both Casimir-Polder effects themselves and their velocity dependence, where the maximum effects are sought with the possibility of using either a single or double plate set-up. Due to the general weakness of both effects, this is an invaluable tool in increasing their detectability, especially as it has been shown that for different separations either the single- or double-plate transition rates can be larger. The calculation of the friction force on the atom could not be completed due to time constraints, however using the obtained results for the transition rates a calculation along the lines of Ref. [3, 4] of the friction force can be determined in a straightforward way.

## 5.2 Outlook

The main extension of this work would be to proceed with the calculation along the lines of Refs. [3, 4] to calculate the velocity dependent Casimir-Polder force on the atom for the two-plate set-up. This is possible using the expressions obtained for the transition rates (3.76), and in principle should not be a substantially larger task than that carried out already in calculating the medium-induced transition rates and frequency shifts of the atom.

The main approximation made in this work which has the possibility of being carried out differently is the consideration of purely non-retarded effects. In general in electrodynamics a problem which is unsolvable in the medium range may be solvable in the non-retarded or retarded limits [16]. An example of this in Casimir-Polder physics is the first formulations of the non-retarded [6] and retarded [7] Casimir-Polder processes between an atom and a perfect conductor. The rationale for carrying out the two-plate calculations in the non-retarded limit was detailed in section 4.1.4, however the work of section 3.1 retains the magnetic field terms and thus is suitable for use in the retarded limit. The retarded limit corresponds in this case to the atom-plate separations $z_A$ being much larger than $c/\omega_A$, with $\omega_A$ the atomic transition frequency. In this regime the effects of the electric field become negligible compared to those of the magnetic field, so markedly different behaviour compared to the non-retarded result is expected. A further contribution to this different behaviour may be that in the retarded limit the influence of the magnetic dipole moment of the atom may be non-negligible, changing the form of the Hamiltonian describing the system dynamics substantially.

A second possibility for the extension of applicability of the work presented here is the insertion of rotating atomic dipole moments. A rotating dipole moment is caused by an atomic Hamiltonian whose parity is odd under time reversal, which leads to the dipole moment being complex rather than real. It has been shown [28] that this can lead to a lateral Casimir-Polder force (a force perpendicular to the direction of propagation of the wave) on an atom near an optical nanofiber. Lateral forces are often accompanied by torque on the atom considered [29], and may thus have applications in opto-mechanical systems or as a quantum mechanical rotor. Such behaviour has yet to be investigated for a two-plate system. At several stages in this work it was assumed that the dipole moments were real for calculational convenience, in principle it should be possible to re-evaluate many results presented here for the more general case of complex dipole moments.

This work was limited to the case of atomic motion parallel to the plate surfaces, so a natural extension would be to include the possibility of a non-zero component of the atomic velocity perpendicular to the plate surface. This could possibly be extended along the lines of the treat-

ment of perpendicular motion for the atom-single plate scenario investigated fully in Ref. [3]. In the work presented here for the two-plate set-up motion was restricted to motion parallel to the plates, because an atom moving far from the parallel trajectory will be absorbed by one of the plates before traversing the full length of the apparatus. This effect is enhanced by the attractive static Casimir-Polder force [6] for atoms not in the centre of the two plates.

The work of the paper by Guo and Jacob [14] which was the motivation for this work considered their system relativistically throughout, an aspect which was not carried over to this investigation of the interaction of an atom with two parallel plates. As it was shown that the velocity condition for the giant two-plate resonance to occur was at odds with the requirements placed on the atomic velocity in this work, a treatment of the atom and two-plate system with a larger range of validity for the velocity could possibly reveal the effects of the plate-plate resonance on the atom. A Lorentz covariant treatment of this system is one promising possibility for extending this work such that it might describe the massive resonance in the set-up envisaged by Guo and Jacob.

# Acknowledgements

Firstly I would like to thank my supervisor Stefan Buhmann, for making a great effort throughout my time in Freiburg to help me make the most of my stay here, and for always being there for questions and queries. I also owe a great deal to Juliane Klatt for always being around and ready to share her detailed knowledge of Macroscopic QED and moving atoms, and also for all her suggestions when it came to writing this report. Special mention must go to Josh Hemmerich and Robert Bennett for general motivation/distraction and help with all things LaTeX and Mathematica related. Finally in Freiburg I would like to thank all of the Quantum Optics and Statistics group under Andreas Buchleitner for making my time with them an absolute pleasure and encouraging an interest in physics I didn't even know I had. Back in Imperial College I'd like to thank Florian Mintert for his Freiburg insider knowledge and advice, and Jonathan Eastwood for his advice and understanding whenever I needed it. And last of all I'd like to thank my parents, my brothers Rob and Matt, my grandparents and everyone else from home for helping me get where I am today and supporting me throughout my studies.

# Bibliography


[1] S. Scheel and S. Y. Buhmann. Casimir-Polder forces on moving atoms. *Phys. Rev. A*, 80(4):042902, 2009.

[2] J. M. Wylie and J. E. Sipe. Quantum electrodynamics near an interface. *Phys. Rev. A*, 30(3):1185, 1984.

[3] J. Klatt, R. Bennett, and S. Y. Buhmann. Spectroscopic signatures of quantum friction. *arXiv:1601.02765*, 2016.

[4] S. Y. Buhmann. *Dispersion Forces II - Many-Body Effects, Excited Atoms, Finite Temperature and Quantum Friction*. Springer-Verlag, Berlin Heidelberg, 2012.

[5] G. Bressi, G. Carugno, R. Onofrio, and G. Ruoso. Measurement of the Casimir Force between Parallel Metallic Surfaces. *Phys. Rev. Lett.*, 88(4):041804, 2002.

[6] J. E. Lennard-Jones. Processes of adsorption and diffusion on solid surfaces. *Trans. Faraday Soc.*, 28(0):333–359, 1932.

[7] H. B. G. Casimir and D. Polder. The Influence of Retardation on the London-van der Waals Forces. *Phys. Rev.*, 73(4):360–372, 1948.

[8] S. Y. Buhmann, H. Safari, D-G. Welsch, and H. T. Dung. Microscopic Origin of Casimir-Polder Forces. *Open Syst Inf Dyn*, 13(4):427–436, 2006.

[9] M. Fichet, F. Schuller, D. Bloch, and M. Ducloy. van der Waals interactions between excited-state atoms and dispersive dielectric surfaces. *Phys. Rev. A*, 51(2):1553, 1995.

[10] D. Raskin and P. Kusch. Interaction between a Neutral Atomic or Molecular Beam and a Conducting Surface. *Phys. Rev.*, 179(3):712, 1969.

[11] A. Anderson, S. Haroche, E. A. Hinds, W. Jhe, and D. Meschede. Measuring the van der Waals forces between a Rydberg atom and a metallic surface. *Phys. Rev. A*, 37(9):3594, 1988.

[12] V. Sandoghdar, C. I. Sukenik, E. A. Hinds, and Serge Haroche. Direct measurement of the van der Waals interaction between an atom and its images in a micron-sized cavity. *Phys. Rev. Lett.*, 68(23):3432, 1992.

[13] C. I. Sukenik, M. G. Boshier, D. Cho, V. Sandoghdar, and E. A. Hinds. Measurement of the Casimir-Polder force. *Phys. Rev. Lett.*, 70(5):560, 1993.

[14] Y. Guo and Z. Jacob. Giant non-equilibrium vacuum friction: Role of singular evanescent wave resonances in moving media. *Opt. Express*, 22:26193–26202, 2014.

[15] S. Weinberg. *Lectures on Quantum Mechanics*. Cambridge University Press, New York, 2012.

[16] J. D. Jackson. *Classical Electrodynamics*. Wiley, New York, 3 edition, 1998.

[17] R. Kubo. The fluctuation-dissipation theorem. *Rep. Prog. Phys.*, 29(1):255, 1966.

[18] S. Y. Buhmann and D-G. Welsch. Dispersion forces in macroscopic quantum electrodynamics. *Progress in Quantum Electronics*, 21(3):51–130, 2007.

[19] H. Dung, S. Y. Buhmann, L. Knöll, D-G. Welsch, S. Scheel, and J. Kästel. Electromagnetic-field quantization and spontaneous decay in left-handed media. *Phys. Rev. A*, 68(4):043816, 2003.

[20] S. Y. Buhmann. *Dispersion Forces I - Macroscopic Quantum Electrodynamics and Ground-State Casimir, Casimir–Polder and van der Waals Forces*. Springer-Verlag, Berlin Heidelberg, 2012.

[21] B. Huttner and S. M. Barnett. Quantization of the electromagnetic field in dielectrics. *Phys. Rev. A*, 46(7):4306, 1992.

[22] S. Weinberg. *The Quantum Theory of Fields*. Cambridge University Press, New York, 2005.

[23] C. Cohen-Tannoudji, J. Dupont-Roc, G. Grynberg. *Photons and Atoms: Introduction to Quantum Electrodynamics*. Wiley, New York, 1989.

[24] S. A. Ellingsen, S. Y. Buhmann, and S. Scheel. Dynamics of thermal Casimir-Polder forces on polar molecules. *Phys. Rev. A*, 79(5):052903, 2009.

[25] H-P. Breuer and F. Petruccione. *The Theory of Open Quantum Systems*. Oxford University Press, 2002.

[26] T. F. Gallagher. *Rydberg Atoms*. Cambridge University Press, New York, 1994.

[27] J. C. Slater. Atomic Radii in Crystals. *The Journal of Chemical Physics*, 41(10):3199–3204, 1964.

[28] S. Scheel, S. Y. Buhmann, C. Clausen, and P. Schneeweiss. Directional spontaneous emission and lateral Casimir-Polder force on an atom close to a nanofiber. *Phys. Rev. A*, 92(4):043819, 2015.

[29] S. B. Wang and C. T. Chan. Lateral optical force on chiral particles near a surface. *Nat. Commun.*, 5:3307, 2014.